ABSTRACT

EVERS, ANNA. Elucidating the Fate of Siderophores in Soil Systems. (Under the direction of Dr. Owen Duckworth).

Iron (Fe) is an essential nutrient for all organisms but is typically held in low solubility (oxyhydr)oxide minerals with limited bioavailability in aerobic environments. Low Fe availability can lead to biological deficiency in alkaline soils where Fe is not available for organism uptake. Consequently, bacteria, fungi, and graminaceous plants have evolved specific strategies for Fe uptake. One such strategy is the production of siderophores, a structurally diverse class of high affinity Fe(III) chelating agents with low molecular masses that are exuded to facilitate the solubilization and uptake of essential nutrients from soils. Siderophores are essential for proper plant nutrition as well as the maintenance of soil quality and the suppression of plant diseases. However, due to analytical limitations, the fate of structurally distinct siderophores in soil systems remains largely unresolved, which motivates the research in this dissertation. In the first chapter, the binding capabilities of a synthetic phytosiderophore proline-2'-deoxymugeneic acid (PDMA) with trace metals were investigated. We conducted spectrophotometric titrations to determine the stability constants of PDMA complexes with manganese (Mn(II)), cobalt (Co(II)), copper (Cu(II)), nickel (Ni(II)), and zinc (Zn(II)), and determined that PDMA complex stability constants correlated with: (1) the hydrolysis constants of metal ions in complexes; (2) the ionic potential of complexed metals; and (3) the corresponding complex stability constants of other mugineic acid type phytosiderophores, as well as the trishydroxamate microbial siderophore desferrioxamine-B (DFOB). These correlations demonstrate the potential, and limitations, on our ability to predict the stability of phytosiderophore complexes with metal ions with different properties. The second chapter describes the interactions of the siderophores DFOB, protochelin, and PDMA with soil

aluminosilicates and metal (oxyhydr)oxides, including montmorillonite, kaolinite, goethite, ferrihydrite, and δ-MnO_2. Apo- and metal-siderophore complex sorption was studied using adsorption isotherm experiments, and the fate of complexes on the mineral surfaces was studied using gallium (Ga) X-ray absorption spectroscopy. In general, positively charged siderophores and complexes (Fe(III)$HDFOB^+$ and Fe(III)H_3PDMA^{2+}) showed similar trends in their fate on mineral surfaces. However, sorption of apo-DFOB and Fe(III)-DFOB was higher than that of PDMA and its complexes, with Fe(III)-PDMA having low sorption, and apo-PDMA negligibly sorbing to soil minerals. Protochelin was the most susceptible to degradation via soil minerals, and its anionic complexes behaved uniquely on the surface of montmorillonite and ferrihydrite. The third chapter presents results that track the fate of Ga-siderophore complexes in soils. Micro-X-ray fluorescence (μ-XRF) mapping paired with μ-EXAFS spectroscopy was utilized to probe the fate of Ga(III) complexes with the siderophore DFOB, protochelin, and PDMA in a Cassville clay soil, a Belhaven muck, and a Gruver series soil. In the Cassville clay, interactions for all siderophores were predominantly through intercalation and sorption processes within Fe- and Mn-oxide-coated clay domains, reflecting the high sorptive capacity of clay-rich systems, and their capacity to act as sinks for siderophores. In the organic-rich Belhaven muck, DFOB and protochelin siderophore complexes sorbed as intact complexes with humic substances and associated Fe phases, but PDMA had low affinity for specific mineral phases and distributed evenly through the muck as a dissociated complex. All three siderophores associated with iron phases in the alkaline soil, emphasizing the critical role of siderophores in sustaining Fe cycling under such conditions. Protochelin induced the highest amount of Fe and Mn dissolution in all three soils, implying that protochelin undergoes degradation within the soil matrix, potentially rendering it unable bind Fe(III) after dissolution. Together, the results of this dissertation aid in

our understanding of how siderophore structure effects their fate in soils and will provide a new angle for managing agricultural systems so that nutrient deficiencies and crop disease susceptibility are minimized.

Elucidating the Fate of Siderophores in Soil Systems

by
Anna Evers

A dissertation submitted to the Graduate Faculty of
North Carolina State University
in partial fulfillment of the
requirements for the degree of
Doctor of Philosophy

Soil Science

Raleigh, North Carolina
2025

APPROVED BY:

Owen Duckworth Committee Chair	Wei Shi
Hui Li	James Harrington
Terri Long	Angela Allen

DEDICATION

This dissertation is dedicated to all the people who have supported me throughout these last 4 years. First and foremost, my gratitude goes to Dr. Owen Duckworth. Thank you for your patience, mentorship, and endless humor. Your support is invaluable and instrumental to my growth as a scientist. I feel incredibly grateful to have worked under your guidance.

To my parents, who have supported me and pushed me to be the best version of myself from the very beginning. I could not have done this without you.

To my best friends and climbing partners, thank you for your endless empathy, encouraging words, adventures, and psych. I am incredibly grateful to have you all by my side and on the other end of a rope.

To all my office mates throughout this time, thank you for nurturing an environment full of tomfoolery, vulnerability, and collaboration. I know our friendships will carry on well beyond this office.

BIOGRAPHY

Anna was born in Offenbach am Main, Germany, but moved to the US as a baby, and grew up in East Brunswick, New Jersey. After graduating from high school, Anna attended the University of Delaware, where she pursued a Bachelor's degree in Chemistry, with an Environmental Concentration. Early in her college years, she spent weekends backpacking and soon became an avid rock climber. It was through the countless hours spent outside pursuing other passions that she realized she also ultimately wanted to bring an aspect of the natural world into her career. Pursuing a PhD had been the plan since high school, so in her second year of college Anna began to pursue undergraduate research. Here, she stumbled upon Dr. Donald Sparks' Environmental Chemistry Lab, where she was first introduced to the field of soil chemistry. She quickly realized she was fascinated by the intersection of chemical principles with environmental applications. Upon graduation in 2021, she began her PhD in soil biogeochemistry at North Carolina State University under the direction of Dr. Owen Duckworth. Here, she worked to understand how differing structures of iron chelators reacted in soil environments. After graduation in 2025, Anna plans to begin a Post Doctoral position.

ACKNOWLEDGMENTS

This research was funded by United States Department of Agriculture—National Institute of Food and Agriculture (USDA-NIFA) Project 2019-06522. This work was also supported by the USDA National Institute of Food and Agriculture, Hatch project NC02951. Portions of this research were carried out at the Stanford Synchrotron Radiation Lightsource, a national user facility operated by Stanford University on behalf of the U.S. Department of Energy, Office of Basic Energy Sciences under Contract No. DE-AC02-76SF00515. Portions of this work were also carried out at the Advanced Light Source, which is supported by the Director, Office of Science, Office of Basic Energy Sciences, of the U.S. Department of Energy under Contract DE-AC02-05CH11231. Throughout this project, we would like to thank Dr. Georgiy Gamov for useful discussion, and Dr. Wayne Robarge for analytical support with ICP-OES measurements.

TABLE OF CONTENTS

LIST OF TABLES

LIST OF FIGURES

AUTHORSHIP STATEMENT

Contributions of Anna Evers and coauthors are listed below for each chapter.

Chapter 1

1. Anna Evers: sole author

Chapter 2

1. Anna Evers: development of methodological details, data analysis, data interpretation, primary writing and editing
2. Jackson Kohn: data collection, data analysis
3. Owen Duckworth: conceptualization, data interpretation, primary writing and editing
4. James Harrington: editing, critical review, and thoughtful discussion
5. Oliver Baars: critical review and editing
6. Kosuke Namba: provision of recourses for experimentation

Chapter 3

1. Anna Evers: development of methodology, data collection, data analysis, data interpretation, primary writing and editing
2. Annaleigh Morgan: data collection
3. Lauren Putney: data collection
4. Tyler Sowers: data collection, critical review
5. Owen Duckworth: development of methodology, data interpretation, primary writing and editing, conceptualization

Chapter 4

1. Anna Evers: development of methodology, data collection, data analysis, data interpretation, primary writing and editing
2. Owen Duckworth: development of methodology, data interpretation, primary writing and editing, critical review, conceptualization

Chapter 5

1. Anna Evers: sole author

Use of generative artificial intelligence: No generative artificial intelligence was used to write this dissertation.

CHAPTER 1: Literature Review

1. Introduction

Trace metals are essential for the metabolic function of all living cells. Iron (Fe) is the most abundant transition metal in the enzymes of microbes and plants (Williams 1991). It is frequently utilized in redox catalysis, including the electron transport chain, and serves as a vital nutrient in the nitrogen cycle via enzymes involved in the catalysis of nitrogen redox reactions (Vraspir and Butler 2009). Although abundant in the earth's crust (approximately 5%), it is typically held in insoluble (oxyhydr)oxide mineral phases that are not readily available for biological uptake at circumneutral pH in soil systems. Due to the low bioavailability of Fe, plants, bacteria, and fungi have developed strategies to facilitate the solubilization and uptake of Fe from soils, in the form of root exudates. Because of the importance of Fe to biological productivity, understanding Fe uptake mechanisms is not only of foremost scientific interest but also critical for developing sustainable agricultural and environmental management strategies that optimize micronutrient cycling and support ecosystem functioning.

2. Nutrient acquisition by plants

Root exudates enhance nutrient acquisition by altering rhizosphere chemistry through processes such as releasing protons and organic acids that lower rhizosphere pH and complex or solubilize nutrients. Plants use two distinct strategies to acquire Fe from soil (Römheld and Marschner 1986). The first strategy (Strategy I) (in most non-graminaceous species) involves the acidification of the rhizosphere through the release of protons (H^+). This release of H^+ lowers the pH and thus solubilizes Fe(III) by promoting its reduction to Fe(II) near the plant root (Fox and Guerinot 1998; Brown and Jolley 1988). The released Fe(II) is taken up by a high-affinity transporter localized on the plasma membrane (Eide et al. 1996; Robinson et al. 1999).

The second strategy (Strategy II), used by graminaceous plants (grasses) does not require the reduction of Fe(III) but instead involves the exudation of small (typically 200-2000 Da) Fe(III)-binding ligands called siderophores. In this strategy, reductive dissociation of Fe(III) from a complex occurs inside the cell (Takagi, Kamei, and Yu 1988). Siderophores released by graminaceous plants are classed as phytosiderophores, and are released in a diurnal pulse, triggered by light (Walter et al. 1995). Grasses have been shown to thrive compared to non-graminaceous plants in calcareous soil environments, providing compelling evidence for the efficacy of siderophores. Additionally, transgenic rice lines harboring genes from barley involved in the synthesis of mugineic acids (a phytosiderophore) have exhibited improved tolerance to low Fe alkaline soils (Suzuki et al. 2008). Studying natural Fe acquisition strategies, such as the production of siderophores — a class of compounds that plants are already producing — may aid in the development of better management strategies to improve plant growth and nutritional content.

3. Chemistry of Siderophores

Graminaceous plants, bacteria, and fungi all release siderophores to help facilitate the solubilization and uptake of essential nutrients from soil (Schwyn and Neilands 1987). Their reported concentrations vary between 10^{-9} to 10^{-6} M in fresh water systems, soils, and the ocean (Duckworth, Holmstrom, et al. 2009; Kraemer 2004; Ahmed and Holmström 2014; Rai et al. 2020b). To date there are more than 500 known structures of siderophores (Boukhalfa et al. 2003). Siderophores typically contain multidentate combinations of catecholate, hydroxamate, carboxylate, and α-hydroxycarboxylate groups arranged in linear, tripodal, or cyclic arrangements (Figure 1) (Crumbliss and Harrington 2009; Hider and Kong 2010).

Siderophores typically have a higher affinity for Fe(III) than Fe(II), and they form high - affinity, stable complexes with ferric iron. In water, Fe(III) is solvated by a total of six water molecules or hydroxide ions, forming an octahedral complex. It is energetically favorable for the siderophore donor atoms to replace the water in the complex (typically using the electron pairs from oxygen for coordination), forming an Fe(III) hexacoordinated complex with a similar octahedral geometry to the aqueous ion (Raymond and Dertz 2004). To satisfy the octahedral coordination preferred by Fe(III), siderophores usually act as hexadentate ligands to form 1:1 complexes. Siderophores may also employ preorganization and rigid complexation structures to enhance affinity(Crumbliss and Harrington 2009). The known stability constants of such 1:1 Fe(III)-siderophore complexes range from K = 10^{30}–10^{50} (Kraemer 2004), which are many orders of magnitude higher than those of most Fe complexes formed by common organic ligands, such as EDTA and oxalate (Cheah et al. 2003; Ngwack and Sigg 1997). Although siderophores typically are thought of as Fe transporters, they can also form complexes with other essential elements such as Mn, Mo, Cu, Co, and Ni (with structure determining the relative affinity), impacting their availability for microbial cells (for DFOB, log $K_{Al(III)}$ = 24.5, log $K_{Cu(II)}$ = 14.1, and log $K_{Zn(II)}$ = 11.1) (Bellinger 2008; Anderegg, l'Eplattenier, and Schwarzenbach 1963). Interestingly, some siderophores bind other hard metal ions with a higher affinity, such as Mn(III) and Co(III), than Fe(III), depending on their structure.

Although siderophores are operationally defined, there are commonalities that are seen through the structures. Plants typically produce carboxylate and α-hydroxycarboxylate phytosiderophores (Kraemer, Crowley, and Kretzschmar 2006) in the mugineic acid family. This group is less structurally diverse than microbial siderophores, with only a few phytosiderophores identified (Kratena et al. 2021; Lemanceau et al. 2009). Additionally, phytosiderophores tend to

have lower stability constants ($K = 10^{11}–10^{17}$) than microbial siderophores. The ecological and evolutionary reasons for the lower stability are not well understood.

Fungi typically produce siderophores with a single type of binding moiety — hydroxamate. However, the chemistry of siderophores produced with this moiety is quite diverse, including coprogens, fusarinines, ferrichromes, and ferrioxamines (Figure 1). Coprogens are characterized as linear dihydroxamate and trihydroxamate ligands; in contrast, fusarinines can take various forms, including monomers, linear dimers, and cyclic trimers, and ferrichromes primarily exist as cyclic hexapeptides (Renshaw et al. 2002). Fungi may also produce a citrate derived- carboxylate siderophore, rhizoferrin, which consists of two molecules of citric acid linked to 1,4-diaminobutane through two amide bonds (Thieken and Winkelmann 1992).

Bacteria produce the most diverse range of siderophores, reflecting their ecological diversity and Fe acquisition strategies. Among these are catecholate, hydroxamate, carboxylate, and mixed-type moieties, enabling bacteria to compete effectively for Fe in diverse environments (Cornelis 2010). A large class of mixed-type siderophores is pyoverdine, a major siderophore with over 100 known structures. Pyoverdines are fluorescent siderophores characterized by a conserved dihydroxyquinoline chromophore attached to a variable peptide chain that comprises 6–12 amino acids, and a side-chain, generally a dicarboxylic acid or an amide that are exuded by all fluorescent *Pseudomonas* species and by *Azotobacter vinelandii* (Meyer 2000; Cornelis 2010). The peptide chain comprises l- and d-amino acids, some of which are unusual. Both the chromophores and the peptide chains of pyoverdines are synthesized by non-ribosomal peptide synthetases (Mossialos et al. 2002; Merriman, Merriman, and Lamont 1995; Lehoux, Sanschagrin, and Levesque 2000).

To represent a variety of siderophore structures and chelating moieties, three siderophores were studied in this dissertation. The first is the widely used tris-hydroxamate microbial siderophore desferrioxamine B (DFOB) (Figure 2), which has been commonly used in experiments due to its commercial availability, as well as in medical applications (Day and Ackrill 1993). It occurs in both terrestrial and marine ecosystems, and serves as a useful model for a large class of microbial siderophores (Essén et al. 2006; Müller and Raymond 1984; McCormack, Worsfold, and Gledhill 2003). The three hydroxamate functional groups provide 6 total binding sites, resulting in 1:1 complex formation, satisfying the octahedral coordination sphere of Fe(III). The stability of the aqueous Fe(III)-DFOB complex arises in part from the efficacy of the hydroxamate functionality as a Lewis base, donating electron density to the central Fe(III). This complexation results in a stable complex (logK=32.02) with considerable delocalization of electron density in the complex core (Edwards and Myneni 2005). Because of the positive charge of the terminal amino group, at relevant soil pHs, both apo-DFOB and Fe(III)-DFOB are cations in solution (e.g., H_4DFOB^+ and $Fe(III)HDFOB^+$). DFOB plays a significant role not only in the biogeochemistry of Fe but also in that of manganese (Mn) and cobalt (Co). The stability constant of the $Mn(II)HDFOB^+$ complex is 29.9 (Duckworth and Sposito 2005), while that of the $Co(III)HDFOB^+$ complex is 37.7 (Duckworth, Bargar, et al. 2009), indicating that the Co complex is approximately five orders of magnitude more stable than the corresponding Fe complex. DFOB interacts with a wide range of biologically important trivalent metal cations and plays a multifaceted role in biogeochemical processes across both terrestrial and marine ecosystems.

The second siderophore used in this thesis is proline-2′-deoxymugineic acid (PDMA) (Figure 2). PDMA is a synthetic analog of the carboxylate natural phytosiderophore 2′-

deoxymugineic acid (DMA). DMA is a common siderophore exuded by *Poaceae* (e.g. rice, corn, and wheat) and contains a highly strained four-membered ring of azetidine-2-carboxylic acid. This makes it relatively unstable and difficult to synthesize by laboratory methods. In response to these limitations, PDMA was developed by (Suzuki et al. 2021), and replaces this 4-membered ring with a more stable 5-membered ring, resulting in a simplified synthetic procedure and improved resistance to biodegradation. PDMA has previously been studied as a potential fertilizer in calcareous soil (Suzuki et al. 2021; Wang et al. 2023) and has been shown to improve Fe nutrition when applied to rice and peanut plants. As noted previously, the stability constants of phytosiderophores are lower than for most microbial siderophores (logK = 17.1 for PDMA); however, plants may also have by higher rates of exudation, with concentratio ns reaching up to 1 mM in the rhizosphere (Römheld 1991).

The third siderophore discussed in this work is protochelin, a bacterial tris-catecholamine siderophore produced by the free-living diazotroph *Azotobacter vinelandii* (Figure 2) (Cornish and Page 1995). Catechol donor groups bind Fe(III) through the conjugated central ring system, which delocalizes electron density (Albrecht-Gary and Crumbliss 1998). Protochelin, unlike the previously mentioned siderophores is less soluble, in part due to its higher molecular weight and hydrophobicity (Harrington et al. 2012). The backbone of the molecule features very few hydrogen bond donor or acceptor sites, and the catechol donor groups of the molecule are likely protonated at pH < 7.5 (Loomis and Raymond 1991), resulting in a neutral charge and highly hydrophobic donor groups at low solution pH (Harris et al. 1979). Protochelin also degrades slowly over time in solution at relevant soil pH (Harrington et al. 2012).

4. Sinks for Siderophores in Soils

Although siderophores have long been recognized for their importance in Fe acquisition in soil systems, we know little about how these structural differences affect their fate and their ability to transport metals in soils (Harrington, Duckworth, and Haselwandter 2015). The traditional paradigm for siderophore activity in soil involves: (1) siderophore release from organisms; (2) Fe solubilization from bio-unavailable sources; and (3) Fe uptake by cells via an active transporter or reductive process (Kraemer 2004; Kraemer, Crowley, and Kretzschmar 2006; Robin et al. 2008; Schenkeveld et al. 2014). For siderophores to bring Fe to a cell, they must be transported as an apo-siderophore (not binding a metal) from the cell to an Fe source, and then as an Fe(III)-siderophore complex back to the cell. Because soils are complicated and dynamic systems, a myriad of reactive agents, including mineral surfaces and organic matter, may disrupt these solubilization or transport processes, both for the free siderophore and complexed siderophore.

Although siderophores are usually released into soils by organisms with the putative intent of being reabsorbed by the organism, there are many reactions in soil systems that may disrupt the transport and uptake of siderophores. Adsorption to minerals, degradation via redox active minerals or enzymes, and competitive uptake by other organisms can all play a role in the fate of a siderophore as it moves through the rhizosphere (Kraemer 2004; Akafia et al. 2014; Duckworth and Sposito 2005; Siebner-Freibach, Hadar, and Chen 2004; Kuhn et al. 2014; Kim et al. 2001). Traditionally, chelation has been thought to protect siderophores from antagonistic effects, as it orients some susceptible moieties away from bulk solution and modifies their electronic configuration (Duckworth, Bargar, and Sposito 2008; Edwards and Myneni 2005), making them less susceptible to redox or surface promoted degradation. This effect has also been observed in biotic systems, where chelation protects siderophore moieties from enzymatic

degradation (Chukwuma, Duckworth, and Baars 2025). Both apo-siderophore and metal-siderophore complexes have previously been shown to adsorb to clays, Fe minerals, and organic matter (Boiteau et al. 2020; Carrasco et al. 2009; Haack, Johnston, and Maurice 2008).

In general, sorption of molecules, including siderophores, to mineral surfaces can be separated into outer sphere sorption, inner sphere sorption, and the formation of ternary complexes. Sorption is controlled by the chemical characteristics of both the sorbent (reactive functional groups or electrostatic charges) and the sorptive (ionic radius, valence, bonding characteristics, hydrophobicity). In an outer sphere complex there is no direct bond, and the ligand is attracted to the surface by electrostatic forces and can be separated from the surface by water molecules (Strawn 2021). Inner sphere complexes are formed when the ligand binds directly to the surface and can be classified by their complex architecture 1) monodentate with one functional group bound to metal surface; 2) mononuclear bidentate with two functional groups bound to one metal site; or 3) bridging (binuclear) bidentate where two groups are bound to two different metal sites (Simanova, Loring, and Persson 2011). Metal-organic complexes, such as Fe(III)-siderophore complexes, can also be bound to surfaces through ternary complexes, where a cation or anion is used as a bridging ion. Ternary complexes can be either type A, where the metal bridges the surface to the ligand, or type B, where the ligand bridges the metal to the surface.

Adsorption isotherms are often utilized to provide a quantitative measure of substance adsorption by soil minerals as a non-mechanistic approach (Sposito 2008). The data are typically presented as a graph of the amount of a solute adsorbed (q) versus the equilibrium solution concentration of the solute. Four common types of isotherms include L-type, H-type, S-type and C-type. Langmuir and Freundlich equations have been widely employed to mathematically

describe L-type adsorption behavior, the most common pattern observed in isotherms (Sposito 2008). The Langmuir equation was developed by Irving Langmuir in 1918 to describe the adsorption of gas molecules on a planar surface. The original equation makes assumptions that: 1) adsorption occurs on surfaces that have a fixed number of identical sites; 2) adsorption is reversible; 3) there is no lateral movement of molecules on the surface; and 4) the surface is homogenous and there is no interaction between adsorbate molecules (Harter and Smith 1981). Because soils are heterogenous surfaces, these assumptions are often invalid, and debate has been had over its validity to model adsorption to soil surfaces. Despite this, it can be used for qualitative and descriptive purposes, and can be expressed as:

$$q = KC_b/(1 + KC_b) \quad (1)$$

where q is the amount of adsorption (adsorbate per unit mass of adsorbent) and C is equilibrium concentration. Although mechanistic information cannot be derived from this purely macroscopic model, it can be used to predict maximum sorption values.

The Freundlich equation was first used to describe gas phase adsorption and solute adsorption and is an empirical model that has been widely used in environmental soil chemistry. It can be expressed as:

$$q = K_d C^{1/n} \quad (2)$$

where K_d is the distribution coefficient, and n is a correction factor. Unlike the Langmuir equation, one of the major disadvantages of the Freundlich equation does not predict an adsorption maximum.

However, it is important to keep in mind that adsorption isotherms are purely descriptions of macroscopic data and do not definitely prove a reaction mechanism (Sparks 2003b). Understanding sorption behavior of siderophores is critical to the interpretation of other

spectroscopic approaches, and helps inform on the mobility, bioavailability, reactivity, and ecological function of siderophores in soil systems.

4.1. Sorption to Clays

A significant number of studies have probed the adsorption of free siderophores and their complexes to clays, including montmorillonite and kaolinite (He et al. 2006; Haack, Johnston, and Maurice 2008; Siebner-Freibach, Hadar, and Chen 2004; Neubauer et al. 2000; Rosenberg and Maurice 2003). Montmorillonite is a 2:1 swelling clay, with the capacity to intercalate (absorb in its interlayers) molecules, and kaolinite is a 1:1 clay, with the available adsorption sites being silicious (Si-O-Si) sites on the basal plane surfaces (Maurice, Haack, and Mishra 2009). Swelling clays and micas have negative permanent structural charge density resulting from isomorphic substitution and may undergo cation exchange. (Maurice, Haack, and Mishra 2009). It is known that clays such as montmorillonite may intercalate many organic compounds, including DFOB (Haack, Johnston, and Maurice 2008). The characteristics of the interlayer molecules (size, structure, orientation, and charge) can change the thickness of the interlayer spacing, which is reflected in changes in the basal plane or interlayer spacing, as typically measured by X-ray diffraction. For most organic molecules and metal complexes, the large size of the molecule results in swelling of interlayers. Metal ions may also intercalate, often resulting in the collapse of interlayer spacing due to electrostatic attraction and bridging of layers. (Siebner-Freibach, Hadar, and Chen 2004) found that Fe(III)HDFOB^{+} sorbs strongly to montmorillonite, but minimally to kaolinite. Fourier transform infrared spectroscopy (FTIR) revealed that intercalation of the intact complex was the dominant sorption mechanism (Siebner-Freibach et al. 2005). The phytosiderophore DMA has previously been shown to exhibit no

sorption to montmorillonite clay due to small amounts of reactive Al and small external surface area (Hiradate and Inoue 1999). The sorption of apo- and complexed hydroxamate siderophores, as well as apo- MA type siderophores to smectites is well understood, however gaps remain regarding the sorption of complexed phytosiderophores and catecholate type siderophores to clays.

4.2. Iron oxides

The significance of Fe bearing minerals as nutrient sources for siderophore promoted Fe acquisition has long been recognized. As discussed above, in most environments, Fe deficiency is not triggered by low total Fe concentrations but by low solubility and dissolution kinetics of Fe bearing mineral phases. Common crystalline Fe oxide phases include hematite (α-Fe_2O_3), magnetite (Fe_3O_4), and goethite (α-FeOOH) (Schwertmann 1989). The solubility of Fe oxides in aerobic systems depends on the properties of the solid and the composition of the solution. Solubilities increase with decreasing particle sizes and increasing bulk lattice energies of Fe oxides. Size and lattice energy are influenced by ageing and isomorphous substitution by metal ions such as aluminum (Al). The solution pH, ionic strength, and the presence of organic ligands are key factors influencing the solubility of Fe oxides.

For the purposes of this thesis, goethite was chosen to represent stable Fe oxides. Goethite has a distorted hexagonal close packing structure consisting of three short O-Fe bonds and three long Fe-OH bonds with four repeat formula units (Cornell and Schwertmann 2003b). When in contact with water, the goethite surface has two types of terminal hydroxyls- a bidentate hydroxo group and a monodentate aquo group that may protonate or deprotonate depending on solution pH (Ghose et al. 2010).

Another class of Fe oxides is short range ordered Fe oxides, which are poorly crystalline Fe oxides where atoms are arranged in a somewhat regular pattern only over a few nanometers. The most common short range ordered Fe oxide is ferrihydrite, which serves as the most important precursor for other crystalline Fe (oxyhydr)oxides (i.e., hematite and goethite) produced in the natural environment during weathering or pedogenic processes (Cornell and Schwertmann 2003a; Hochella Jr et al. 2008). Ferrihydrite may control the soluble Fe concentrations in soil solutions due to its high solubility, surface area, and kinetic lability even if it represents only a minor Fe pool. Even with the considerable attention given to the chemical and physical properties of ferrihydrite in previous research, there is no consensus on the crystal structure of this mineral. It is generally considered to be poorly ordered, and designated as "two-line" or "six-line" on the basis of the number of poorly defined, broadened maxima observed in X-ray diffraction (XRD) patterns (Michel et al. 2007). The surface of both goethite and ferrihydrite contains reactive oxygens, leading to an overall negative surface charge on the minerals (if pH is less than the point of zero charge of a mineral).

Extensive research has focused on the adsorption behavior of both free siderophores and their Fe(III) complexes on Fe oxide surfaces (Kraemer et al. 1999; Kraemer et al. 2002; Neubauer, Furrer, and Schulin 2002; Kraemer 2004). The hydroxamic groups of DFOB are thought to be coordinated to the surface of goethite either inner-spherically, or outer spherically but protonated. Fe(III)HDFOB^{+} has been shown to sorb in part as a type A ternary complex to the surface of goethite (Simanova, Loring, and Persson 2011). However, most studies have focused on the siderophore DFOB and thus knowledge gaps exist as to the adsorption behavior of other binding moieties to these minerals.

4.3. Organic Matter

Soil organic matter (SOM) may also interact with siderophores and their complexes. Humic substances are amongst the most widely distributed organic materials on the planet (Stevenson 1994), and contribute vital properties to soils, including sequestration, mobilization, and oxidative or reductive transformation of molecules (Sutton and Sposito 2005). Humic substances are currently defined as supramolecular associations, in which many relatively small and chemically diverse organic molecules form clusters linked by hydrogen bonds and hydrophobic interactions (Piccolo 2001). This results in the concept of a micellar structure for organic matter, where hydrophilic exterior regions shield hydrophobic regions from water molecules (Wandruszka, Engebreatson, and Yates 1999).

Because Fe is ubiquitous in soils, it plays an important role in the stabilization of organic matter in soil (Jambor and Dutrizac 1998). However, the binding strength of Fe to siderophores is higher than that of Fe to organic matter, so Fe in this pool represents a possible labile source of Fe (Gustafsson et al. 2007). SOM may also act as a potential sink for siderophores, as siderophores can adsorb to negative sites on humic substances or minerals via bridging with multivalent cations (Harrington, Duckworth, and Haselwandter 2015). For the siderophore DFOB, it has been shown that an excess of DFOB removed around 75% of Fe from organic matter, and lowered the distribution of molecular weights, perhaps due to the removal of bridging Fe (Kuhn et al. 2014). Siderophores may strongly interact with SOM through hydrogen bonding, by bridging complexes with strongly bound ions or nanoparticles, or via hydrophobic partitioning. Higashi et. al. found that the formation of DFOB·humic substances (HS) (or possibly DFOB·metal·HS) caused significant decreases in the formation of the Fe(III)-DFOB complex (M. Higashi, W-M. Fan, and N. Lane 1998) . The results showed that such organic ligand–HS interactions do occur for DFOB, which significantly alter the metal ion chemistry and

probably affect bioavailability. Additionally, the adsorption of siderophores pyoverdin and enterobactin to alkaline soils containing organic matter has been studied. It was concluded that cation-bridged aggregation of OM favors the stabilization of larger molecules with more nucleophilic functional groups based on the increased adsorption of pyoverdine over enterobactin (Boiteau et al. 2020). Additionally, it was found that siderophores associated with organic carbon coatings rather than to bare mineral, indicating that SOM is a sink for siderophores (Boiteau et al. 2020). SOM can act as both an Fe source and a sink for siderophores, and these interactions need to be studied with greater depth.

4.4. Manganese Oxides

Manganese is commonly found as Mn(II), Mn(III) or Mn(IV) in natural environments in a diverse suite of minerals (Post 1999). Mn(II) is favored under reducing conditions and is predominantly associated with ferromagnesian silicates and other Fe-bearing minerals. During mineral weathering, Mn(II) associated with these primary minerals may be oxidized to Mn(III) and Mn(IV) either at the mineral surface or in solution. (Robson 1988). For the purposes of this dissertation, the Mn oxide to be discussed is birnessite. Birnessite consists of stacked sheets of edge-sharing Mn octahedra, a layered arrangement known as a phyllomanganate structure (Remucal and Ginder-Vogel 2014). Mn atoms in the layers are mainly Mn^{4+} but Mn^{3+} can be a minor component. The layers also contain varying amounts of uncoordinated oxygen atoms around point defects of missing Mn, known as cationic vacant sites, which are often sites of oxidation and sorption (Schacht and Ginder-Vogel 2018). The high number of vacancy sites results in high redox activity (Morgan 2000). As a result, most studies of the dissolution of Mn hydr(oxides) have focused on reductive pathways, and have shown that ligands promote

dissolution via reductive dissolution (Klewicki and Morgan 1999; McArdell, Stone, and Tian 1998).

5. Siderophore Induced Mineral Dissolution Mechanisms

Dissolution of metal hydr(oxides) plays an important role in the fate of siderophores and their ability to increase nutrient availability, as it can lead to siderophore degradation, coupled with the release of free metal into the rhizosphere. The dissolution of metal oxides may occur via several different reactions, including ligand-promoted, reductive, and proton-promoted pathways. For the purpose of this thesis, ligand promoted dissolution and reductive dissolution are discussed.

5.1. Non-reductive ligand promoted dissolution

Ligand-promoted dissolution involves surface complex formation between the ligand and a metal ion at the surface of the mineral, which destabilizes the metal-oxygen bonds, and mobilizes the metal into solution (Kraemer 2004; Wehrli, Wieland, and Furrer 1990). This is followed by regeneration of the surface site and transport of the detached metal into solution, typically as a part of a metal-ligand complex.

Non-reductive siderophore promoted dissolution has been extensively studied for soil minerals (Kraemer 2004; Kraemer, Crowley, and Kretzschmar 2006). Siderophores promote Fe dissolution from a wide range of Fe minerals, however most studies have again focused on the siderophore DFOB (Cheah et al. 2003; Cocozza et al. 2002; Liermann et al. 2000; Yoshida, Hayashi, and Ohmoto 2002; Cervini-Silva and Sposito 2002). DFOB-promoted dissolution of Fe hydroxides occurs via a pH-independent, ligand-promoted (non-reductive) process that occurs on the surface of the mineral (Cocozza et al. 2002; Hersman, Lloyd, and Sposito 1995). Other hydroxamate type siderophores have been shown to exhibit similar surface controlled non reductive behavior (Cocozza et al. 2002; Hersman, Lloyd, and Sposito 1995).

The dissolution of chromium (Cr) from hydroxide minerals has been studied by Duckworth et. al., who found that at pH 5, a proton promoted dissolution mechanism occurred, and at pH 8, a ligand promoted dissolution mechanism was observed (Duckworth et al. 2014). At high pH, Mn oxides have also been found to dissolve via ligand promoted pathways (Duckworth and Sposito 2005).

5.2. Reductive dissolution

Because transition metals may be prone to redox reactions, changes in oxidation state have a dramatic impact on both their solubility and speciation. Under anoxic conditions, oxides of Fe(III) and Mn(III,IV) can be reduced to their divalent oxidation state, greatly increasing solubility. Additionally, in aerobic environments at neutral pH, adsorbed ligand can act as a reductant to promote reductive dissolution of oxides (Stumm 1987). Reductive dissolution involves electron transfer between ligands and the surface metal, with the ligand being oxidized and the surface being reduced. This process also results in the detachment of the metal from the surface and is concomitant with the degradation of the siderophore.

Several factors determine which mechanism occurs within a system. One key factor is the redox activity of the siderophore functional group (Figure 1). For instance, hydroxamate-type siderophores such as DFOB are not highly redox active and therefore typically facilitate metal mobilization through ligand-promoted dissolution (Kraemer 2004). In contrast, catecholate groups are much more redox active and can be readily oxidized to quinones (Dubbin and Bullough 2017; French et al. 2024). Another important factor is the strength of surface interactions; when the binding between the siderophore and mineral surface is weaker, as in the case of outer-sphere interactions, electron transfer is less likely to occur (Cheah et al. 2003).

Finally, environmental conditions such as soil pH and redox potential also play a crucial role in influencing which mechanism predominates.

The dissolution of Mn minerals via DFOB has also been researched. Lloyd et. al. found that for manganite (MnOOH) reductive dissolution occurred; and Duckworth et. al. found non-reductive dissolution occurred at pH > 6.5 leading to the conclusion that DFOB dissolves Mn oxides via a reductive pathway at pH < 7, and a ligand promoted pathway at pH > 7 (Duckworth and Sposito 2007, 2005; Lloyd 1999). This was later confirmed for other Mn oxides (birnessite, pyrolusite) of differing oxidation numbers ((Peña et al. 2007; Duckworth and Sposito 2007). A similar observation has been made for the dissolution of heterogenite (CoOOH) (Bi, Hesterberg, and Duckworth 2010). Because reductive dissolution results in siderophore oxidation, Mn oxide dissolution at acidic pH may provide a significant abiotic sink for siderophores in soils (Duckworth and Sposito 2007) and inhibit for Fe uptake (Kang and Peña 2023). Although Fe oxides are typically reduced via ligand promoted pathways, in the absence of light at pH = 6, hydrolysis of the terminal hydroxamate group of DFOB at the Fe-hydroxide surface may produce decomposition products of acetate and an oxidized hydroxylamine-DFOB fragment, suggesting a reductive dissolution pathway for goethite dissolution (Simanova, Persson, and Loring 2010).

5.3. Synergistic dissolution

Siderophores are not produced in isolation by microbes and plants, but are co-exuded with other low molecular mass organic acids, such as citrate and oxalate (Cheah et al. 2003; Reichard, Kretzschmar, and Kraemer 2007). The secretion of these low molecular mass acids is known to be part of a strategy to promote mineral solubility and increase their bioavailability. Low molecular mass organic acids can behave like catalysts, known as synergistic dissolution.

Dissolution is synergistic if the reactivity in a multicomponent system exceeds the sum of reaction rates in corresponding single ligand systems. The dissolution of Fe oxide minerals in the presence of oxalate has been studied, and Cheah et. al. proposed the following reaction mechanism: 1) adsorption of carboxylate at mineral surface; 2) formation of a highly labile Fe(III)-carboxylate surface species; 3) detachment of the complex; 4) substitution of the carboxylate with a siderophore; and 5) reabsorption of the freed carboxylate to the mineral surface (Cheah et al. 2003). This was investigated on a molecular scale by Simanova et. al., who concluded that type A oxalate-Fe(III)-goethite complexes form at the water-goethite interface (Simanova 2011). Since the ternary complex is connected to the surface via only two bonds that need to be broken, Fe in this ternary complex is most likely more labile and therefore more accessible to siderophores than the Fe in the crystal lattice. A similar observation was made with MnO_2 in the presence of DFOB and low molecular mass organic acids (Saal and Duckworth, 2010). The presence of citrate and oxalate enhanced the DFOB-promoted rate of dissolution of δ-MnO_2 across a wide range of pH. Citrate–DFOB mixtures enhance both reductive and complex-forming dissolution rates, while oxalate–DFOB mixtures enhance only reductive dissolution rates and the production of Mn(II) (Saal and Duckworth 2010). On the contrary, when looking at dissolution rates of Cr oxides in the presence of oxalate and DFOB, no synergistic dissolution was observed, as Cr exchange between the oxalate and DFOB is slow and limits the process (Saad et al. 2017).

6. Technical Approaches

Technical approaches to studying reactions with siderophores in soils have typically been limited to extraction of the siderophore from the system, or assay quantification (Rai et al. 2020a; Powell et al. 1980). The success with siderophore extraction has mostly been limited to

hydroxamate type siderophores such as DFOB, leaving the occurrence of other metal siderophore complexes poorly resolved. These analytical limitations are due to strong adsorption to soil particles and the abundance of Fe in soil environments.

The background concentrations of Fe (ca. 100–100,000 mg kg^{-1} (Sparks 2003a)) in soils makes probing Fe atoms in siderophore complexes by element specific techniques, such as X-ray absorption spectroscopy (XAS) or X-ray fluorescence (XRF) analysis, unfeasible. However, low abundance yet chemically similar metals have been successfully used to probe chemistries of systems with significant competing background signals (Hagvall, Persson, and Karlsson 2014). Gallium (Ga) is a non-redox active metal that occurs at very low concentrations in environmental systems and has similar physicochemical properties to Fe. Fe(III) and Ga(III) ions show extensive similarities in nuclear radius, coordination chemistry, ionization potential, electronegativity, electron affinity, and tendency to ionic bonding, which make many biological systems unable to distinguish between these two metals and leads to Ga(III) incorporation in siderophores as well as in several Fe(III)-containing enzymes (Chitambar and Narasimhan 1991). (Nicolafrancesco et al. 2019) investigated the local coordination structure of Ga(III)-pyoverdin complexes using multiple spectroscopic techniques and determined that the electronic structure and coordination geometry of the Ga(III)-pyoverdin complex is analogous to that of the Fe(III)-pyoverdin complex.

The use of Ga(III)-siderophore complexes allowed for measuring the K-edge Ga extended X-ray absorption fine structure (EXAFS) spectra (Hagvall, Persson, and Karlsson 2014). EXAFS is an element specific technique in which a high energy X-ray allows for the excitation of a core electron. This vacancy in the core shell results in the relaxation of an outer electron to fill this vacancy, and an X-ray is emitted. EXAFS relies on an interference effect

using the wave nature of the photoelectron. These oscillations off neighboring atoms can be measured as changes in intensity of incident or fluoresced X-rays. EXAFS is highly useful for probing the local coordination environment as well as the oxidation state of an element of interest.

Another synchrotron technique that can be used to probe the fate of siderophores in soils is micro-X-ray fluorescence (μ-XRF) (Majumdar et al. 2012). μ-XRF uses the same foundational principles as XRF (adsorption of X-rays by a sample leaving a vacancy, followed by the release of a secondary X-ray as an outer electron relaxed to fill the hole) but adds an element of spatial mapping. Unlike conventional spatial XRF, which has a typical spatial resolution ranging in diameter from several hundred micrometers up to several millimeters, μ-XRF uses X-ray optics to restrict the excitation beam size or focus the excitation beam to a small spot on the sample surface so that small features on the sample can be analyzed. It can also be paired with μ-EXAFS to obtain more detailed information on specific map areas. In this dissertation, EXAFS and μ-XRF mapping are combined to track Ga(III)-siderophore complexes through soil and to discern which soil components are associating with siderophore complexes.

7. Objectives

The overarching objective of this dissertation is to investigate the fate of apo siderophores and metal-siderophore complexes in soil systems. This was investigated over three objectives organized into chapters:

1. Determining the stability constants of the siderophore PDMA with the trace metal nutrients Mn(II), Co(II), Cu(II), and Zn(II) to better understand the effectiveness of PDMA as a trace metal fertilizer and its impacts on trace metal biogeochemistry.

2. Understand how apo-DFOB, apo-PDMA, and apo-protochelin and their metal complexes react and bind to antagonistic soil minerals to aid in our understanding of Fe cycling in soils.
3. Investigate the fate of DFOB, PDMA, and protochelin complexes in three unique soils (high clay, high organic matter, and calcareous) to understand how siderophore structure determines its fate in distinctive soil environments.
4. A final chapter will provide reflections on the research as well as an outlook on the applications, implications, and potential next steps for this line of inquiry.

REFERENCES

Ahmed, Engy, and Sara J. M. Holmström. 2014. 'The effect of soil horizon and mineral type on the distribution of siderophores in soil', *Geochimica et Cosmochimica Acta*, 131: 184-95.

Akafia, Martin M., James M. Harrington, John R. Bargar, and Owen W. Duckworth. 2014. 'Metal oxyhydroxide dissolution as promoted by structurally diverse siderophores and oxalate', *Geochimica et Cosmochimica Acta*, 141: 258-69.

Albrecht-Gary, A. M., and A. L. Crumbliss. 1998. 'Coordination chemistry of siderophores: thermodynamics and kinetics of iron chelation and release', *Met Ions Biol Syst*, 35: 239-327.

Anderegg, G, F l'Eplattenier, and G Schwarzenbach. 1963. 'Hydroxamatkomplexe III. Eisen (III)-Austausch zwischen Sideraminen und Komplexonen. Diskussion der Bildungskonstanten der Hydroxamatkomplexe', *Helvetica chimica acta*, 46: 1409-22.

Bellinger, D. C. 2008. 'Neurological and behavioral consequences of childhood lead exposure', *PLoS Med*, 5: e115.

Bi, Yuqiang, Dean L. Hesterberg, and Owen W. Duckworth. 2010. 'Siderophore-promoted dissolution of cobalt from hydroxide minerals', *Geochimica et Cosmochimica Acta*, 74: 2915-25.

Boiteau, Rene M., Ravi Kukkadapu, John B. Cliff, Chuck R. Smallwood, Libor Kovarik, Mark G. Wirth, Mark H. Engelhard, Tamas Varga, Alice Dohnalkova, Daniel E. Perea, Thomas Wietsma, James J. Moran, and Kirsten S. Hofmockel. 2020. 'Calcareous organic matter coatings sequester siderophores in alkaline soils', *Science of The Total Environment*, 724: 138250.

Boukhalfa, Hakim, Joe Lack, Sean D. Reilly, Larry Hersman, and Mary P. Neu. 2003. 'Siderophore Production and Facilitated Uptake of Iron and Plutonium in P. Putida', *AIP Conference Proceedings*, 673: 343-44.

Brown, John C., and Von D. Jolley. 1988. 'Strategy I and strategy II mechanisms affecting iron availability to plants may be established too narrow or limited', *Journal of Plant Nutrition*, 11: 1077-98.

Carrasco, Naraya, Ruben Kretzschmar, Jide Xu, and Stephan M. Kraemer. 2009. 'Adsorption of hydroxamate siderophores and EDTA on goethite in the presence of the surfactant sodium dodecyl sulfate', *Geochemical Transactions*, 10: 5.

Cervini-Silva, Javiera, and Garrison Sposito. 2002. 'Steady-State Dissolution Kinetics of Aluminum-Goethite in the Presence of Desferrioxamine-B and Oxalate Ligands', *Environmental Science & Technology*, 36: 337-42.

Cheah, Singfoong, Stephan Kraemer, Javiera Cervini-Silva, and Garrison Sposito. 2003. 'Steady-state dissolution kinetics of goethite in the presence of desferrioxamine B and oxalate ligands: Implications for the microbial acquisition of iron', *Chemical Geology*, 198: 63-75.

Chitambar, Christopher R, and Jana Narasimhan. 1991. 'Targeting iron-dependent DNA synthesis with gallium and transferrin-gallium', *Pathobiology*, 59: 3-10.

Chukwuma, Chinazam Emmanuel, Owen William Duckworth, and Oliver Baars. 2025. 'Degradation of catecholate, hydroxamate, and carboxylate model siderophores by extracellular enzymes', *PLoS One*, 20: e0330432.

Cocozza, Claudio, Calvin C. G. Tsao, Sing-Foong Cheah, Stephan M. Kraemer, Kenneth N. Raymond, Teodoro M. Miano, and Garrison Sposito. 2002. 'Temperature dependence of

goethite dissolution promoted by trihydroxamate siderophores', *Geochimica et Cosmochimica Acta*, 66: 431-38.
Cornelis, P. 2010. 'Iron uptake and metabolism in pseudomonads', *Appl Microbiol Biotechnol*, 86: 1637-45.
Cornell, Rochelle M, and Udo Schwertmann. 2003a. *The iron oxides: structure, properties, reactions, occurrences and uses* (John Wiley & Sons).
———. 2003b. *The iron oxides: structure, properties, reactions, occurrences, and uses* (Wiley-vch Weinheim).
Cornish, Anthony S., and William J. Page. 1995. 'Production of the triacetecholate siderophore protochelin by Azotobacter vinelandii', *BioMetals*, 8: 332-38.
Crumbliss, Alvin L., and James M. Harrington. 2009. 'Iron sequestration by small molecules: Thermodynamic and kinetic studies of natural siderophores and synthetic model compounds.' in Rudi van Eldik and Colin D. Hubbard (eds.), *Advances in Inorganic Chemistry* (Academic Press).
Day, J. P., and P. Ackrill. 1993. 'The chemistry of desferrioxamine chelation for aluminum overload in renal dialysis patients', *Ther Drug Monit*, 15: 598-601.
Dubbin, William E., and Florence Bullough. 2017. 'Dissolution of Al-Substituted Goethite in the Presence of Ferrichrome and Enterobactin at pH 6.5', *Aquatic Geochemistry*, 23: 61-74.
Duckworth, Owen, Sara Holmstrom, Jasquelin Peña, and Garrison Sposito. 2009. 'Biogeochemistry of iron oxidation in a circumneutral freshwater habitat', *Chemical Geology*, 260: 149-58.
Duckworth, Owen W., Martin M. Akafia, Megan Y. Andrews, and John R. Bargar. 2014. 'Siderophore-promoted dissolution of chromium from hydroxide minerals', *Environmental Science: Processes & Impacts*, 16: 1348-59.
Duckworth, Owen W., John R. Bargar, Andrzej A. Jarzecki, Oyeyemi Oyerinde, Thomas G. Spiro, and Garrison Sposito. 2009. 'The exceptionally stable cobalt(III)–desferrioxamine B complex', *Marine Chemistry*, 113: 114-22.
Duckworth, Owen W., John R. Bargar, and Garrison Sposito. 2008. 'Sorption of ferric iron from ferrioxamine B to synthetic and biogenic layer type manganese oxides', *Geochimica et Cosmochimica Acta*, 72: 3371-80.
Duckworth, Owen W., and Garrison Sposito. 2005. 'Siderophore−Manganese(III) Interactions. I. Air-Oxidation of Manganese(II) Promoted by Desferrioxamine B', *Environmental Science & Technology*, 39: 6037-44.
———. 2007. 'Siderophore-promoted dissolution of synthetic and biogenic layer-type Mn oxides', *Chemical Geology*, 242: 497-508.
Edwards, David C., and Satish C. B. Myneni. 2005. 'Hard and Soft X-ray Absorption Spectroscopic Investigation of Aqueous Fe(III)−Hydroxamate Siderophore Complexes', *The Journal of Physical Chemistry A*, 109: 10249-56.
Eide, D., M. Broderius, J. Fett, and M. L. Guerinot. 1996. 'A novel iron-regulated metal transporter from plants identified by functional expression in yeast', *Proc Natl Acad Sci U S A*, 93: 5624-8.
Essén, Sofia A, Dan Bylund, Sara JM Holmström, My Moberg, and Ulla S Lundström. 2006. 'Quantification of hydroxamate siderophores in soil solutions of podzolic soil profiles in Sweden', *BioMetals*, 19: 269-82.
Fox, T. C., and M. L. Guerinot. 1998. 'MOLECULAR BIOLOGY OF CATION TRANSPORT IN PLANTS', *Annu Rev Plant Physiol Plant Mol Biol*, 49: 669-96.

French, K. S., E. Chukwuma, I. Linshitz, K. Namba, O. W. Duckworth, M. A. Cubeta, and O. Baars. 2024. 'Inactivation of siderophore iron-chelating moieties by the fungal wheat root symbiont Pyrenophora biseptata', *Environ Microbiol Rep*, 16: e13234.

Ghose, Sanjit, Glenn Waychunas, Thomas Trainor, and Peter Eng. 2010. 'Hydrated goethite (a-FeOOH) (100) interface structure: Ordered water and surface functional groups', *Geochimica et Cosmochimica Acta*, 74: 1943-53.

Gustafsson, Jon Petter, Ingmar Persson, Dan Berggren Kleja, and Joris WJ Van Schaik. 2007. 'Binding of iron (III) to organic soils: EXAFS spectroscopy and chemical equilibrium modeling', *Environmental Science & Technology*, 41: 1232-37.

Haack, Elizabeth A., Cliff T. Johnston, and Patricia A. Maurice. 2008. 'Mechanisms of siderophore sorption to smectite and siderophore-enhanced release of structural Fe3+', *Geochimica et Cosmochimica Acta*, 72: 3381-97.

Hagvall, Kristoffer, Per Persson, and Torbjörn Karlsson. 2014. 'Spectroscopic characterization of the coordination chemistry and hydrolysis of gallium(III) in the presence of aquatic organic matter', *Geochimica et Cosmochimica Acta*, 146: 76-89.

Harrington, James M., John R. Bargar, Andrzej A. Jarzecki, James G. Roberts, Leslie A. Sombers, and Owen W. Duckworth. 2012. 'Trace metal complexation by the triscatecholate siderophore protochelin: structure and stability', *BioMetals*, 25: 393-412.

Harrington, James M., Owen W. Duckworth, and Kurt Haselwandter. 2015. 'The fate of siderophores: antagonistic environmental interactions in exudate-mediated micronutrient uptake', *BioMetals*, 28: 461-72.

Harris, Wesley R., Carl J. Carrano, Stephen R. Cooper, Stephen R. Sofen, Alex E. Avdeef, James V. McArdle, and Kenneth N. Raymond. 1979. 'Coordination chemistry of microbial iron transport compounds. 19. Stability constants and electrochemical behavior of ferric enterobactin and model complexes', *Journal of the American Chemical Society*, 101: 6097-104.

Harter, Robert D, and Gordon Smith. 1981. 'Langmuir equation and alternate methods of studying “adsorption” reactions in soils', *Chemistry in the soil environment*, 40: 167-82.

He, Hongping, Ray L. Frost, Thor Bostrom, Peng Yuan, Loc Duong, Dan Yang, Yunfei Xi, and J. Theo Kloprogge. 2006. 'Changes in the morphology of organoclays with HDTMA+ surfactant loading', *Applied Clay Science*, 31: 262-71.

Hersman, Larry, Thomas Lloyd, and Garrison Sposito. 1995. 'Siderophore-promoted dissolution of hematite', *Geochimica et Cosmochimica Acta*, 59: 3327-30.

Hider, Robert C., and Xiaole Kong. 2010. 'Chemistry and biology of siderophores', *Natural Product Reports*, 27: 637-57.

Hiradate, S., and K. Inoue. 1999. 'Interactions of Mugineic Acid with Allophane, Imogolite, Montmorillonite and Gibbsite.' in J. Berthelin, P. M. Huang, J. M. Bollag and F. Andreux (eds.), *Effect of Mineral-Organic-Microorganism Interactions on Soil and Freshwater Environments* (Springer US: Boston, MA).

Hochella Jr, Michael F, Steven K Lower, Patricia A Maurice, R Lee Penn, Nita Sahai, Donald L Sparks, and Benjamin S Twining. 2008. 'Nanominerals, mineral nanoparticles, and earth systems', *Science*, 319: 1631-35.

Jambor, John L, and John E Dutrizac. 1998. 'Occurrence and constitution of natural and synthetic ferrihydrite, a widespread iron oxyhydroxide', *Chemical Reviews*, 98: 2549-86.

Kang, Kyounglim, and Jasquelin Peña. 2023. 'Siderophore-Mediated Mobilization of Manganese Limits Iron Solubility in Mixed Mineral Systems', *ACS Earth and Space Chemistry*, 7: 662-75.
Kim, Chulhwan, W. Walter Lorenz, J. Todd Hoopes, and F. D. Dean Jeffrey. 2001. 'Oxidation of Phenolate Siderophores by the Multicopper Oxidase Encoded by the Escherichia coli yacK Gene', *Journal of bacteriology*, 183: 4866-75.
Klewicki, J. K., and J. J. Morgan. 1999. 'Dissolution of β-MnOOH particles by ligands: pyrophosphate, ethylenediaminetetraacetate, and citrate', *Geochimica et Cosmochimica Acta*, 63: 3017-24.
Kraemer, S. M., D. E. Crowley, and R. Kretzschmar. 2006. 'Geochemical Aspects of Phytosiderophore-Promoted Iron Acquisition by Plants.' in, *Advances in Agronomy* (Academic Press).
Kraemer, S. M., J. Xu, K. N. Raymond, and G. Sposito. 2002. 'Adsorption of Pb(ll) and Eu(III) by oxide minerals in the presence of natural and synthetic hydroxamate siderophores', *Environ Sci Technol*, 36: 1287-91.
Kraemer, Stephan M. 2004. 'Iron oxide dissolution and solubility in the presence of siderophores', *Aquatic Sciences*, 66: 3-18.
Kraemer, Stephan M., Singfoong Cheah, Rita Zapf, Jide Xu, Kenneth N Raymond, and Garrison Sposito. 1999. 'Effect of hydroxamate siderophores on Fe release and Pb(II) adsorption by goethite', *Geochimica et Cosmochimica Acta*, 63: 3003-08.
Kratena, N., T. Gökler, L. Maltrovsky, E. Oburger, and C. Stanetty. 2021. 'A Unified Approach to Phytosiderophore Natural Products', *Chemistry*, 27: 577-80.
Kuhn, Keshia M., Patricia A. Maurice, Elisabeth Neubauer, Thilo Hofmann, and Frank von der Kammer. 2014. 'Accessibility of Humic-Associated Fe to a Microbial Siderophore: Implications for Bioavailability', *Environmental Science & Technology*, 48: 1015-22.
Lehoux, Dario E, François Sanschagrin, and Roger C Levesque. 2000. 'Genomics of the 35-kb pvd locus and analysis of novel pvdIJK genes implicated in pyoverdine biosynthesis in Pseudomonas aeruginosa', *FEMS microbiology letters*, 190: 141-46.
Lemanceau, Philippe, Petra Bauer, Stephan Kraemer, and Jean-François Briat. 2009. 'Iron dynamics in the rhizosphere as a case study for analyzing interactions between soils, plants and microbes', *Plant and Soil*, 321: 513-35.
Liermann, Laura J, Birgitta E Kalinowski, Susan L Brantley, and James G Ferry. 2000. 'Role of bacterial siderophores in dissolution of hornblende', *Geochimica et Cosmochimica Acta*, 64: 587-602.
Lloyd, Thomas. 1999. *Dissolution of Fe (III)-and Mn (III, IV)-(hydr) oxides by deferrioxamine B* (California Institute of Technology).
Loomis, Lawrence D., and Kenneth N. Raymond. 1991. 'Solution equilibria of enterobactin and metal-enterobactin complexes', *Inorganic Chemistry*, 30: 906-11.
M. Higashi, Richard, Teresa W-M. Fan, and Andrew N. Lane. 1998. 'Association of desferrioxamine with humic substances and their interaction with cadmium(II) as studied by pyrolysis–gas chromatography–mass spectrometry and nuclear magnetic resonance spectroscopy†', *Analyst*, 123: 911-18.
Majumdar, Sanghamitra, Jose R. Peralta-Videa, Hiram Castillo-Michel, Jie Hong, Cyren M. Rico, and Jorge L. Gardea-Torresdey. 2012. 'Applications of synchrotron μ-XRF to study the distribution of biologically important elements in different environmental matrices: A review', *Analytica Chimica Acta*, 755: 1-16.

Maurice, Patricia A., Elizabeth A. Haack, and Bhoopesh Mishra. 2009. 'Siderophore sorption to clays', *BioMetals*, 22: 649-58.
McArdell, Christa S., Alan T. Stone, and Jiaher Tian. 1998. 'Reaction of EDTA and Related Aminocarboxylate Chelating Agents with CoIIIOOH (Heterogenite) and MnIIIOOH (Manganite)', *Environmental Science & Technology*, 32: 2923-30.
McCormack, Paul, Paul J Worsfold, and Martha Gledhill. 2003. 'Separation and detection of siderophores produced by marine bacterioplankton using high-performance liquid chromatography with electrospray ionization mass spectrometry', *Analytical Chemistry*, 75: 2647-52.
Merriman, Tony R, Marilyn E Merriman, and Iain L Lamont. 1995. 'Nucleotide sequence of pvdD, a pyoverdine biosynthetic gene from Pseudomonas aeruginosa: PvdD has similarity to peptide synthetases', *Journal of bacteriology*, 177: 252-58.
Meyer, Jean-Marie. 2000. 'Pyoverdines: pigments, siderophores and potential taxonomic markers of fluorescent Pseudomonas species', *Archives of microbiology*, 174: 135-42.
Michel, F. Marc, Lars Ehm, Sytle M. Antao, Peter L. Lee, Peter J. Chupas, Gang Liu, Daniel R. Strongin, Martin A. A. Schoonen, Brian L. Phillips, and John B. Parise. 2007. 'The Structure of Ferrihydrite, a Nanocrystalline Material', *Science*, 316: 1726-29.
Morgan, J. J. 2000. 'Manganese in natural waters and earth's crust: its availability to organisms', *Met Ions Biol Syst*, 37: 1-34.
Mossialos, Dimitris, Urs Ochsner, Christine Baysse, Patrice Chablain, Jean-Paul Pirnay, Nico Koedam, Herbert Budzikiewicz, Diana Uría Fernández, Mathias Schäfer, and Jacques Ravel. 2002. 'Identification of new, conserved, non-ribosomal peptide synthetases from fluorescent pseudomonads involved in the biosynthesis of the siderophore pyoverdine', *Molecular microbiology*, 45: 1673-85.
Müller, G, and KENNETH N Raymond. 1984. 'Specificity and mechanism of ferrioxamine-mediated iron transport in Streptomyces pilosus', *Journal of bacteriology*, 160: 304-12.
Neubauer, U., G. Furrer, and R. Schulin. 2002. 'Heavy metal sorption on soil minerals affected by the siderophore desferrioxamine B: the role of Fe(III) (hydr)oxides and dissolved Fe(III)', *European Journal of Soil Science*, 53: 45-55.
Neubauer, Uta, Bernd Nowack, Gerhard Furrer, and Rainer Schulin. 2000. 'Heavy metal sorption on clay minerals affected by the siderophore desferrioxamine B', *Environmental Science & Technology*, 34: 2749-55.
Ngwack, Bernd, and Laura Sigg. 1997. 'Dissolution of Fe(III) (hydr) oxides by metal-EDTA complexes', *Geochimica et Cosmochimica Acta*, 61: 951-63.
Nicolafrancesco, Chiara, Francesco Porcaro, Igor Pis, Silvia Nappini, Laura Simonelli, Carlo Marini, Emanuela Frangipani, Daniela Visaggio, Paolo Visca, Settimio Mobilio, Carlo Meneghini, Ilaria Fratoddi, Giovanna Iucci, and Chiara Battocchio. 2019. 'Gallium- and Iron-Pyoverdine Coordination Compounds Investigated by X-ray Photoelectron Spectroscopy and X-ray Absorption Spectroscopy', *Inorganic Chemistry*, 58: 4935-44.
Peña, Jasquelin, Owen W. Duckworth, John R. Bargar, and Garrison Sposito. 2007. 'Dissolution of hausmannite (Mn3O4) in the presence of the trihydroxamate siderophore desferrioxamine B', *Geochimica et Cosmochimica Acta*, 71: 5661-71.
Piccolo, Alessandro. 2001. 'The supramolecular structure of humic substances', *Soil science*, 166: 810-32.

Post, Jeffrey E. 1999. 'Manganese oxide minerals: Crystal structures and economic and environmental significance', *Proceedings of the National Academy of Sciences*, 96: 3447-54.
Powell, P. E., G. R. Cline, C. P. P. Reid, and P. J. Szaniszlo. 1980. 'Occurrence of hydroxamate siderophore iron chelators in soils', *Nature*, 287: 833-34.
Rai, V., N. Fisher, O. W. Duckworth, and O. Baars. 2020a. 'Extraction and Detection of Structurally Diverse Siderophores in Soil', *Front Microbiol*, 11: 581508.
Rai, Vineeta, Nathaniel Fisher, Owen W. Duckworth, and Oliver Baars. 2020b. 'Extraction and Detection of Structurally Diverse Siderophores in Soil', *Frontiers in Microbiology*, Volume 11 - 2020.
Raymond, Kenneth N., and Emily A. Dertz. 2004. 'Biochemical and Physical Properties of Siderophores.' in, *Iron Transport in Bacteria*.
Reichard, PU, Ruben Kretzschmar, and Stephan M Kraemer. 2007. 'Dissolution mechanisms of goethite in the presence of siderophores and organic acids', *Geochimica et Cosmochimica Acta*, 71: 5635-50.
Remucal, Christina K., and Matthew Ginder-Vogel. 2014. 'A critical review of the reactivity of manganese oxides with organic contaminants', *Environmental Science: Processes & Impacts*, 16: 1247-66.
Renshaw, Joanna C., Geoff D. Robson, Anthony P. J. Trinci, Marilyn G. Wiebe, Francis R. Livens, David Collison, and Robin J. Taylor. 2002. 'Fungal siderophores: structures, functions and applications', *Mycological Research*, 106: 1123-42.
Robin, A., G. Vansuyt, P. Hinsinger, J. M. Meyer, J. F. Briat, and P. Lemanceau. 2008. 'Chapter 4 Iron Dynamics in the Rhizosphere: Consequences for Plant Health and Nutrition.' in, *Advances in Agronomy* (Academic Press).
Robinson, N. J., C. M. Procter, E. L. Connolly, and M. L. Guerinot. 1999. 'A ferric-chelate reductase for iron uptake from soils', *Nature*, 397: 694-7.
Robson, A. D. 1988. 'Manganese in Soils and Plants — An Overview.' in Robin D. Graham, Robert J. Hannam and Nicholas C. Uren (eds.), *Manganese in Soils and Plants: Proceedings of the International Symposium on 'Manganese in Soils and Plants' held at the Waite Agricultural Research Institute, The University of Adelaide, Glen Osmond, South Australia, August 22–26, 1988 as an Australian Bicentennial Event* (Springer Netherlands: Dordrecht).
Römheld, V. 1991. 'The role of phytosiderophores in acquisition of iron and other micronutrients in graminaceous species: an ecological approach', *Plant and Soil*, 130: 127-34.
Römheld, V., and H. Marschner. 1986. 'Evidence for a specific uptake system for iron phytosiderophores in roots of grasses', *Plant Physiol*, 80: 175-80.
Rosenberg, Dana R, and Patricia A Maurice. 2003. 'Siderophore adsorption to and dissolution of kaolinite at pH 3 to 7 and 22° C', *Geochimica et Cosmochimica Acta*, 67: 223-29.
Saad, Emily M., Jingying Sun, Shuo Chen, Olaf J. Borkiewicz, Mengqiang Zhu, Owen W. Duckworth, and Yuanzhi Tang. 2017. 'Siderophore and Organic Acid Promoted Dissolution and Transformation of Cr(III)-Fe(III)-(oxy)hydroxides', *Environmental Science & Technology*, 51: 3223-32.
Saal, Lauren B., and Owen W. Duckworth. 2010. 'Synergistic Dissolution of Manganese Oxides as Promoted by Siderophores and Small Organic Acids', *Soil Science Society of America Journal*, 74: 2021-31.

Schacht, Lily, and Matthew Ginder-Vogel. 2018. 'Arsenite Depletion by Manganese Oxides: A Case Study on the Limitations of Observed First Order Rate Constants', *Soil Systems*, 2: 39.
Schenkeveld, W. D. C., Y. Schindlegger, E. Oburger, M. Puschenreiter, S. Hann, and S. M. Kraemer. 2014. 'Geochemical Processes Constraining Iron Uptake in Strategy II Fe Acquisition', *Environmental Science & Technology*, 48: 12662-70.
Schwertmann, Udo; Taylor, R.M. . 1989. *Iron Oxides.* (Soil Science Society of America).
Schwyn, B., and J. B. Neilands. 1987. 'Universal chemical assay for the detection and determination of siderophores', *Anal Biochem*, 160: 47-56.
Siebner-Freibach, H., Y. Hadar, and Y. Chen. 2004. 'Interaction of Iron Chelating Agents with Clay Minerals', *Soil Science Society of America Journal*, 68: 470-80.
Siebner-Freibach, Hagar, Shmuel Yariv, Yitzhak Lapides, Yitzhak Hadar, and Yona Chen. 2005. 'Thermo-FTIR Spectroscopic Study of the Siderophore Ferrioxamine B: Spectral Analysis and Stereochemical Implications of Iron Chelation, pH, and Temperature', *Journal of Agricultural and Food Chemistry*, 53: 3434-43.
Simanova, Anna A. . 2011. 'Molecular Perspectives on Goethite Dissolution in the Presence of Oxalate and Desferrioxamine-B', Doctoral Thesis Umea University.
Simanova, Anna A., John S. Loring, and Per Persson. 2011. 'Formation of Ternary Metal-Oxalate Surface Complexes on α-FeOOH Particles', *The Journal of Physical Chemistry C*, 115: 21191-98.
Simanova, Anna A., Per Persson, and John S. Loring. 2010. 'Evidence for ligand hydrolysis and Fe(III) reduction in the dissolution of goethite by desferrioxamine-B', *Geochimica et Cosmochimica Acta*, 74: 6706-20.
Sparks, Donald L. 2003a. '2 - Inorganic Soil Components.' in Donald L. Sparks (ed.), *Environmental Soil Chemistry (Second Edition)* (Academic Press: Burlington).
———. 2003b. '5 - Sorption Phenomena on Soils.' in Donald L. Sparks (ed.), *Environmental Soil Chemistry (Second Edition)* (Academic Press: Burlington).
Sposito, Garrison. 2008. *The chemistry of soils* (Oxford university press).
Stevenson, Frank J. 1994. *Humus chemistry: genesis, composition, reactions* (John Wiley & Sons).
Strawn, Daniel G. 2021. 'Sorption Mechanisms of Chemicals in Soils', *Soil Systems*, 5: 13.
Stumm, Werner. 1987. *Aquatic surface chemistry: Chemical processes at the particle-water interface* (John Wiley & Sons).
Sutton, Rebecca, and Garrison Sposito. 2005. 'Molecular Structure in Soil Humic Substances: The New View', *Environmental Science & Technology*, 39: 9009-15.
Suzuki, Motofumi, Kendi Claudio Morikawa, Hiromi NAKANISHI, Michiko TAKAHASHI, Masahiko SAIGUSA, Satoshi MORI, and Naoko K. NISHIZAWA. 2008. 'Transgenic rice lines that include barley genes have increased tolerance to low iron availability in a calcareous paddy soil', *Soil Science & Plant Nutrition*, 54: 77-85.
Suzuki, Motofumi, Atsumi Urabe, Sayaka Sasaki, Ryo Tsugawa, Satoshi Nishio, Haruka Mukaiyama, Yoshiko Murata, Hiroshi Masuda, May Sann Aung, Akane Mera, Masaki Takeuchi, Keijo Fukushima, Michika Kanaki, Kaori Kobayashi, Yuichi Chiba, Binod Babu Shrestha, Hiromi Nakanishi, Takehiro Watanabe, Atsushi Nakayama, Hiromichi Fujino, Takanori Kobayashi, Keiji Tanino, Naoko K. Nishizawa, and Kosuke Namba. 2021. 'Development of a mugineic acid family phytosiderophore analog as an iron fertilizer', *Nature Communications*, 12: 1558.

Takagi, Sei-ichi, Shigeru Kamei, and Ming-Ho Yu. 1988. 'Efficiency of iron extraction from soil by mugineic acid family phytosiderophores', *Journal of Plant Nutrition*, 11: 643-51.
Thieken, Andrea, and Günther Winkelmann. 1992. 'Rhizoferrin: a complexone type siderophore of the mocorales and entomophthorales (Zygomycetes)', *FEMS microbiology letters*, 94: 37-41.
Vraspir, J. M., and A. Butler. 2009. 'Chemistry of marine ligands and siderophores', *Ann Rev Mar Sci*, 1: 43-63.
Walter, A., A. Pich, G. Scholz, H. Marschner, and V. Römheld. 1995. 'Diurnal Variations in Release of Phytosiderophores and in Concentrations of Phytosiderophores and Nicotianamine in Roots and Shoots of Barley', *Journal of Plant Physiology*, 147: 191-96.
Wandruszka, R von, RR Engebreatson, and LM Yates, III. 1999. 'Humic acid pseudomicelles in dilute aqueous solution: fluorescence and surface tension measurements'.
Wang, T., N. Wang, Q. Lu, S. Lang, K. Wang, L. Niu, M. Suzuki, and Y. Zuo. 2023. 'The active Fe chelator proline-2'-deoxymugineic acid enhances peanut yield by improving soil Fe availability and plant Fe status', *Plant Cell Environ*, 46: 239-50.
Wehrli, Bernhard, Erich Wieland, and Gerhard Furrer. 1990. 'Chemical mechanisms in the dissolution kinetics of minerals; the aspect of active sites: Dedicated to Werner Stumm for his 65th birthday', *Aquatic Sciences*, 52: 3-31.
Williams, D. F. 1991. "The Biological Chemistry of the Elements." In.
Yoshida, Takahiro, Ken-ichiro Hayashi, and Hiroshi Ohmoto. 2002. 'Dissolution of iron hydroxides by marine bacterial siderophore', *Chemical Geology*, 184: 1-9.

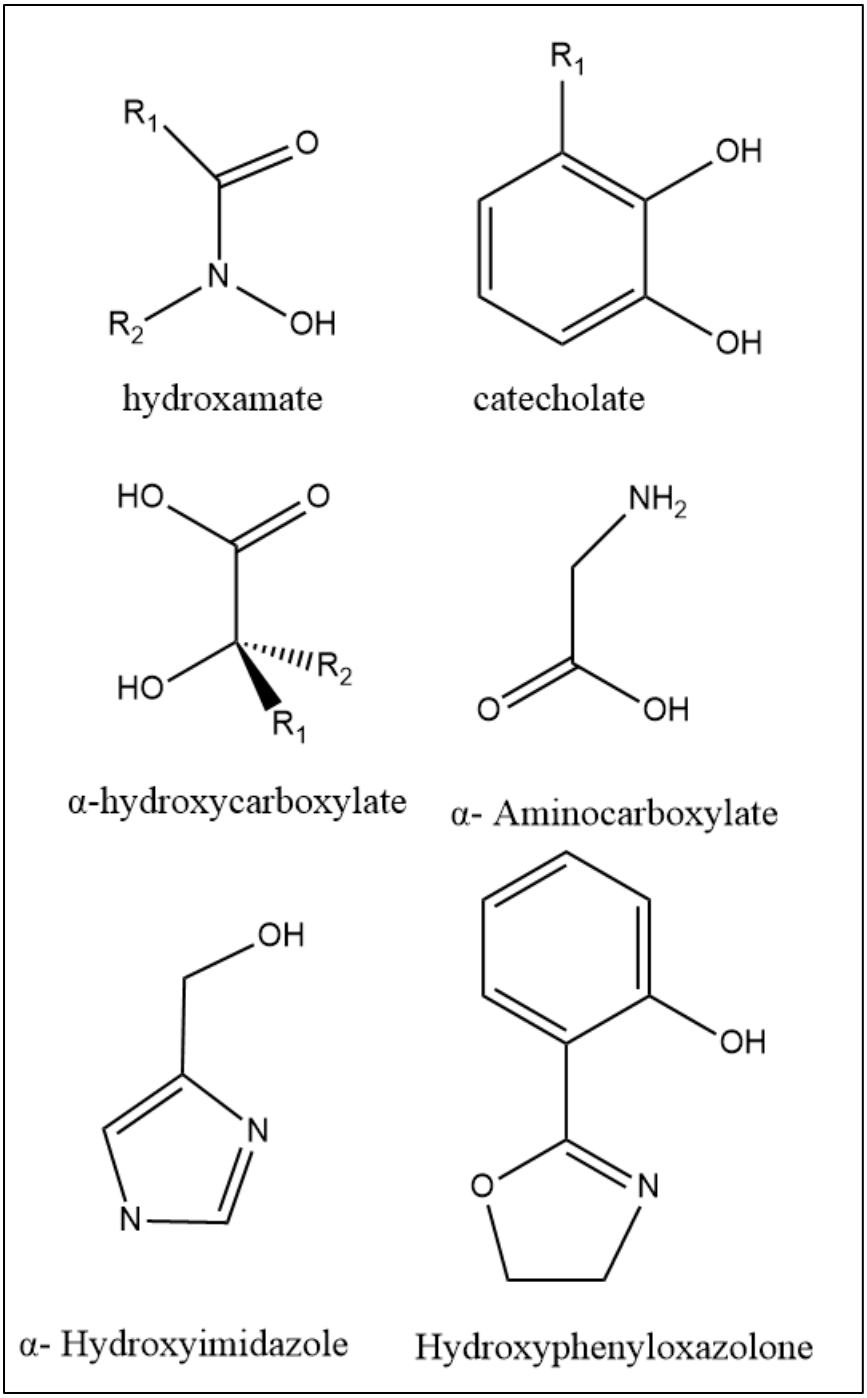

Figure 1.1. Structures of hydroxamate, catecholate, α-hydroxycarboxylate, α-aminocarboxylate, α-hydroxyimidazole and hyroxyphenyloxazolone binding moieties.

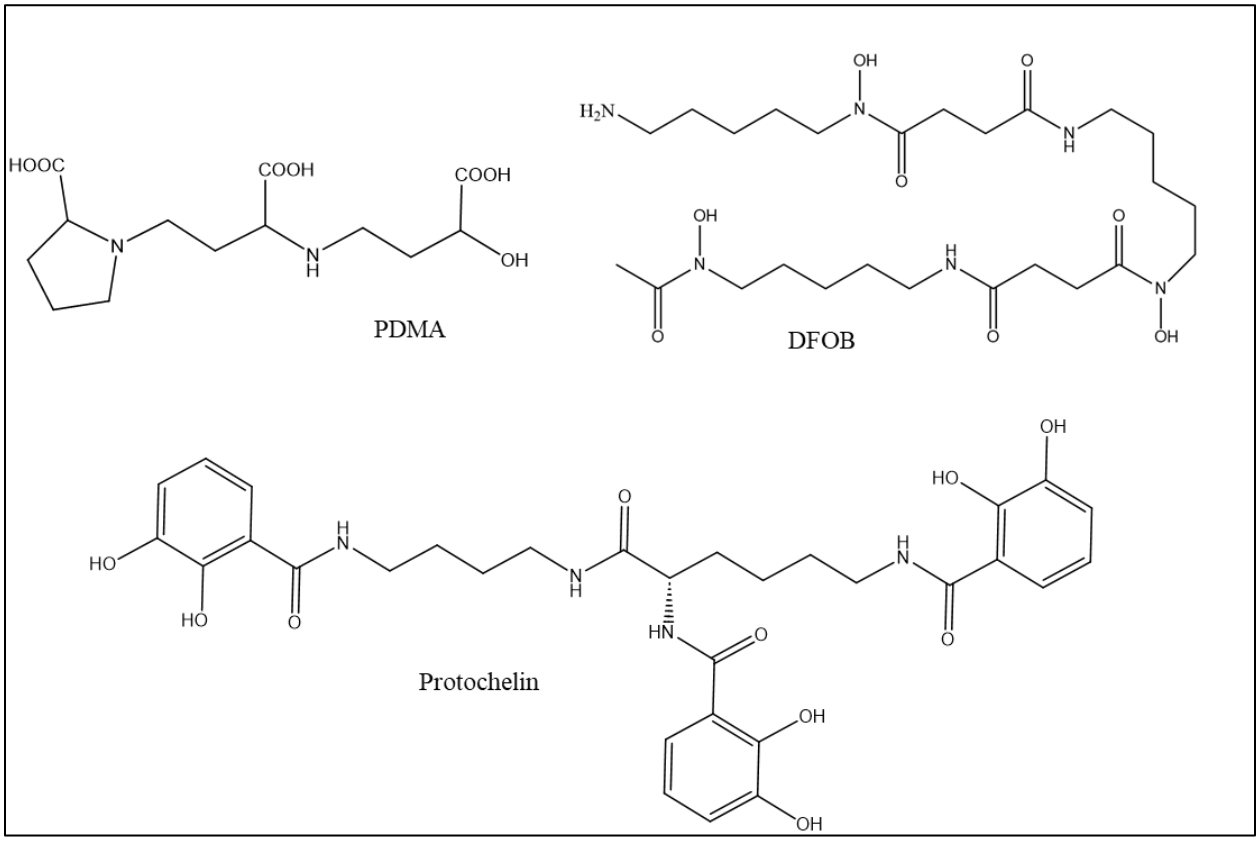

Figure 1.2. Structures of the siderophores proline-2᾽-deoxymugineic acid (PMDA), desferrioxamine-B (DFOB), and protochelin

CHAPTER 2: Stability of metal ion complexes with the synthetic phytosiderophore proline-2′-deoxymugineic acid

Published: Evers A, Kohn J, Baars O, Harrington JM, Namba K, Duckworth OW. Stability of metal ion complexes with the synthetic phytosiderophore proline-2'-deoxymugineic acid. Biometals. 2024 Dec;37(6):1599-1607. doi: 10.1007/s10534-024-00629-7. Epub 2024 Aug 28. PMID: 39198338.

Introduction

Essential trace metals, including Mn, Fe, Co, Ni, Cu, and Zn, are required by plants, microbes, and humans, largely for use in metalloenzymes required for proper metabolic function (Alloway 2008, Alloway 2013). In humans, inadequate dietary micronutrient concentrations of crops grown in deficient soils can contribute to “hidden hunger”, which occurs when nutritional requirements are not properly met despite sufficient calorie consumption (Muthayya, Rah et al. 2013). Currently, about 30% of plants growing on cultivated soils worldwide are deficient in iron and 50% of world cereal crops (wheat, maize, barley, and rice) are deficient in zinc, leading to significant decreases in agricultural yield and nutritional value, while also increasing crop susceptibility to chlorosis and other developmental defects (Alloway 2013, Das 2014). Nutrient deficiencies can stem from several issues, including the insolubility of trace metal nutrients preventing their dissolution into the bioavailable pool. (Khush, Lee et al. 2012).

To facilitate the uptake of poorly bioavailable essential nutrients, graminaceous plants, as well as many bacteria and fungi, have developed the ability to exude low molecular weight organic ligands (metallophores) when experiencing trace metal deficiency stress (Schenkeveld, Schindlegger et al. 2014, Kraemer, Duckworth et al. 2015). The most widely recognized class of metallophores is siderophores (from the Greek: “iron carriers”), a structurally broad group of

molecules that have large binding affinities for Fe(III), but have also been shown to bind with and impact the biogeochemical cycling of other elements (Treeby, Marschner et al. 1989, Kraemer, Duckworth et al. 2015, Suzuki, Urabe et al. 2021). Once exuded, siderophores can mobilize metal cations from poorlysolubility soil minerals into the bioavailable pool by forming high affinity soluble complexes (Treeby, Marschner et al. 1989, Dhungana and Crumbliss 2005).

2'- deoxymugineic acid (DMA) is a phytosiderophore, a subclass of α-hydroxycarboxylate siderophores secreted by plants (Figure 1), that is exuded by rice plants during metal deficiency stress and has been shown to effectively bind with many trace metal nutrients (Sugiura, Tanaka et al. 1981, Dell'mour, Koellensperger et al. 2010). Because of its binding affinities for trace metals, synthetic DMA has been tested as a soil amendment to increase nutrient availability across a wide range of agricultural settings, particularly in calcareoussoils like those that comprise approximately one third of Earth's total land area (Kraemer, Crowley et al. 2006). However, DMA contains a highly strained 4-membered azetidine ring that contributes to the relative instability of the molecule (Suzuki, Urabe et al. 2021). Recently, a more stable synthetic DMA analog, proline 2′-deoxymugineic acid (PDMA; Figure 1), was developed which shows a comparable binding affinity with Fe^{3+} (Suzuki, Urabe et al. 2021). By replacing the strained 4-membered azetidine ring in DMA with the 5-membered pyrrolidine ring in PDMA, the synthesis costs and susceptibility to microbial degradation were reduced (Suzuki, Urabe et al. 2021).

Preliminary laboratory experiments indicate that PDMA can mobilize Fe(III) with similar efficiency as DMA, but less is known about how PDMA interacts with other trace metal nutrients (Suzuki, Urabe et al. 2021). Direct observation and accurate measurements of siderophore dynamics in natural rhizosphere ecosystems are difficult to facilitate due to the

inaccessibility of high-resolution in situ techniques and the complexity of natural soil substrates (Northover, Mao et al. 2022). Consequently, laboratory experiments and geochemical models are commonly used to study trace metal acquisition and transport (Di Bonito, Lofts et al. 2018). However, these models require accurate thermodynamic parameters to reflect the behavior of siderophores in soil environments. The goals of this study are to: (1) use spectrophotometric titrations to quantify the stability constants of PDMA with Mn(II), Co(II), Ni(II), Cu(II), and Zn(II); and (2) to compare the values with known stability constants of other metal-siderophore complexes, which can provide insights into metal-phytosiderophore complex formation and fate in the environment. Our results are critical for further understanding the potential effectiveness of PDMA as a trace metal fertilizer and its impacts on trace metal biogeochemistry.

Materials and Methods

Materials. All solutions were prepared using ASTM Type 1 (>18.2 MΩ·cm) deionized water (DI). Unless otherwise noted, all chemicals used were of reagent grade from Fisher Scientific (Hampton, NH) or Sigma-Aldrich (St. Louis, MO). Proline-2′-deoxymugineic acid PDMA was provided as PDMA·2HCl by Aichi Steel Corporation (Japan) (Suzuki, Urabe et al. 2021).

Spectrophotometric titrations. Solutions containing 1.0 mM of metal ion (as the salts MnSO4 ·H2O, Co(NO3)2 ·6H2O, NiCl2 ·6H2O, CuCl2, or ZnSO4 ·7H2O) and 1.0 mM PDMA were prepared in a matching 0.1 M NaCl or NaNO3 background electrolyte in deionized water, depending on which electrolyte had a lower formation constant with the metal ion. These metal-PDMA solutions were shielded from light with aluminum foil and titrated within a few hours of preparation to limit potential degradation of the siderophore. Solutions were N2 purged for at least 1 hour prior to use in the titrations.

Titrations were conducted using an autotitrator (888 Titrando, Metrohm, Switzerland) equipped with a combination glass electrode and a UV-visible miniature spectrophotometer (FLAME-T-UV-VIS-ES, OceanOptics) with a equipped with a dip probe (1 cm pathlength) and a deuterium-halogen light source (DH-mini UV-Vis-NIR, OceanOptics, FL, USA). The autotitrator electrode was calibrated by measuring electromotive force (emf; mV) as a function of known proton concentrations using commercially standardized 0.1 M HCl and NaOH.

Solutions were pH adjusted to pH = 2.6 with 0.1 M HCl and 50 mL aliquots of the metal ion-PDMA solution were transferred into an aluminum foil covered reaction flask and titrated with 0.2 mL doses of commercially standardized 0.1 M NaOH every minute under constant stirring. During the titration, stable emf readings were collected after each dose of titrant. After each stable reading, UV-visible spectra were immediately collected between 200–800 nm. Titrations were terminated after the pH of solution reached 11.5 (Doydora, Baars et al. 2022). This process was performed in duplicate for each metal-PDMA solution.

Determination of Stability Constants. The UV-visible absorbance (200–800 nm) and pH data from each titration was fit in the chemical equilibria modeling program KEV (Meshkov and Gamov 2019) to determine stability constants of MIIHPDMA- complexes with individual trace metals. For Mn(II), which did not have a measurable shift in spectrophotometric data, only pH data was used in stability constant determination. It has been previously shown that divalent metal ions form pentadentate complexes with DMA at alkaline pH (Sugiura, Tanaka et al. 1981), and we thus assume our final species to be $M^{II}HPDMA^{-}$. By calculating the amount of protons consumed in excess of those required to change the pH of water (3 ± 0.5 for all titrations), the species at the beginning of the titration was inferred to be $M^{II}H_4PDMA^{2+}$. The molar absorptivity constants for $M^{II}H_4PDMA^{2+}$ and $M^{II}HPDMA^{-}$ were thus determined from the first and last

spectra of each titration. KEV was further parametrized with all species present in the titration, including metal hydrolysis species and metal ligand species, by using known thermodynamic data (Schecher 2001).

Results and Discussion

Binding of metal ions by phytosiderophores. The pK_a values for different functional groups in PDMA (Figure 1) are: $pK_{a1} = 2.01$, $pK_{a2} = 2.47$, $pK_{a3} = 3.12$, $pK_{a4} = 7.63$, and $pK_{a5} = 9.23$ (Suzuki, Urabe et al. 2021). It is worth noting that PDMA has very basic pKa6 (i.e., $pK_a > 14$) associated with the terminal α-hydroxyl group. For DMA, the dissociation constant for the α-hydroxyl group has been estimated to be $10^{-17.1}$ by using the Taft equation (Perrin, Dempsey et al. 1981); based on the similarity of the molecules, we assume the pKa_6 to be comparable for PDMA.

Siderophore complexes with metal ions have been shown to change with the pH-dependent protonation state of the siderophore (Kim, Duckworth et al. 2009). We modelled metal-PDMA to undergo deprotonation reactions as the pH increased during the titration from an initially acidic solution (pH = 2.6):

$$M^{II}H_4PDMA^{2+} \leftrightarrow M^{II}HPDMA^{-} + 3H^{+} \qquad (1)$$

where successive deprotonation reactions free up electron pairs and create a more negative charge in PDMA to produce stronger PDMA metal interactions.

The terminal α-hydroxyl group remains protonated and is not thought to bind with divalent metal ions at both environmental pH values and over the range of our titrations, resulting in a pentadentate complex at the final pH of our experiments (Murakami, Kunio et al. 1989). This has resulted in the reporting of stability constants using a once protonated phytosiderophore as the reference state such that:

$$M(II) + L^{3-} \rightarrow M(II)L^{1} \qquad K_{ML} \; (2)$$

where L = $HDMA^{3-}$ or the equivalent protonation state of another physiderophore. By this formalism, $K_{ML} = \beta_{110}$, where beta is the cumulative formation constant such that β_{MLH} represent the reaction from the formation of individual components. However, it is worth noting that strongly Lewis acidic trivalent cations are thought to form hexadendate complexes (e.g., $Fe(III)DMA^{-1}$) where the final α-hydroxyl group deprotonates and bonds to the ligand (Murakami, Kunio et al. 1989), resulting in a formation formation constant experession:

$$Fe(III) + LH_{1-}^{4-} \rightarrow Fe(III)LH_{1-}^{-} \qquad K_{MLH_{-1}} \quad (3)$$

where LH_{1-} = DMA^{4-} or the equivalent protonation state of another phytosiderophore. By this formalism, the formation constant is related to cumulative formation constant through division by the acidity constant of the terminal binding moiety $K_{MLH_{1-}} = (\beta_{111-})/ K_{a6.}$

These formalisms have led to some inconsistences in the reporting of stability constants. For example, the Fe(III)DMA complex stability constant has been reported as 15.7 and 31.35, dependent on whether $HDMA^{3-}$ ($\log\beta_{111-}$) or DMA^{4-} ($\log K_{MLH_{1-}}$) was used as the reference state (Shenker, Fan et al. 2001, Dell'mour, Koellensperger et al. 2010). It is worth noting that, when the stability constant is corrected for the deprotonation of the α-hydroxyl group, the $K_{MLH_{1-}}$ shows a difference between Fe(III) and divalent cations that more is typical of other siderophores and ligands with hard base binding moieties (Supplementary Information Table S1).

Spectrophotometric titrations of metal-PDMA solutions. The UV-visible spectra of metal-PDMA complexes during titrations are shown in Figure 2. For PDMA complexes with Co(II), Zn(II), Cu(II), and Ni(II), spectral shifts were observed as the solution changed from low to high pH, reflecting changes in light absorption among the intermediate species in equation 1. For example, solutions with Co(II) and PDMA, a shift of A_{max} was observed from 262 to 272 nm, with a 0.2 unit

absorbance increase (Figure 2). In contrast, Mn(II) does not show a spectral shift in the UV-visible range (Figure S1).

Determination of Stability Constants. Using the spectrophotometric titration data, we calculated the stability constants for $M^{II}HPDMA^-$ ($LogK_{ML}$), with Mn(II), Ni(II), Cu(II), Co(II), and Zn(II), in KEV (Table 1). The resulting stability constants are similar to those previously obtained stability constants for other phytosiderophores, such as mugineic acid (MA), 2'-deoxymugineic acid (DMA), 3-hydroxymugineic acid (HMA) and 3-epi-hydroxymugineic acid (epi-HMA) (supplementary material Table S1). The $Fe(III)PDMA^-$ stability constant was previously determined by Suzuki et al. (2021), and adjusted to $logK_{MLH-1} = 34.2$, considering the deprotonation of the α-hydroxyl group.

Lewis acidity and binding. The affnity of ligands for metal ions has previously been correlated to several parameters, including ionic potential (z/r), and hydrolysis constant (KOH) of cations (Hancock and Martell 1989, Hernlem, Vane et al. 1999). These correlations not only provide insights into the interactions between binding ligands and metal ions, they can facilitate the estimation of affinity constants for metals for which there is no experimental data (Duckworth, Akafia et al. 2014).

Because ligand complexation is fundamentally a Lewis acid-base interaction, some aspects of siderophore stability constants can be attributed to the hard-soft acid/base theory. Figure 3a presents a linear correlation of $logK_{PDMA}$ with the ionic potential of the corresponding metal ion ($R^2 = 0.87$). This phenomenon can be rationalized by noting that the Pearson's hardness of the metal ion is related to the strength of interaction with the Lewis bases in the siderophore binding moieties. Similarly, Figure 3b presents a correlation of $logK_{PDMA}$ versus the logarithm of the hydrolysis constant ($logK_{OH}$) ($R^2 = 0.96$). Because siderophores feature negatively charged

oxygen donor groups (in the case of PDMA, carboxylate groups and a hydroxyl group), it is assumed that the ability of the metal ion to attract the binding groups on the ligand trends with the affinity of the metal ion for hydroxide ions (Hernlem, Vane et al. 1999).

Despite its utility in explaining fundamental chemistry, Hernlem et al. (1999) noted that using z/r as a predictor of unknown ligand-metal stability constants may be superfluous because the relationship with $\log K_{OH}$ yields a stronger correlation (Figure 3). The resulting equation, which may be used to estimate stability constants from tabulated hydrolysis constants, is:

$$\log K_{OH} = (0.32 \pm 0.02)\log K - (13.6 \pm 0.3) \quad (4)$$

where logK is the the K_{ML} or the K_{MLH-1} depending on the metal in question. Estimates of PDMA stability constants determined by equation 4 are presented in the supporting information (supplementary material Table S2).

Estimation of phytosiderophore stability. Unlike structurally diverse microbial siderophores, phytosiderophores are closely structurally related. As seen in the Figure 1, the main difference between phytosiderophores is the presence and position of hydroxyl groups not associated in metal binding. Synthetic PDMA has the added change of having a five membered ring instead of a four membered ring, making it more resistant to microbial degradation in the rhizosphere environment than natural phytosiderophores (Suzuki, Urabe et al. 2021). The homology of these ligands suggest commonalities in the binding affinities of these ligands.

To that end, we constructed log-log plots of the stability constants for PDMA that we determined against known literature stability constants for the other phytosiderophores, as well as the commonly used trishydroxamate siderophore DFOB. Regressions for all the siderophores with PDMA show strong linear trends, with $R^2 = 0.90–0.94$ (Table 2). Because PDMA is easier to obtain, more stable and more inexpensive than a lot of other phytosiderophores such as

mugineic acid (MA), 2'-deoxymugineic acid (DMA), and 3-epi-hydroxymugineic acid (epi-HMA), it could be used as an alternative to these siderophores, and as a predictor of metal stability constants with MA, DMA, and epi-HMA.

When regressing the stability constants for PDMA with those of the trishydroxamate DFOB, an $R^2 = 0.90$ was observed from the relationship:

$$\log K_{HDFOB} = (0.85 \pm 0.10)\log K - (1 \pm 1) \quad (5)$$

This correlation was previously discounted because of the aforementioned inconsistencies in reporting of the hexadentate Fe(III) binding constants (with phytosiderophore constants being orders of magnitude smaller than DFOB) and the structural differences between the ligands (viz. amine groups associated with complexation by PDMA). It is worth noting here that Al(III), another known hexadentate phytosiderophore complex, also falls onto the line created by this regression, with a $\log K_{MLH1-}$=23.9 for MA and $\log K_{ML}$=22.2 for DFOB (Yoshimura, Kohdr et al. 2011). Because DFOB has a large thermodynamic database of siderophore-metal ion interactions, using DFOB as a predictor for PMDA, and potentially other phytosiderophores, could allow for estimation of a large number of ions that may be used in models of siderophores in the environment.

Table S2 shows estimated binding affinities for PDMA as calculated by equations 2 and 3 (e.g., estimation from hydrolysis and DFOB binding constants). In general, estimated errors are greater for $\log K_{DFOB}$ estimated constants than from hydrolysis constants. In general, there is reasonable agreement (difference in logK values less than 2) for divalent cations as well as Al(III) and Ga(III). Greater discrepancies appear for large cations that have non-octahedral or pentadentate coordination (e.g., La(III) or Pb(II) and hard cations with high affinities (e.g., In(III), Co(III), and Mn(III)). Previous studies have noted that for hard ions, steric effects may have

significant impacts on the relative affinity for specific metal ions ions (Harrington, Bargar et al. 2012). This suggests that caution may be needed when estimating the binding constants of ligands that have differing coordination chemistries (e.g., steric contracts, moiety preorganization, or complex architectures), and that more $\log K_{MLH_{1-}}$ values for hexadentate trivalent metals are needed to further empirically confirm this relationship The values in Table S2 provide potential end member estimates for phytosiderophores with metal ions that lack values, as well as illustrate the limits of this approach, and may help to guide future measurements to improve our ability to estimate logK values.

Conclusions and Implications

This study determined the stability constants of synthetic mugineic acid derivative siderophore – PDMA – with the metals ions Mn(II), Co(II), Ni(II), Cu(II), and Zn(II) via potentiometric and spectrophotometric titrations. Spectrophotometric shifts were observed, acting as an indication that the ligand was deprotonating and binding with the metal complex as pH increased. The hydrolysis constant and the ionic potential of the metal ion may be used as predictors of stability constants with PDMA. Stability constants were also regressed against the stability constants of other mugineic acid type phytosiderophores, as well as the trishydroxamate microbial DFOB, showing that known constants for these siderophores could also act as predictors, with specific caveats and limitations related to different coordination chemistries with different metals. Being able to estimate the stability of PDMA with different micronutrients can help predict PDMA's possibility as a fertilizer, while estimates with several metal cations could predict the plausibility in contaminant remediation scenarios.

REFERENCES

Alloway, Brian J. 2008. 'Micronutrients and Crop Production: An Introduction.' in Brian J. Alloway (ed.), *Micronutrient Deficiencies in Global Crop Production* (Springer Netherlands: Dordrecht).

———. 2013. 'Bioavailability of Elements in Soil.' in Olle Selinus (ed.), *Essentials of Medical Geology: Revised Edition* (Springer Netherlands: Dordrecht).

Das, S. 2014. 'Role of Micronutrient in Rice Cultivation and Management Strategy in Organic Agriculture—A Reappraisal.', *Agricultural Sciences*, 5: 765-69.

Dell'mour, Madeleine, Gunda Koellensperger, Joselito P. Quirino, Paul R. Haddad, Christian Stanetty, Eva Oburger, Markus Puschenreiter, and Stephan Hann. 2010. 'Complexation of metals by phytosiderophores revealed by CE-ESI-MS and CE-ICP-MS', *ELECTROPHORESIS*, 31: 1201-07.

Dhungana, Suraj, and Alvin L. Crumbliss. 2005. 'Coordination Chemistry and Redox Processes in Siderophore-Mediated Iron Transport', *Geomicrobiology Journal*, 22: 87-98.

Di Bonito, Marcello, Sthephen Lofts, and Jan E. Groenenberg. 2018. 'Chapter 11 - Models of Geochemical Speciation: Structure and Applications.' in Benedetto De Vivo, Harvey E. Belkin and Annamaria Lima (eds.), *Environmental Geochemistry (Second Edition)* (Elsevier).

Doydora, S. A., O. Baars, J. M. Harrington, and O. W. Duckworth. 2022. 'Salicylate coordination in metal-protochelin complexes', *BioMetals*, 35: 87-98.

Duckworth, Owen W., Martin M. Akafia, Megan Y. Andrews, and John R. Bargar. 2014. 'Siderophore-promoted dissolution of chromium from hydroxide minerals', *Environmental Science: Processes & Impacts*, 16: 1348-59.

Hancock, Robert D., and Arthur E. Martell. 1989. 'Ligand design for selective complexation of metal ions in aqueous solution', *Chemical Reviews*, 89: 1875-914.

Harrington, James M., John R. Bargar, Andrzej A. Jarzecki, James G. Roberts, Leslie A. Sombers, and Owen W. Duckworth. 2012. 'Trace metal complexation by the triscatecholate siderophore protochelin: structure and stability', *BioMetals*, 25: 393-412.

Hernlem, Bradley J., Leland M. Vane, and Gregory D. Sayles. 1999. 'The application of siderophores for metal recovery and waste remediation: examination of correlations for prediction of metal affinities', *Water Research*, 33: 951-60.

Khush, Gurdev S., Sichul Lee, Jung-Il Cho, and Jong-Seong Jeon. 2012. 'Biofortification of crops for reducing malnutrition', *Plant Biotechnology Reports*, 6: 195-202.

Kim, Dongwook, Owen W. Duckworth, and Timothy J. Strathmann. 2009. 'Hydroxamate siderophore-promoted reactions between iron(II) and nitroaromatic groundwater contaminants', *Geochimica et Cosmochimica Acta*, 73: 1297-311.

Kraemer, S. M., D. E. Crowley, and R. Kretzschmar. 2006. 'Geochemical Aspects of Phytosiderophore-Promoted Iron Acquisition by Plants.' in, *Advances in Agronomy* (Academic Press).

Kraemer, Stephan M., Owen W. Duckworth, James M. Harrington, and Walter D. C. Schenkeveld. 2015. 'Metallophores and Trace Metal Biogeochemistry', *Aquatic Geochemistry*, 21: 159-95.

Meshkov, A. N., and G. A. Gamov. 2019. 'KEV: A free software for calculating the equilibrium composition and determining the equilibrium constants using UV–Vis and potentiometric data', *Talanta*, 198: 200-05.

Murakami, Takasu, Ise Kunio, Hayakawa Minato, Kamei Shigeru, and Takagi Sei-ichi. 1989. 'Stabilities of Metal Complexes of Mugineic Acids and Their Specific Affinities for Iron(III)', *Chemistry Letters*, 18: 2137-40.

Muthayya, S., J. H. Rah, J. D. Sugimoto, F. F. Roos, K. Kraemer, and R. E. Black. 2013. 'The global hidden hunger indices and maps: an advocacy tool for action', *PLoS One*, 8: e67860.

Northover, George H. R., Yiru Mao, Salvador Blasco, Ramon Vilar, Enrique Garcia-España, Claudia Rocco, Md Hanif, and Dominik J. Weiss. 2022. 'Synergistic use of siderophores and weak organic ligands during zinc transport in the rhizosphere controlled by pH and ion strength gradients', *Scientific Reports*, 12: 6774.

Perrin, DD. , B Dempsey, and EP Serjeant. 1981. *pKa Prediction for OrganicAcids and Bases* (Chapman & Hall: London).

Schecher, WD. 2001. 'Thermochemical data used in MINEQL+ version 4.5 with comparisons to versions 4.07 and earlier', *Environmental Research Software*.

Schenkeveld, W. D. C., Y. Schindlegger, E. Oburger, M. Puschenreiter, S. Hann, and S. M. Kraemer. 2014. 'Geochemical Processes Constraining Iron Uptake in Strategy II Fe Acquisition', *Environmental Science & Technology*, 48: 12662-70.

Shenker, M., T. W. Fan, and D. E. Crowley. 2001. 'Phytosiderophores influence on cadmium mobilization and uptake by wheat and barley plants', *J Environ Qual*, 30: 2091-8.

Sugiura, Yukio, Hisashi Tanaka, Yoshiki Mino, Toshimasa Ishida, Nagayo Ota, Masatoshi Inoue, Kyosuke Nomoto, Himeko Yoshioka, and Tsunematsu Takemoto. 1981. 'Structure, properties, and transport mechanism of iron(III) complex of mugineic acid, a possible phytosiderophore', *Journal of the American Chemical Society*, 103: 6979-82.

Suzuki, Motofumi, Atsumi Urabe, Sayaka Sasaki, Ryo Tsugawa, Satoshi Nishio, Haruka Mukaiyama, Yoshiko Murata, Hiroshi Masuda, May Sann Aung, Akane Mera, Masaki Takeuchi, Keijo Fukushima, Michika Kanaki, Kaori Kobayashi, Yuichi Chiba, Binod Babu Shrestha, Hiromi Nakanishi, Takehiro Watanabe, Atsushi Nakayama, Hiromichi Fujino, Takanori Kobayashi, Keiji Tanino, Naoko K. Nishizawa, and Kosuke Namba. 2021. 'Development of a mugineic acid family phytosiderophore analog as an iron fertilizer', *Nature Communications*, 12: 1558.

Treeby, M., H. Marschner, and V. Römheld. 1989. 'Mobilization of iron and other micronutrient cations from a calcareous soil by plant-borne, microbial, and synthetic metal chelators', *Plant and Soil*, 114: 217-26.

Yoshimura, Etsuro, Hicham Kohdr, Satoshi Mori, and Robert C. Hider. 2011. 'The binding of aluminum to mugineic acid and related compounds as studied by potentiometric titration', *BioMetals*, 24: 723-27.

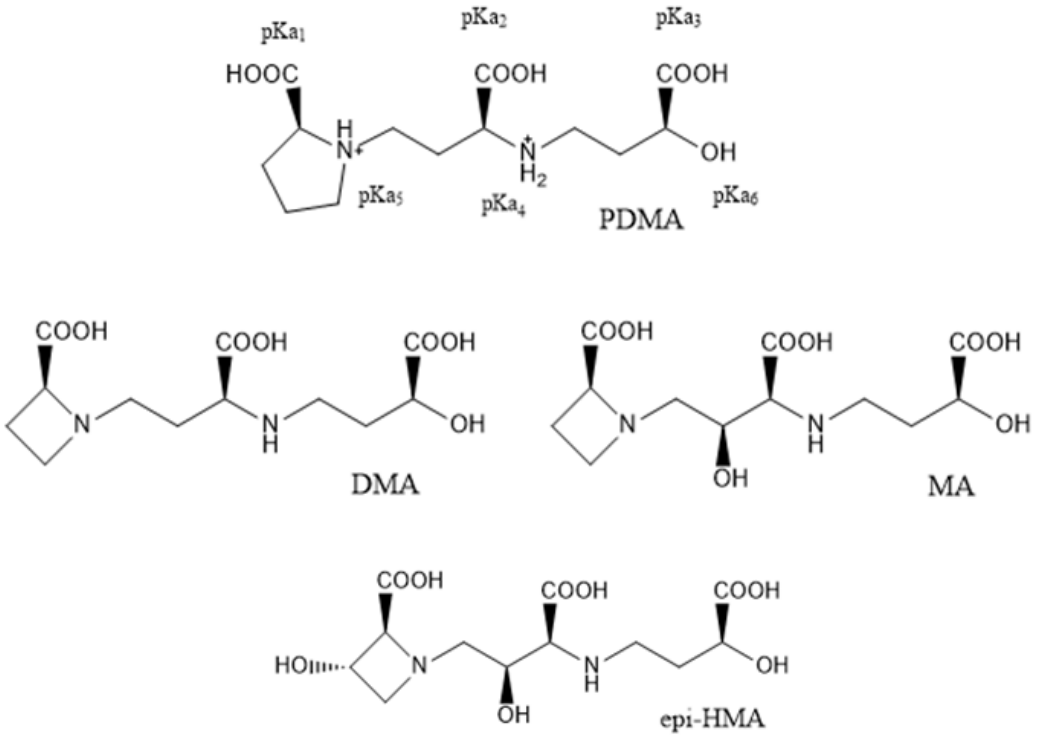

Figure 2.1 Structures of the phytosiderophores proline-2′-deoxymugineic acid (PDMA), 2′-deoxymugineic acid (DMA), mugineic acid (MA), and 3-Epi-3-hydroxymugineic (epi-HMA).

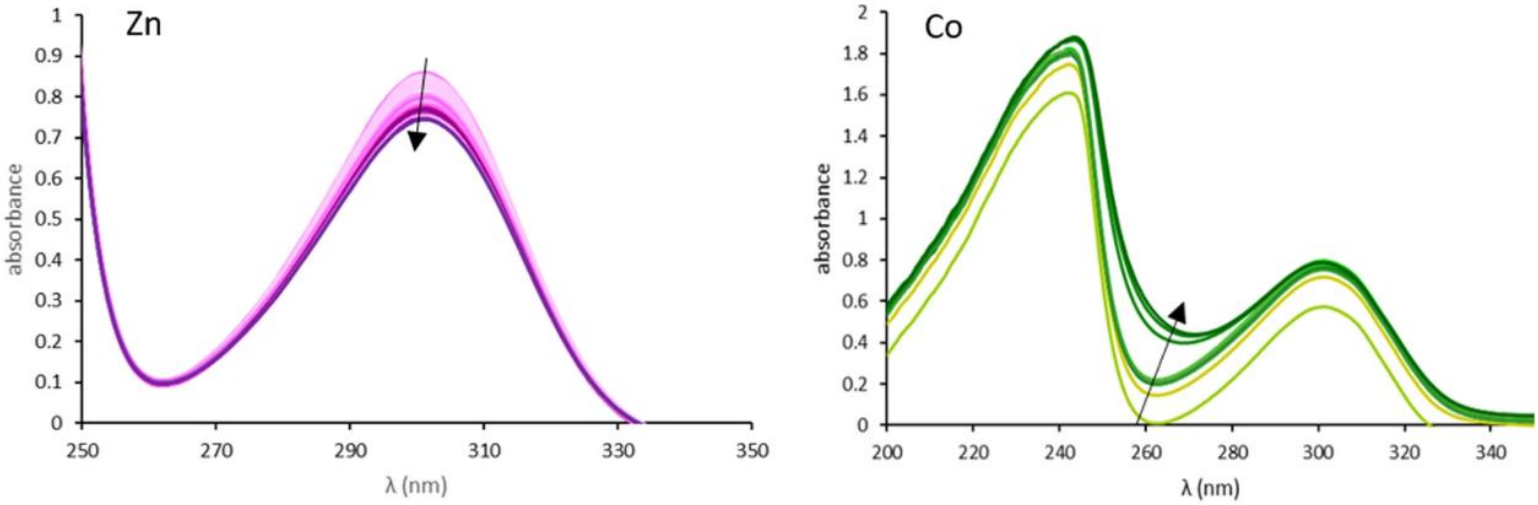

Figure 2.2. Spectrophotometric titration for zinc and cobalt titration of M^{II}- proline-2′-deoxymugineic acid (PDMA) systems. [M^{II}-PDMA] = 1.0×10^{-3} M, I = 0.10 M. Arrows indicate the direction of spectral shifts. Other elements along with potentiometric titrations in Supplementary Information Figure S1.

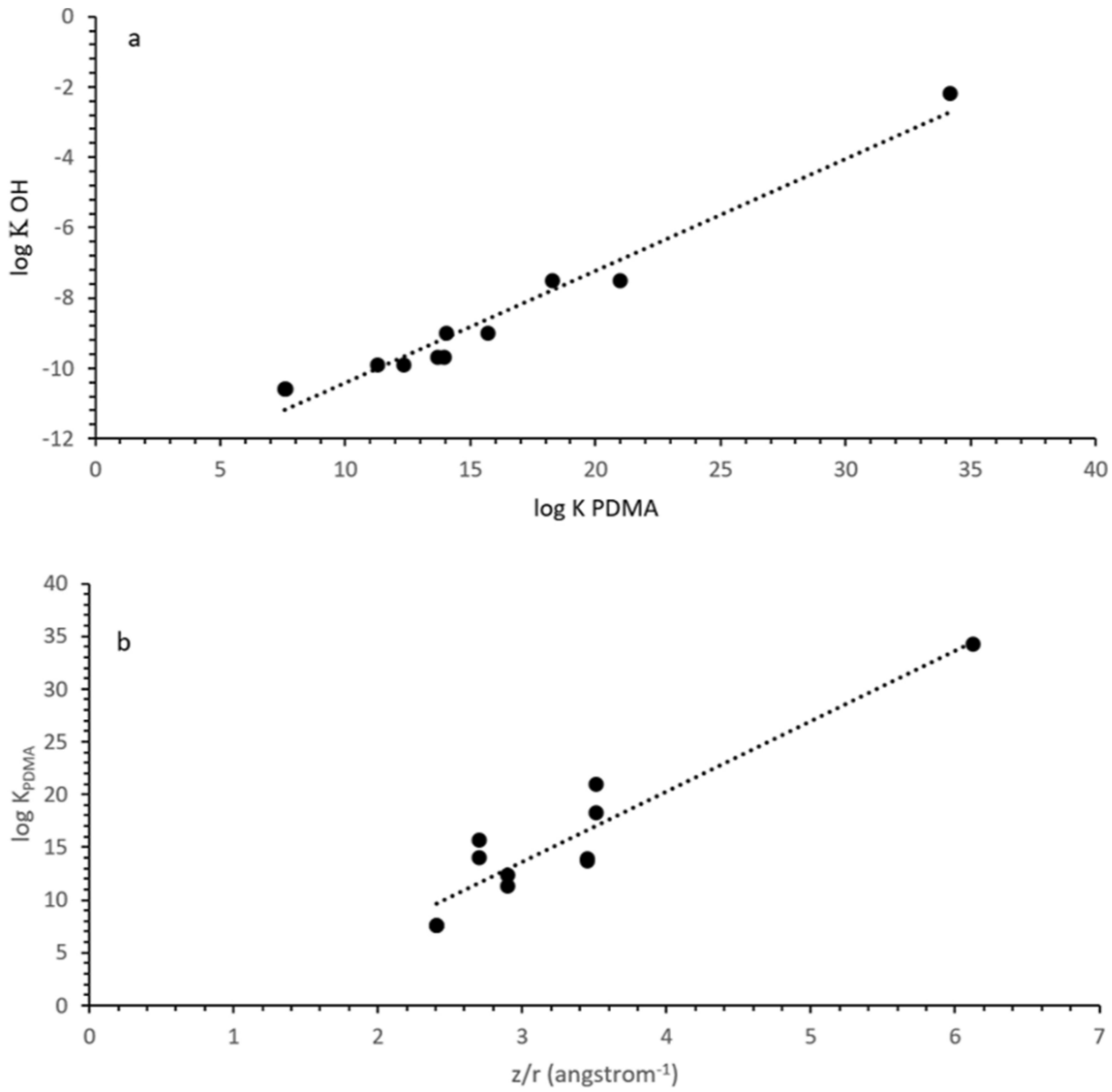

Figure 2.3. (a) First hydrolysis constant for metal ions regressed against proline-2′-deoxymugineic acid (PDMA) stability constants. (b) Ionic potential of metals regressed against proline-2′-deoxymugineic acid (PDMA) stability constants.

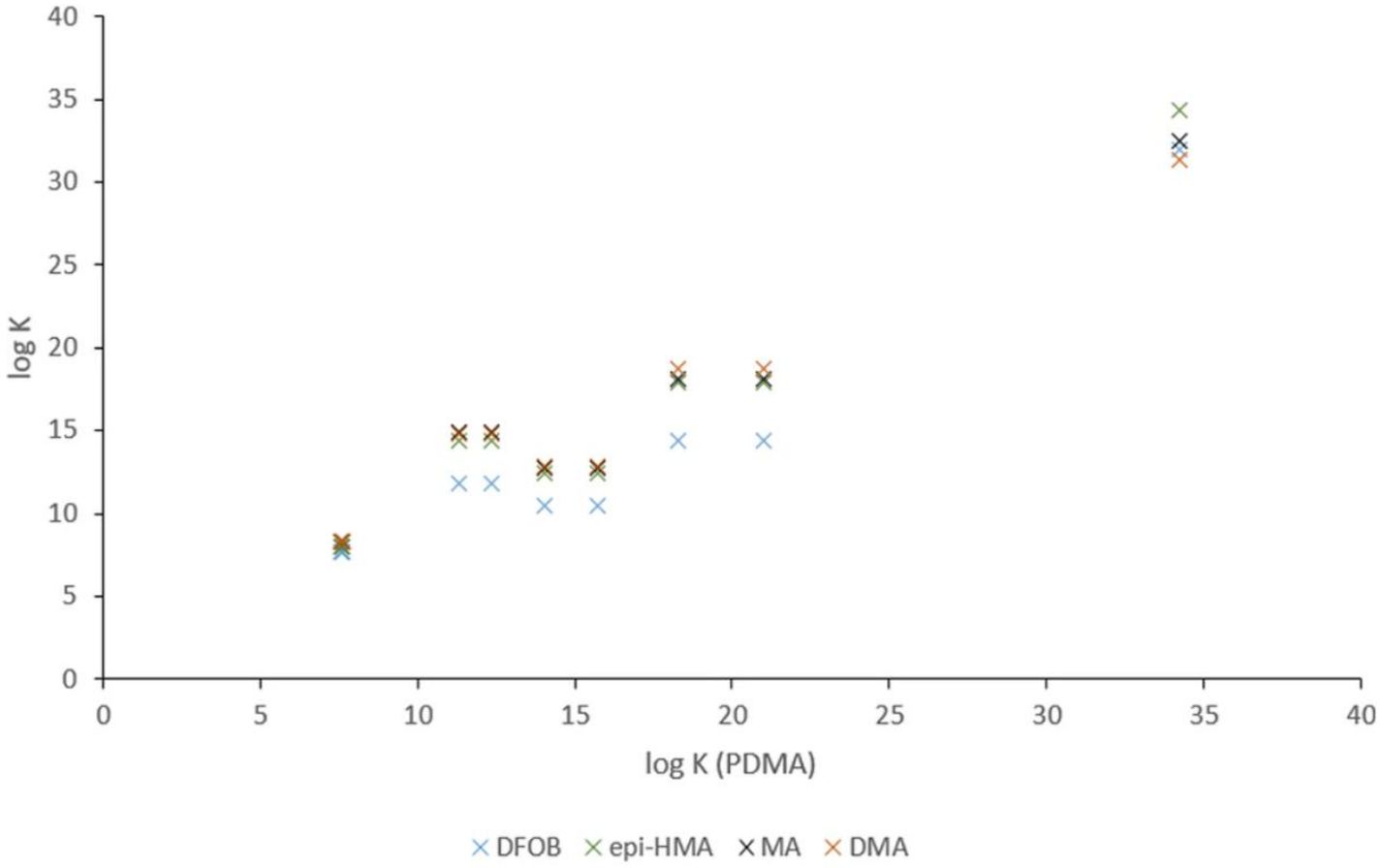

Figure 2.4. Regression of proline-2′-deoxymugineic acid (PDMA) stability constants against stability constants for 2′- deoxymugineic acid (DMA), mugineic acid (MA), and 3-Epi-3-hydroxymugineic (epi-HMA), and desferrioxamine B (DFOB).

Table 2.1. Stability constants, standard deviations, R^2 values for divalent metal-PDMA complexes calculated by KEV from spectrophotometric titration data (in duplicate*)*.

$M(II)HPDMA^{3-}$ complex	$LogK_{ML}$	R^2	$LogK_{ML}$	R^2
Mn(II)	7.6 ± 0.2	0.99	7.6 ± 0.3	0.98
Co(II)	13.9 ± 0.6	0.97	13.7 ± 0.5	0.96
Ni(II)	12.3 ± 0.5	0.99	11.3 ± 0.5	0.92
Cu(II)	18 ± 1	0.99	21 ± 1	0.96
Zn(II)	14.0 ± 0.1	1.00	15.7 ± 0.2	0.92

Table 2.2. Regression statistics for the regression of PDMA with HMA, DMA, MA, epi-HMA, and DFOB. Stability constants are from: DMA (Murakami et al. 1989); MA (Murakami et al. 1989); epi-HMA(Murakami et al. 1989); and DFOB (Hernlem, Vane, and Sayles 1996)

siderophore	slope	intercept	R^2
DMA	0.82 ± 0.07	1 ± 1	0.93
MA	0.85 ± 0.08	1 ± 1	0.93
epiHMA	0.92 ± 0.07	1 ± 1	0.94
DFOB	0.85 ± 0.07	2 ± 1	0.90

CHAPTER 3: Probing the Fate of Structurally Distinct Siderophores with Reactive Soil Components

1. Introduction

Iron (Fe) is an essential nutrient for all organisms. However, in aerobic environments, such as many soils and surface waters, it is typically held in low solubility (oxyhydr)oxide minerals with limited bioavailability. This lack of availability can lead to biological Fe deficiency in alkaline soils where Fe is abundant but not available for organism uptake. Consequently, bacteria, fungi, and graminaceous plants have evolved specific strategies for Fe uptake. One such strategy is the production of siderophores, a structurally diverse class of high affinity Fe(III) chelating agents with low molecular masses (typically 200–2000 Da) that are exuded to facilitate the solubilization and uptake of essential nutrients from soils (Schwyn and Neilands 1987). Siderophores typically contain multidentate combinations of catecholate, hydroxamate, carboxylate, and α-hydroxycarboxylate groups arranged in linear, tripodal, or cyclic arrangements (Crumbliss and Harrington 2009; Hider and Kong 2010).

Grasses, bacteria, and fungi all release structurally distinct siderophores. For example, grasses produce carboxylate-bearing mugineic acid type siderophore whereas fungi most commonly produce hydroxamate siderophores (Römheld and Marschner 1986; Renshaw et al. 2002). Currently, we know little about how these structural differences affect their fate and their ability to transport metals in soils (Harrington, Duckworth, and Haselwandter 2015). The traditional paradigm for siderophore activity in soil involves: (1) siderophore release from organisms; (2) Fe solubilization from bio-unavailable sources; and (3) Fe uptake by cells via an active transporter or reductive process (Kraemer 2004; Kraemer, Crowley, and Kretzschmar 2006; Robin et al. 2008). For siderophores to bring nutrients to a cell, they must be transported as an apo-siderophore from the cell to a Fe source, and then as a Fe(III)-siderophore complex back to the

cell. Because soils are complicated and dynamic systems, a myriad of reactive agents, including mineral surfaces, may disrupt these solubilization and transport processes.

Interactions of metal-siderophore complexes with reactive soil components are currently poorly resolved, largely due to soil complexity and analytical limitations. The background concentrations of Fe (ca. 100–100,000 mg kg^{-1} (Sparks 2003a)) in soils makes probing Fe atoms in siderophore complexes by element specific techniques, such as X-ray absorption spectroscopy (XAS) or X-ray fluorescence (XRF) analysis, unfeasible. However, low abundance yet chemically similar metals have been successfully used to probe chemistries of systems with significant competing background signals (Hagvall, Persson, and Karlsson 2014).

Gallium (Ga) is found in trace amounts in soils and has physicochemical properties similar to Fe. The coordination chemistry of Ga is similar to that of the high-spin ferric ion, with similar electronic configurations (filled 3d for Ga^{3+} and half-filled 3d for Fe^{3+}) and ionic radii in octahedral coordination (0.62 Å for Ga^{3+} and 0.65Å for Fe^{3+}) (Green and Welch 1989). Therefore, many biological systems cannot distinguish between the two metals (Bonchi et al. 2014). Additionally, the stability constants (log K) of Ga(III) and Fe(III)- complexes with the siderophore DFOB are similar (29.49 and 32.02, respectively), so Ga(III)-siderophore behavior should reflect that of Fe(III)-siderophore. Although Ga does not have an environmental redox chemistry, the reduction of Fe(III)-siderophore complexes is generally unfavorable due to thermodynamic stabilization of the trivalent state by ligand binding, further making Ga an effective proxy for Fe in complexes.

A significant number of studies have previously probed the adsorption of siderophores (most commonly DFOB) to clay minerals (as reviewed in (Maurice, Haack, and Mishra 2009)) and oxides (Kraemer et al. 1999; Neubauer, Furrer, and Schulin 2002). However, specific information about the sorption of structurally diverse apo-siderophore and metal siderophore

complexes to reactive soil components is lacking. In this study, we use the trishydroxamate siderophore desferrioxamine-B (DFOB), the triscatecholamide siderophore protochelin, and the carboxylate mugineic acid derivative phytosiderophore proline-2'-deoxymugeneic acid (PDMA) to probe how differing siderophore structures and binding moieties impact siderophore interactions with soil mineral surfaces (Figure 1). Using Ga(III)-siderophore complexes allowed for measuring the K-edge Ga extended X-ray absorption fine structure (EXAFS) spectra for Ga(III)-siderophore complexes sorbed onto mineral surfaces, elucidating the surface structure of siderophore sorption as well as the fate of the complex upon sorption. Pairing the structural EXAFS information with traditional isotherm experiments provided a deeper understanding of how structurally distinct siderophores interact with a myriad of reactive soil components. Understanding how apo-siderophores and metal-siderophores react and bind in soils aids in our understanding of Fe cycling in soil, potentially facilitating the development of better management strategies to improve crop yield and Fe content.

2. Methods

2.1. Materials. All **s**olutions were prepared using ASTM Type 1 (>18.2 MΩ·cm) deionized water (DI). Unless otherwise noted, all chemicals used were of reagent grade from Fisher Scientific (Hampton, NH) or Sigma-Aldrich (St. Louis, MO). The three siderophores examined in this study were chosen for their structural diversity. The mesylate salt of the trishydroxamate siderophore DFOB was purchased from Sigma Aldrich (>92.5%) and used without any further purification. Protochelin (a triscatecholamide siderophore) was synthesized by the Duke University Small Molecules Custom Synthesis Facility (Harrington, Bargar, et al. 2012). Proline-2′-deoxymugineic acid PDMA was provided as PDMA·2HCl by Aichi Steel Corporation (Japan) (Suzuki et al. 2021).

The Fe minerals ferrihydrite and goethite were synthesized by established methods (Cornell and Schwertmann 2003). The turbostratic phyllomanganate δ-MnO_2 was also synthesized by established methods (Villalobos et al. 2003) and had been previously described (Duckworth, Bargar, and Sposito 2008). Standard kaolinite (KGa-1b) and montmorillonite (Na-Swy-1) were sourced from the Clay Mineral Society (Chantilly, VA) and used as received. A 3-point Brunauer-Emmett-Teller (BET) specific surface area analysis was determined with a Quantichrome NovaTouch LX4. Oriented X-ray diffraction (XRD) patterns were collected on air dried Na-Swy-1 samples over 3–80° 2θ using a Rigaku Smartlab X-ray Diffractometer (Cu Kα radiation). The diffractometer was operated at 40 kV and 44 mA, with step size and scan speed of 0.02° 2θ and 1.123 seconds, respectively.

2.2. Sorption Experiments. Sorption experiments were performed with apo-siderophores, and with Fe(III)- and Ga(III)-siderophore complexes in triplicate. DFOB, PDMA, and protochelin isotherms were conducted with a solid to solution ratio of 2 g/L, 10 mM 2-(N-morpholino)ethanesulfonic acid (MES) buffer, and 0.02 M KCl background electrolyte, at pH 6. For Fe(III)- and Ga(III)-siderophore isotherms, $FeCl_3$ and $GaCl_3$ (respectively) were added in a 1:1 stoichiometric ratio to the siderophore stock solution prior to addition to the isotherm.

Initial concentrations included 0, 10, 50, 100, 150, 200, 250, 300, 400, and 500 μM siderophore or siderophore complex. Concentrations were selected to encompass a range of natural siderophore concentrations in rhizosphere environments. Clay minerals and δ-MnO_2 were equilibrated for 24 hours, whereas ferrihydrite and goethite isotherms were equilibrated for 2 hours to prevent mineral dissolution. All samples were shielded from light to prevent photodegradation and filtered through a 0.2 μm filter to end the experiment. Iron-siderophore isotherms were immediately analyzed by UV-visible miniature spectrophotometer (FLAME-T-UV-VIS-ES,

OceanOptics) with a deuterium-halogen light source (DH-mini UV-Vis-NIR, OceanOptics, FL, USA). For apo-DFOB and apo-protochelin analysis, $FeCl_3$ was added in a 1.2:1 Fe: siderophore ratio. Fe(III)-siderophore complexes were analyzed at 425 nm for DFOB (ε_{425} = 2700 M^{-1} cm^{-1}; Bi, Hesterberg et al. 2010), 308 nm for Fe(III)-PDMA (ε_{308} = 4600 M^{-1} cm^{-1}), and 545 for Fe(III)-Protochelin (ε_{545} = 9195 M^{-1} cm^{-1}; Harrington, Bargar et al. 2012). For apo-PDMA a Cu-CAS assay, composed of 100µM $CuCl_2$, 210 µM CAS, 40mM MES, at pH 5.7 was used. Cu-CAS assay was added to filtered samples, and absorbance measured at 582 nm (Shenker, Chen, and Hadar 1995).

The sorbed concentrations of Fe(III)-siderophore, apo-siderophore, and Ga(III)-siderophore were calculated as the difference between the initial aqueous concentration and their post-sorption aqueous concentration (c):

$$c^{sorbed} = c^{initial} - c^{final} \quad (1)$$

Non-linear optimization in a preprogrammed Excel spreadsheet (Bolster and Hornberger 2007) was used to fit to Langmuir and Freundlich models.

2.3. Mineral dissolution. To determine if mineral phases dissolved during experiments, dissolved Fe and Mn were quantified in solution via inductively coupled plasma-optical emission spectrometry (ICP-OES; Perkin Elmer Optima 800).

In apo-siderophore isotherms with goethite and ferrihydrite, dissolved Fe was measured in solution. As a result, a portion of siderophore was Fe bound in solution and no longer available to interact with the mineral surface, referred to below as c^{bound}. For these isotherms, c^{sorbed} was calculated via the following equation:

$$c^{sorbed} = c^{initial} - (c^{final} - c^{bound}) \quad (2)$$

In experiments with δ-MnO_2, dissolved Mn was found for both apo-siderophore and Fe-siderophore complexes. Because siderophore promoted dissolution of Mn may occur by reductive dissolution with concomitant siderophore degradation, it is important to note that in sorption experiments where degradation occurs, isotherms calculated by difference are impacted by the loss of siderophore. In this case, equation 1 is thus modified such that:

$$c^{sorbed} + c^{degraded} = c^{initial} - c^{final} \quad (3)$$

2.4.Gallium-siderophore complex sorption experiments. To prepare samples for XAS measurements, a subset of isotherm experiments were conducted. Ga(III) and Ga(III)-siderophore solutions (1 mM) were exposed to mineral surfaces at pH 6 and a suspension loading of 2 g/L. After the equilibration period of either 24 or 2 hours (dependent on mineral identity as described above), the suspension was passed through 0.2 μm filter and the filtrate was analyzed for Ga concentration via inductive coupled plasma-optical emission spectrometry (ICP-OES; Perkin Elmer Optima 800). Solids were collected and air dried for XAS measurement.

2.5. X-ray absorption spectroscopy. Gallium K-edge extended X-ray absorption fine structure (EXAFS) spectra were collected at room temperature at Stanford Synchrotron Radiation Lightsource (SSRL) or the Advanced Photon Source. Spectra were collected for most Ga(III)-siderophore sorbed to mineral surfaces, free Ga sorbed to mineral surfaces, and aqueous Ga(III)-PDMA and Ga(III)-protochelin complexes. Aqueous Ga(III) complexes (1 mM Ga) were prepared on site at pH 6. Beamline 11–2 [Si (220) variable-exit monochromator] was operated at room temperature by using either a 100-element germanium or passivated implanted planar silicon (PIPS) detector equipped with Soller slits and a Zn filter. For Fe minerals, aluminum foil was used to attenuate Fe fluorescence. Sample holders had a 2.5 mm by 30 mm aperture covered with 0.0005-in. thick Kapton tape. Harmonics were rejected by using a Rh coated flat cutoff mirror.

The beam was calibrated using an elemental Ga standard by setting the energy to the first inflection point at the K-edge (10367 eV). Additionally, spectra of Ga(III) and Ga(III)-siderophore complexes sorbed to goethite were collected at the Advanced Photon Source at Argonne National Laboratory Sector 10. Energy was calibrated to the rhenium L_{III} edge (10535 eV). Three consecutive spectra, which showed no sign of beam damage, were averaged for each sample to improve signal-to-noise ratio.

Spectra were energy calibrated, averaged, background-subtracted, splined, and least square fit (Kelly, Hesterberg et al. 2008) using the SixPACK interface (Webb 2005), which makes use of the IFEFFIT code (Newville 2001). To confirm their molecular structure, standard spectra, including aqueous Ga(III)-siderophore complexes and Ga(III) sorbed to mineral surfaces, were fit to existing structural models using an amplitude reduction factor of $S_0 = 1.0$ (Duckworth, Bargar, and Sposito 2009b). Paths were generated for a Ga(III)-DFOB complex and Ga(III) sorbed to δ-MnO_2, alumina, and hematite using Feff 9 (Rehr et al. 2010). Specifically, Ga(III)-protochelin and Ga(III)-PDMA were fit existing models based on the structure of Fe(III)-protochelin and Fe(III)-DFOB (Harrington, Bargar, et al. 2012; Harrington, Parker, et al. 2012). Existing models of cations sorbed to birnessite (Duckworth, Bargar, and Sposito 2008), kaolinite (O'Day, Parks, and Brown 1994), and ferrihydrite (Whitaker and Duckworth 2018) were used for Ga(III) sorbed to δ-MnO_2, kaolinite and montmorillonite, and goethite and ferrihydrite, respectively. Using the standards above, linear combination fitting with the spectra of the Ga(III)-sorbed to minerals surfaces and the aqueous Ga(III)-siderophore complexes (Kruft et al. 2013) was used to analyze the spectra of Ga(III)-siderophore complex reacted with corresponding mineral surface to better understand surface complexation structures for on the mineral surface.

3. Results

3.1. DFOB isotherms. The surface area normalized adsorption isotherms for apo-DFOB and Fe(III)-DFOB, presented in Figure 2 and 3, represent the equilibrium adorption capacities of mineral surfaces as functions of increasing initial siderophore concentrations. Apo-DFOB showed sorption affinity in the order of montmorillonite> kaolinite> goethite> δ-MnO_2> ferrihydrite. All DFOB isotherms were modeled with a Freundlich isotherm. Best fits were determined by model efficiency. The Freundlich sorption constant (K_f), exponential constant (n), and model efficiency (E) are shown in Table 1.

For Fe(III)-DFOB, sorption was observed onto montmorillonite clay, δ-MnO_2, and goethite. The greatest sorption maximum occurred on montmorillonite clay, with an S_{max} of 8.4 μmol m^{-1}, followed by goethite (S_{max} = 0.8 μmol m^{-1}) and δ-MnO_2, (S_{max} = 0.4 μmol m^{-1}). Fe(III)-DFOB isotherms were modeled with a Langmuir isotherm (Table 2). No sorption was observed for ferrihydrite or kaolinite. Although different models gave best fits, similar sorption was seen between DFOB and Fe(III)-DFOB to montmorillonite.

3.2.Gallium-DFOB complex isotherms. Gallium-DFOB complex sorption experiments were conducted to ensure that Ga(III)-siderophore complex behavior mirrored the sorption of Fe chelated siderophores. To preserve small quantities of siderophores, these isotherms were only conducted with DFOB. Ga(III)-DFOB sorption plotted with Fe(III)-DFOB sorption is shown in Figure 3. Because Fe(III)-DFOB only showed sorption to goethite, montmorillonite, and δ-MnO_2, only these three minerals were used for the verification.

Ga(III)-DFOB and Fe(III)-DFOB sorbed to montmorillonite had similar S_{max} values (8.0 μmol/m^2 vs 8.4 μmol/m^2). The sorption of both metal-siderophore complexes onto δ-MnO_2 also displayed similar Smax values (0.5 μmol/m^2 vs 0.4 μmol/m^2). Ga(III) and Fe(III)-DFOB sorption

to goethite resulted in S_{max} values of 0.76 μmol/m^2 and 0.80 μmol/m^2. The overall similarity in sorption amounts and behaviors (Table 2) suggests that the behavior of Ga(III)-siderophore complexes is representative of that of the Fe(III)-siderophore complex.

3.3 PDMA isotherms. Surface area normalized sorption isotherms for Fe(III)-PDMA (Figure 4) complexes were best fit with sorption maxima such that S_{max} was in the order montmorillonite> δ-MnO_2> goethite> ferrihydrite. No sorption was observed to kaolinite. The greatest sorption was to montmorillonite, and both isotherms for both montmorillonite and δ-MnO_2 showed a high degree of linearity (n value of 1), indicating that a maximum capacity was not reached. Fit parameters are in Table 3. In contrast, no sorption was observed for uncomplexed PDMA (Figure 5) to montmorillonite, kaolinite, ferrihydrite, and goethite.

3.4.Protochelin isotherms. For surface area normalized apo-protochelin isotherms (Figure 6) sorption affinity was in the order of montmorillonite> goethite> δ-MnO_2> ferrihydrite> kaolinite. Sorption to montmorillonite was linear with increasing concentration, whereas sorption data for ferrihydrite and goethite were fit with Langmuir models and showed clear sorption maxima. Fe(III)-protochelin isotherms (Figure 7) showed similar amounts of sorption to montmorillonite and goethite, along with lower sorption to δ-MnO_2.

3.5. Additional changes to sorbents or solution composition. Siderophore promoted mineral dissolution consistent with ligand-promoted or reductive dissolution was observed in many isotherms. Apo-DFOB isotherms with goethite and δ-MnO_2 resulted in dissolved Fe and Mn in solution, respectively (SI Figure 1). For the PDMA δ-MnO_2 isotherm, dissolved Mn concentration increased with increasing initial concentrations of siderophore, with significant dissolution occurring at 250 μM initial siderophore concentration (SI Figure 2). Both apo- and Fe(III)-protochelin isotherms resulted in similar amounts of dissolved Mn in solution, with significant

amounts of dissolution occurring after 100 μM of initial siderophore (SI Figure 3). Protochelin isotherms with ferrihydrite and goethite also resulted in dissolved Fe in solution.

Additional color changes and visible signs of degradation were observed in apo- and Fe(III)-protochelin isotherms, suggesting reactions other than simple sorption. Suspensions containing montmorillonite clay and δ-MnO_2 turned green and brown, respectively upon the addition of apo-protochelin and metal-protochelin complex. The formation of brown precipitates has been attributed to redox chemistry resulting in reactions involving catechol groups in protochelin (Harrington, Bargar, et al. 2012).

3.6. EXAFS structure fitting of standard spectra. Spectra of aqueous Ga(III)-siderophore complexes and Ga(III) sorbed to mineral surfaces accompanied by fits existing models (Harrington, Bargar, et al. 2012; Duckworth, Bargar, and Sposito 2009b; Whitaker and Duckworth 2018; O'Day, Parks, and Brown 1994) are shown in supplemental Figure 4 and 5, with fit parameters reported in supporting Table 1. For all standards, fits had a first shell with 5.8–8.4 (±20%) oxygen atoms at a distance of 1.91–1.98 Å from Ga, consistent with hexadentate coordination of Ga(III). Aqueous complexes were found to have a layered coordination structure, consistent with the central Ga(III) being surrounded by the first oxygen coordination shell and other atoms in the molecule at longer distances (Harrington, Bargar, et al. 2012; Harrington, Parker, et al. 2012; Edwards and Myneni 2005; Duckworth et al. 2009; Duckworth, Bargar, and Sposito 2009b). For Ga(III) sorbed to ferrihydrite and goethite, the model was fit with two second shell Fe atoms, suggesting the possible presence of mononuclear and binuclear inner sphere complexes (Whitaker and Duckworth 2018). For δ-MnO_2, an existing two-site model was best fit with a specific sorption of 86% of Ga(III) at edge sites, and 14% at phyllomanganate sheet vacancies (Duckworth, Bargar, and Sposito 2008). For clay minerals, shells containing Ga-Al and

Ga-Ga scattering paths were used, suggesting clustering of sorbed Ga(III) atoms on mineral surfaces (O'Day, Parks, and Brown 1994). These results are consistent with other studies of the sorption of metal ions to mineral surfaces, confirming the molecular structure of our standards.

3.7. EXAFS linear combination fits. Figure 8, 9 and 10 shows the Ga K-edge EXAFS for Ga(III)-DFOB, Ga(III)-protochelin, and Ga(III)-PDMA complexes reacted with mineral suspensions. Fits are represented as dashed lines. Table 7 shows the results of the least square fit results for Ga(III)-siderophore complexes. These results were determined by using free Ga metal sorbed onto a mineral and aqueous Ga(III)-siderophore complex as standards in least square fitting, with percentages presented in the table representing the percentage of the least square fit made up of aqueous Ga(III)-siderophore complex.

For ferrihydrite, Ga(III)-DFOB and Ga(III)-PDMA were best fit by 100% free Ga metal. Ga(III)-protochelin was best fit by 100% aqueous Ga(III)-protochelin complex. All goethite spectra were best fit with a ratio of around 33% aqueous Ga(III)-siderophore complex and around 66% Ga sorbed to the surface of goethite. For montmorillonite, Ga(III)-DFOB was best fit with 100% of the spectra of aqueous Ga(III)-DFOB complex. Ga(III)-PDMA montmorillonite was best fit with 70% aqueous Ga(III)-PDMA, and 30% Ga sorbed to montmorillonite. Ga(III)-protochelin montmorillonite resulted in a fit of 28% aqueous complex, and 72% free Ga sorbed to montmorillonite. Ga(III)-DFOB and Ga(III)-PDMA with kaolinite were best fit with 100% Ga sorbed to the surface of kaolinite. Ga(III)-protochelin onto kaolinite was best fit with 28% aqueous siderophore complex and 72% Ga on the surface. All three Ga(III)-siderophore complexes had best fits of 100% Ga sorbed to the mineral surface for δ-MnO_2.

3.8. Structural changes of montmorillonite. XRD analysis was conducted on air dried samples of apo-siderophore and Ga(III)-siderophore complexes sorbed to montmorillonite clay to investigate

whether structural changes consistent with intercalation, uptake of the complex between phyllosilicate layers, were occurring. This has been previously observed for apo-DFOB sorption to smectite clays (Haack, Johnston, and Maurice 2008). Na-montmorillonite has characteristic reflections present at 2θ = 6.38°, 19.92°, 20.82°, 26.66°, 28.72°, 34.92°, 50.15°, 54.08° and 61.97° (Sarier, Onder, and Ersoy 2010). The typical XRD reflection of Na-montmorillonite related to the basal spacing *d*(001) between the clay platelets appears at 2θ = 6.38° (6.26 Å). Cations may take on different orientations in the interlayer, sorbing either parallel between opposing layers, or in intermediate orientations. (He et al. 2006). The results of the change in basal spacing due to the absorption of siderophores is presented in Table 8. The absorption of free Ga caused a decrease in *d*-spacing of 1.04 Å, as expected with the introduction of a large highly charged cation. DFOB sorption caused an increase in d spacing of 0.52 Å, and Ga(III)-DFOB sorption resulted in an increase of 0.62 Å. PDMA absorption caused a decrease in *d*-spacing of 1.14 Å, whereas Ga(III)-PDMA increased the basal spacing by 0.11 Å. For protochelin, *d*-spacing decreased by 0.6 Å, along with a decrease of 0.43 Å for Ga(III)-protochelin absorption. Ga(III)-protochelin was the only complexed siderophore causing a decrease in d-spacing. It is again worth noting that the montmorillonite clay turned a pronounced blue-green upon the sorption of the Ga(III)-protochelin complex. The XRD spectra for all siderophores and siderophore complexes (except that of Ga(III)-protochelin) no longer showed a reflection peak of 2θ = 28.72° (Figure 9). Changes in these reflections are typically attributed to the delamination and disorientation of clay platelets (Sarier, Onder, and Ersoy 2010).

4. Discussion

4.1. Mechanisms of interaction of siderophores and siderophore metal complexes with surfaces.

Previous studies of siderophores and other organic acids have demonstrated a wide range of

potential interactions with mineral surfaces. The individual binding groups of DFOB (hydroxamate), PDMA (α-aminocarboxylate and α-hydroxycarboxylate), and protochelin (catechol) may all uniquely interact with the contrasting surfaces of the minerals studied. Similarly, the complexes of these siderophores may interact differently based on the charge and structure of the complex. Adsorbates have either attractive electrostatic forces holding them near the surface (outer sphere), or have direct chemical bonds with surface functional groups (inner sphere adsorption and ternary complex formation) (Strawn 2021).

4.1.1. Adsorption. Adsorption is controlled by the chemical characteristics of both the sorbent (reactive functional groups or electrostatic charges) and the sorptive (ionic radius, valence, bonding characteristics, hydrophobicity). In an outer sphere complex there is no direct bond, and the ligand is attracted to the surface by electrostatic forces and can be separated from the surface by water molecules (Strawn 2021). Inner sphere complexes be classified as: 1) monodentate with one functional group bound to metal surface; 2) mononuclear bidentate with two functional groups bound to one metal site; or 3) bridging (binuclear) bidentate where two groups are bound to two different metal sites (Simanova, Loring, and Persson 2011).

Metal-organic complexes can also be bound to surfaces through ternary complexes, where a cation or anion is used as a bridging ion. Ternary complexes can be either type A, where the metal bridges the surface to the ligand, or type B, where the ligand bridges the metal to the surface. $Fe(III)HDFOB^{+}$ has been shown to sorb in part as a type A ternary complex to the surface of goethite (Simanova, Loring, and Persson 2011). In the case of complexes, it is also possible that the surface may promote dissociation of the complex, and with potential separate sorption or solubilization of the siderophore and metal ion.

4.1.2. Dissolution. Siderophores may promote dissolution of minerals via non-reductive or reductive pathways. Non-reductive dissolution includes proton promoted dissolution and ligand-controlled dissolution. Proton promoted dissolution is pH dependent and involves the protonation of Fe ion pairs at the mineral surface. Ligand controlled dissolution involves surface complex formation between the ligand and the mineral, followed by detachment of the surficial metal center. The ligand promoted dissolution occurs by destabilizing the coordination of the Fe ions at the surface (Kraemer 2004). In the absence of small organics, siderophores are generally thought to dissolve ferric minerals via a non-reductive ligand promoted dissolution mechanism, resulting in ferric siderophore complexes.

4.1.3. Reductive dissolution with concomitant siderophore oxidation. Siderophores may also promote dissolution via reductive dissolution pathways. Reductive dissolution involves the reduction of a metal hydroxide mineral, often leading to the release of a soluble form of the metal. Siderophore-promoted reductive dissolution at acidic pH has been demonstrated for a variety of Mn (oxyhydr)oxides, including δ-MnO_2, and leads to the release of a reduced metal ion into solution, accompanied by the oxidation of the siderophore (Duckworth and Sposito 2005; Harrington, Parker, et al. 2012; Duckworth and Sposito 2007; Peña et al. 2007) by the generalized reaction:

$$Mn(III,IV)O_2 + H_4DFOB^+ \rightarrow Mn^{2+} + DFOB_{ox} \quad (3)$$

where DFOB is degraded in the process. (Akafia et al. 2014) also saw oxidation of binding groups in protochelin reacted with Mn oxides, where the catechol groups oxidized to quinones.

4.1.4. Intercalation. Intercalation refers to a compound being inserted between the layers of a layered clay mineral. Swelling clays and micas have negative permanent structural charge density resulting from isomorphic substitution and may undergo cation exchange. (Maurice, Haack, and

Mishra 2009). It is known that for clays such as montmorillonite that many organic compounds, including DFOB, may absorb into the clay interlayers. The characteristics of the interlayer molecules (size, structure, orientation, and charge) can change the thickness of the interlayer spacing (*d*(001)), which is measurable through XRD. For most organic molecules and metal complexes, the large size of the molecule results in swelling of interlayers. Metal ions may also intercalate, often resulting in collapse of interlayer spacing due to electrostatic attraction and bridging of layers.

4.2 Siderophore and siderophore complex interactions with mineral surfaces. Siderophores and metal-complexes have a potentially rich diversity of interactions with different mineral surfaces, depending on the siderophore structure and mineral surface. Based on the discussion above and our spectroscopic and wet chemical investigations, we explore the possible interactions present in our experimental systems.

4.2.1. Montmorillonite. Apo-siderophores showed contrasting behaviors in their interactions with the expansive 2:1 clay montmorillonite. DFOB showed a linear isotherm (c-type isotherm) with montmorillonite, indicating that the sorption capacity was not reached, which is consistent with intercalation (Sparks 2003b). This interpretation is also supported by the XRD data, where sorption of DFOB to montmorillonite caused an increase in *d*(001). In contrast, PDMA isotherms showed no appreciable sorption to montmorillonite. The structurally analogous mugineic acid siderophore DMA, has previously been shown to exhibit no sorption to montmorillonite clay due to small amounts of reactive Al and small external surface area (Hiradate and Inoue 1999). However, the XRD data showed a decrease in *d*(001) spacing of 1.14 Å (Table 8), indicating that a reaction causing the clay layer to collapse did occur, which suggests some solute-sorbent interaction that results in structural rearrangement.

When protochelin was reacted with montmorillonite, a linear isotherm was also observed, however the clay turned a blue-green color upon interaction with the siderophore, which may suggest siderophore degradation. Protochelin has been shown to degrade via hydrolysis and oxidation, resulting in the formation of benzoquinone groups or coupled hydroxylated aromatic compounds, one of which could be responsible for the change in color observed (Dubme, Hider, and Khodr 1997; Harrington, Bargar, et al. 2012). This suggests that equation (1) is not applicable for measurements. Because equation (2) has an additional unknown degradation term, our isotherms likely overestimate sorption. Although approaches such as mass spectrometry have been used to quantify protochelin, there are significant barriers to the recovery and quantitation of both protochelin and its degradation products (Rai et al. 2020; French et al. 2024). It is worth noting that the montmorillonite *d*-spacing decreased by 0.6 Å upon interaction with protochelin (Table 8), so it is possible that either protochelin or degradation fragments were intercalated in the interlayer of the clay.

Montmorillonite has been shown to intercalate metal-DFOB complexes (Maurice, Haack, and Mishra 2009) in part because DFOB forms positive complexes with trivalent metals ($M(III)HDFOB^{+}$) that are electrostatically attached to negative layers in the clay. Fe(III)-DFOB showed a similar affinity for montmorillonite as DFOB. However, the sorption data were best fit with a Langmuir isotherm, indicating that a sorption capacity was reached. Linear combination fitting of the EXAFS spectra showed no dissociation of the complex upon adsorption to the clay, and XRD data showed an increase in *d*(001) of 0.62 Å (Table 8). This increase is consistent with the size of the Ga(III)-DFOB complex in the horizontal orientation (Kruft et al. 2013), suggesting that the Fe(III)-DFOB complex is intercalating into the montmorillonite interlayers as well. The montmorillonite Fe(III)-PDMA isotherm was also linear, however amounts of sorption were lower

compared to Fe(III)-DFOB (S_{max} = 1.6 μm/m^2 and 6 μm/m^2, respectively). The EXAFS LCF data for the Ga(III)-PDMA complex showed 30% dissociation of the complex, indicating that most of the complex stayed intact. When paired with an increase in basal spacing by 0.11 Å (Table 8), this suggests that Fe(III)-PDMA is also intercalating into the montmorillonite, with a lesser component of dissociation from the complex, instead interacting directly with the surface. It is worth noting that PDMA also forms positive complexes with trivalent metals ($M(III)H_3PDMA^{2+}$) (Suzuki et al. 2021).

Fe(III)-protochelin onto montmorillonite had similar results as apo-protochelin, where the suspension turned a blue-green color. The metal-protochelin complexes are significantly larger and more hydrophobic than corresponding metal-DFOB and metal-PDMA complexes, making them sterically less favorable to intercalate into the clay. Additionally, Ga(III)-protochelin and Fe(III)-protochelin complexes are negative ($Ga(III)Proto^{3-}$) at circumneutral pH, which would be repelled from the negative layer charges of montmorillonite. Fits of EXAFS data indicated Ga(III)-protochelin was the only siderophore complex where the majority of the complex dissociated (67%) when interacting with montmorillonite, and the basal spacing decreased (-0.43 Å) (Table 8). The decrease in d-spacing was not as great as that of free Ga(III), possibly indicating intercalation of both Ga(III) dissociated from complexes and degradation products.

4.2.2 Kaolinite. In contrast to the 2:1 clay montmorillonite, the 1:1 clay kaolinite does not typically intercalate cations (Maurice, Haack, and Mishra 2009). For surface area normalized isotherms, DFOB showed the greatest adsorption affinity for kaolinite, followed by protochelin. For 1:1 clays like kaolinite, siderophores can bind the Si–O–Si sites on the basal plane surfaces (Maurice, Haack, and Mishra 2009), which are available to organics. Adsorption of DFOB to kaolinite has been shown to be consistent with cation-like behavior, suggesting that the adsorption of DFOB to

kaolinite is partially electrostatically driven (Maurice, Haack, and Mishra 2009). Fe(III)-DFOB and Fe(III)-PDMA both showed no affinity for kaolinite, and the EXAFS data were best fit 100% Ga(III) sorbed to the kaolinite surface, suggesting that Ga associated with the mineral surface had dissociated from the mineral, and that siderophores from complexes likely interact similarly to those introduced as apo-siderophores.

4.2.3. Ferrihydrite and goethite. Sorption of DFOB and protochelin to goethite were best fit Freundlich and Langmuir isotherms, respectively. Previous studies (Kraemer et al. 1999) showed similar amounts of sorption for DFOB to goethite, as well as similar sorption behaviors. Additionally, DFOB caused Fe dissolution (SI Figure 4), which has been previously observed (Cocozza et al. 2002; Holmén and Casey 1996; Kraemer 2004). In contrast, apo-PDMA did not appreciably sorb to goethite. Previous studies (Reichard 2005) found adsorption of DMA (structurally identical to PDMA except for a 4 membered azetidine ring) on the scale of nmol/m^2 accompanied by the dissolution of Fe into solution. For metal-siderophore complexes, Fe(III)-DFOB and Fe(III)-PDMA sorption to goethite resulted in Langmuir isotherms with no additional Fe dissolution into solution. Fe(III)-protochelin was best fit with a linear isotherm, along with low amounts of Fe dissolution, indicating that some metal exchange (and possible degradation) was occurring.

The LCF results for EXAFS spectra of the Ga(III)-siderophore complexes sorbed to goethite were best fit with similar percentages (~33%) of intact complexes. This ratio suggests two possibilities. The first is that two separate populations of Ga(III) exist at the surface — approximately 1/3 as an intact complex, and 2/3 with direct sorption of Ga(III) to the surface from complex dissociation. It is unlikely that Ga(III)-DFOB, Ga(III)-PDMA, and Ga(III)- protochelin are forming outer sphere complexes onto goethite due to electrostatic repulsions between

positively charged complexes and the surface (Simanova, Loring, and Persson 2011; Borer et al. 2009).The second possibility is that all three siderophore complexes are forming some type of ternary complexes to the surface of goethite. It this case, it is plausible that Ga(III) may be directly sorbing to the surface with a hydroxamate group binding to the opposing side (type A complex). This type of complex is potentially consistent with fit results, since ~1/3 of potential coordination sites would contain a hydroxamate moiety. This is consistent with previous work that suggest a Type A ternary complex for Fe(III)-DFOB on goethite (Simanova, Loring, and Persson 2011). Additional spectroscopic approaches may help to test this sorption model, although we note that previous research proposed binding of two hydroxamates to distinct sites on the goethite surface, potentially complicating interpretations (Borer et al. 2009).

Once surface area normalized, all three siderophores showed low affinities for ferrihydrite. Ga(III)-DFOB and Ga(III)-PDMA both showed 100% separation of the complex upon sorption. The surface of ferrihydrite contains more reactive oxygens than that of goethite (Cudennec and Lecerf 2006). In contrast, Ga(III)-protochelin remained an intact complex upon sorption to ferrihydrite. Ga(III)-protochelin also showed significantly less Fe dissolution from the ferrihydrite than the Ga(III)-DFOB and Ga(III)-PDMA (SI Table 2), further supporting their dissociative behavior being distinct from Ga(III)-protochelin. The Ga(III)-protochelin complex behaves differently than the Ga(III)-DFOB/PDMA complexes on the surface of ferrihydrite due to its negative charge ($Ga(III)Proto^{3-}$ vs $Ga(III)HDFOB^{+}$ and $Ga(III)H_3PDMA^{2+}$) and its highly hydrophobic backbone. Previous workers have noted the formation of other stable, negatively charged organic complexes, such as $Me(C_2O_4)_3^{3-}$, on the surface of Fe(III) (oxy)hydroxides (Simanova, Loring, and Persson 2011). At the water goethite interface, C_2O_4 formed electrostatically attracted outer sphere surface species, hydrogen bonded outer sphere species, and

two inner sphere oxalate complexes. $Co(III)(C_2O_4)_3^{3-}$ complex was found to adsorb to the water goethite interface outer spherically. $Fe(III)(C_2O_4)_3^{3-}$ were found to initially adsorb outer sphere but decomposed to the same surface species as the oxalate system over time. $Ga(III)(C_2O_4)_3^{3-}$ complexes were found to coordinate inner spherically through a type A ternary complex to the goethite surface (Simanova, Persson, and Loring 2010). Based on this previous research, it is likely that the Ga(III)-Protochelin^{3-} is adsorbing outer spherically to the ferrihydrite water interface and remaining an intact complex. The difference in behavior of the metal siderophore complexes on the iron minerals can be attributed to the high surface area of ferrihydrite, as well as the point of zero charge (PZC) of ferrihydrite (7.8-8.5 (Whitaker and Duckworth 2018) vs. 9.3 (Simanova, Loring, and Persson 2011), respectively), causing the surface of ferrihydrite to be less negatively charged than that of goethite at experimental pH.

It is important to note that we are using Ga(III) as a surrogate for Fe(III) to probe reactions at surfaces. As a result, reactions with the Ga(III) may be occurring that would not typically happen in Fe systems. Especially in Fe rich environments such as experiments with Fe oxides, there is a possibility that Ga(III) is being exchanged out of the siderophore complex for Fe(III) (driven by small changes in stability constants), impacting results. Additionally, Fe(III) may be reduced, which does not occur with Ga(III) (Harrington and Crumbliss 2009). However, the hard base-bearing moieties in high affinity multidentate siderophores greatly favor binding of Fe(III) and alter the electrochemical potential of Fe in complexes such that Fe(III) reduction is thermodynamically disfavored. Additionally, it is possible that exchange reactions between Fe on surfaces are common, and cryptic cycling of Fe minerals has been shown to control key aspects of Fe biogeochemistry (Kappler and Bryce 2017). It is also worth noting that Mn has been shown to interfere with siderophore mediated Fe transport (Kang and Peña 2023; Duckworth, Bargar, and

Sposito 2009a) , and thus the reactivity of Ga(III)-siderophore complexes may help to elucidate these processes.

4.2.4. δ-MnO_2. DFOB, PDMA, protochelin, Fe(III)-DFOB, Fe(III)-PDMA, and Fe(III)-protochelin all showed linear isotherms when reacted with δ-MnO_2. All Ga(III)-siderophore complexes were best fit with 100% the Ga(III)- δ-MnO_2, suggesting that Ga quantitatively dissociates from the complex when reacting with the surface of δ-MnO_2. (Duckworth, Bargar, and Sposito 2008) saw the sorption of Fe to Mn oxide surfaces resulting from the dissociation of Fe(III)$HDFOB^+$ complexes, consistent with our observations of Ga(III)-siderophore complexes behavior. δ-MnO_2 is a strong oxidant with large redox potential (Bricker 1965), and readily undergoes redox reactions with a range of organic molecules (Remucal and Ginder-Vogel 2014), including siderophores (Duckworth and Sposito 2007). Additionally, δ-MnO_2 has structural octahedral cationic vacancies in phyllomanganate layers, and these sites and the edges of layers are strong sorption sites for metal cations (Appelo and Postma 1999; Manceau, Lanson, and Drits 2002; Tebo et al. 2004; Wang et al. 2018).

The dissolution of Mn from the δ-MnO_2 suggests reductive dissolution is occurring, and that both the apo and Fe(III)-siderophore are being degraded. (Duckworth and Sposito 2005) previously observed the reductive dissolution of manganite upon reaction with DFOB, resulting in the oxidization/degradation of the siderophore, and protochelin has been shown to degrade via oxidation of the catechol groups (Harrington, Parker, et al. 2012; French et al. 2024). All apo and Fe(III)-siderophore complex pairs (e.g., apo-DFOB/Fe(III)-DFOB) had similar amounts of total siderophore lost ($c^{sorbed} + c^{degraded}$) with the δ-$MnO_2$, accompanied by Mn dissolution. Dissolved Mn in the PDMA sample also is likely an indicator of oxidation of the carboxyl groups of the siderophore, however there is little literature on the degradation products of mugineic acid

type siderophores. The similar amounts of dissolution in apo and complexed siderophores suggest that complexation does not protect siderophores from degradation via redox active mineral surfaces. Because we did not quantify degradation productions or total siderophore remaining at the end of experiments, it is important to note that in the case of all siderophore δ-MnO_2 isotherms, the isotherm is representative of degradation in addition to possible sorption.

5. Conclusions

Adsorption onto the soil solid phase is thought to account for a significant portion of siderophore loss from the rhizosphere (Reichman and Parker 2005) and the total concentrations of siderophores in soils (Ahmed and Holmström 2014; Rai et al. 2020). Similarly, sorbed Fe(III)-siderophore complexes sorbed to surfaces may be an important labile form of iron for soil organisms (Harrington, Duckworth, and Haselwandter 2015). It is consequently important to gain detailed structural information on the surface complexation structures of both apo-siderophores and metal-siderophore complexes mineral surfaces to understand their role in iron mobilization. This study shows that clays may be a sink for siderophores in soils, either intercalating them as for DFOB, or degrading them as for protochelin. Reactive manganese minerals may also act as a sink, degrading siderophores and their complexes. The synthetic siderophore PDMA contains an L-proline ring to replace the unstable azetidine-2-carboxylic acid group found in natural phytosiderophores. PDMA did not adsorb to soil minerals, consistent with its development as potential as an Fe fertilizer (Suzuki et al. 2021). However, complexed PDMA sorbed to mineral surfaces, likely due to changes in electrostatics and orientation of the carbon backbone away from the binding sites. Additionally, it has previously been shown to be resilient against enzymatic degradation (Chukwuma, Duckworth, and Baars 2025). Protochelin was found to have unique behavior from DFOB and PDMA with montmorillonite and ferrihydrite largely resulting from its

hydrophilic backbone, redox reactivity of its binding moieties, and negative charge as complex. Overall, this study demonstrates the effects of siderophore structural diversity on siderophore-soil mineral interactions. The hydrophobicity, charge, and size of siderophores and their complexes drive changes in reactivity with charged mineral surfaces and interlayers, which has direct implications for the availability of Fe and other nutrients to microbes and plants.

The use of Ga(III) in siderophore complexes is allowing us to begin to gain understanding of what siderophore structure and sorption behaviors look like on mineral surfaces and may help to inform future studies in more complex systems. Further studies are required to better establish how structurally distinct siderophores interact in various whole soil environments to help develop sustainable methods of biofortifying crops to combat nutrient deficiencies.

REFERENCES

Ahmed, Engy, and Sara J. M. Holmström. 2014. 'The effect of soil horizon and mineral type on the distribution of siderophores in soil', *Geochimica et Cosmochimica Acta*, 131: 184-95.

Akafia, Martin M., James M. Harrington, John R. Bargar, and Owen W. Duckworth. 2014. 'Metal oxyhydroxide dissolution as promoted by structurally diverse siderophores and oxalate', *Geochimica et Cosmochimica Acta*, 141: 258-69.

Appelo, CAJ, and Dieke Postma. 1999. 'A consistent model for surface complexation on birnessite (− MnO2) and its application to a column experiment', *Geochimica et Cosmochimica Acta*, 63: 3039-48.

Bolster, Carl H., and George M. Hornberger. 2007. 'On the Use of Linearized Langmuir Equations', *Soil Science Society of America Journal*, 71: 1796-806.

Bonchi, C., F. Imperi, F. Minandri, P. Visca, and E. Frangipani. 2014. 'Repurposing of gallium-based drugs for antibacterial therapy', *Biofactors*, 40: 303-12.

Borer, Paul, Stephan J. Hug, Barbara Sulzberger, Stephan M. Kraemer, and Ruben Kretzschmar. 2009. 'ATR-FTIR spectroscopic study of the adsorption of desferrioxamine B and aerobactin to the surface of lepidocrocite (γ-FeOOH)', *Geochimica et Cosmochimica Acta*, 73: 4661-72.

Bricker, Owen. 1965. 'Some stability relations in the system Mn-O2-H2O at 25° and one atmosphere total pressure', *American Mineralogist*, 50: 1296-354.

Chukwuma, Chinazam Emmanuel, Owen William Duckworth, and Oliver Baars. 2025. 'Degradation of catecholate, hydroxamate, and carboxylate model siderophores by extracellular enzymes', *PLoS One*, 20: e0330432.

Cocozza, Claudio, Calvin C. G. Tsao, Sing-Foong Cheah, Stephan M. Kraemer, Kenneth N. Raymond, Teodoro M. Miano, and Garrison Sposito. 2002. 'Temperature dependence of goethite dissolution promoted by trihydroxamate siderophores', *Geochimica et Cosmochimica Acta*, 66: 431-38.

Cornell, Rochelle M, and Udo Schwertmann. 2003. *The iron oxides: structure, properties, reactions, occurrences, and uses* (Wiley-vch Weinheim).

Crumbliss, Alvin L., and James M. Harrington. 2009. 'Iron sequestration by small molecules: Thermodynamic and kinetic studies of natural siderophores and synthetic model compounds.' in Rudi van Eldik and Colin D. Hubbard (eds.), *Advances in Inorganic Chemistry* (Academic Press).

Cudennec, Yannick, and André Lecerf. 2006. 'The transformation of ferrihydrite into goethite or hematite, revisited', *Journal of Solid State Chemistry*, 179: 716-22.

Dubme, Anne-Kathrin, Robert Charles Hider, and Hicham Hussein Khodr. 1997. 'Synthesis and Iron-Binding Properties of Protochelin, the Tris (catecholamide) Siderophore of Azotobacter vinelandii', *Chemische Berichte*, 130: 969-73.

Duckworth, Owen W., John R. Bargar, Andrzej A. Jarzecki, Oyeyemi Oyerinde, Thomas G. Spiro, and Garrison Sposito. 2009. 'The exceptionally stable cobalt(III)–desferrioxamine B complex', *Marine Chemistry*, 113: 114-22.

Duckworth, Owen W., John R. Bargar, and Garrison Sposito. 2008. 'Sorption of ferric iron from ferrioxamine B to synthetic and biogenic layer type manganese oxides', *Geochimica et Cosmochimica Acta*, 72: 3371-80.

———. 2009a. 'Coupled biogeochemical cycling of iron and manganese as mediated by microbial siderophores', *BioMetals*, 22: 605-13.

———. 2009b. 'Quantitative Structure−Activity Relationships for Aqueous Metal−Siderophore Complexes', *Environmental Science & Technology*, 43: 343-49.
Duckworth, Owen W., and Garrison Sposito. 2005. 'Siderophore−Manganese(III) Interactions. I. Air-Oxidation of Manganese(II) Promoted by Desferrioxamine B', *Environmental Science & Technology*, 39: 6037-44.
———. 2007. 'Siderophore-promoted dissolution of synthetic and biogenic layer-type Mn oxides', *Chemical Geology*, 242: 497-508.
Edwards, David C., and Satish C. B. Myneni. 2005. 'Hard and Soft X-ray Absorption Spectroscopic Investigation of Aqueous Fe(III)−Hydroxamate Siderophore Complexes', *The Journal of Physical Chemistry A*, 109: 10249-56.
French, K. S., E. Chukwuma, I. Linshitz, K. Namba, O. W. Duckworth, M. A. Cubeta, and O. Baars. 2024. 'Inactivation of siderophore iron-chelating moieties by the fungal wheat root symbiont Pyrenophora biseptata', *Environ Microbiol Rep*, 16: e13234.
Green, M. A., and M. J. Welch. 1989. 'Gallium radiopharmaceutical chemistry', *Int J Rad Appl Instrum B*, 16: 435-48.
Haack, Elizabeth A., Cliff T. Johnston, and Patricia A. Maurice. 2008. 'Mechanisms of siderophore sorption to smectite and siderophore-enhanced release of structural Fe3+', *Geochimica et Cosmochimica Acta*, 72: 3381-97.
Hagvall, Kristoffer, Per Persson, and Torbjörn Karlsson. 2014. 'Spectroscopic characterization of the coordination chemistry and hydrolysis of gallium(III) in the presence of aquatic organic matter', *Geochimica et Cosmochimica Acta*, 146: 76-89.
Harrington, James M., John R. Bargar, Andrzej A. Jarzecki, James G. Roberts, Leslie A. Sombers, and Owen W. Duckworth. 2012. 'Trace metal complexation by the triscatecholate siderophore protochelin: structure and stability', *BioMetals*, 25: 393-412.
Harrington, James M., and Alvin L. Crumbliss. 2009. 'The redox hypothesis in siderophore-mediated iron uptake', *BioMetals*, 22: 679-89.
Harrington, James M., Owen W. Duckworth, and Kurt Haselwandter. 2015. 'The fate of siderophores: antagonistic environmental interactions in exudate-mediated micronutrient uptake', *BioMetals*, 28: 461-72.
Harrington, James M., Dorothy L. Parker, John R. Bargar, Andrzej A. Jarzecki, Bradley M. Tebo, Garrison Sposito, and Owen W. Duckworth. 2012. 'Structural dependence of Mn complexation by siderophores: Donor group dependence on complex stability and reactivity', *Geochimica et Cosmochimica Acta*, 88: 106-19.
He, Hongping, Ray L. Frost, Thor Bostrom, Peng Yuan, Loc Duong, Dan Yang, Yunfei Xi, and J. Theo Kloprogge. 2006. 'Changes in the morphology of organoclays with HDTMA+ surfactant loading', *Applied Clay Science*, 31: 262-71.
Hider, Robert C., and Xiaole Kong. 2010. 'Chemistry and biology of siderophores', *Natural Product Reports*, 27: 637-57.
Hiradate, S., and K. Inoue. 1999. 'Interactions of Mugineic Acid with Allophane, Imogolite, Montmorillonite and Gibbsite.' in J. Berthelin, P. M. Huang, J. M. Bollag and F. Andreux (eds.), *Effect of Mineral-Organic-Microorganism Interactions on Soil and Freshwater Environments* (Springer US: Boston, MA).
Holmén, Britt A., and William H. Casey. 1996. 'Hydroxamate ligands, surface chemistry, and the mechanism of ligand-promoted dissolution of goethite [α-FeOOH(s)]', *Geochimica et Cosmochimica Acta*, 60: 4403-16.

Kang, Kyounglim, and Jasquelin Peña. 2023. 'Siderophore-Mediated Mobilization of Manganese Limits Iron Solubility in Mixed Mineral Systems', *ACS Earth and Space Chemistry*, 7: 662-75.

Kappler, Andreas, and Casey Bryce. 2017. 'Cryptic biogeochemical cycles: unravelling hidden redox reactions', *Environmental Microbiology*, 19: 842-46.

Kraemer, S. M., D. E. Crowley, and R. Kretzschmar. 2006. 'Geochemical Aspects of Phytosiderophore-Promoted Iron Acquisition by Plants.' in, *Advances in Agronomy* (Academic Press).

Kraemer, Stephan M. 2004. 'Iron oxide dissolution and solubility in the presence of siderophores', *Aquatic Sciences*, 66: 3-18.

Kraemer, Stephan M., Singfoong Cheah, Rita Zapf, Jide Xu, Kenneth N Raymond, and Garrison Sposito. 1999. 'Effect of hydroxamate siderophores on Fe release and Pb(II) adsorption by goethite', *Geochimica et Cosmochimica Acta*, 63: 3003-08.

Kruft, Bonnie I., James M. Harrington, Owen W. Duckworth, and Andrzej A. Jarzęcki. 2013. 'Quantum mechanical investigation of aqueous desferrioxamine B metal complexes: Trends in structure, binding, and infrared spectroscopy', *Journal of Inorganic Biochemistry*, 129: 150-61.

Manceau, Alain, Bruno Lanson, and Victor A Drits. 2002. 'Structure of heavy metal sorbed birnessite. Part III: Results from powder and polarized extended X-ray absorption fine structure spectroscopy', *Geochimica et Cosmochimica Acta*, 66: 2639-63.

Maurice, Patricia A., Elizabeth A. Haack, and Bhoopesh Mishra. 2009. 'Siderophore sorption to clays', *BioMetals*, 22: 649-58.

Neubauer, U., G. Furrer, and R. Schulin. 2002. 'Heavy metal sorption on soil minerals affected by the siderophore desferrioxamine B: the role of Fe(III) (hydr)oxides and dissolved Fe(III)', *European Journal of Soil Science*, 53: 45-55.

Newville, Matthew. 2001. 'IFEFFIT: interactive XAFS analysis and FEFF fitting', *Journal of synchrotron radiation*, 8: 322-24.

O'Day, Peggy A., George A. Parks, and Gordon E. Brown. 1994. 'Molecular Structure and Binding Sites of Cobalt(II) Surface Complexes on Kaolinite from X-Ray Absorption Spectroscopy', *Clays and Clay Minerals*, 42: 337-55.

Peña, Jasquelin, Owen W. Duckworth, John R. Bargar, and Garrison Sposito. 2007. 'Dissolution of hausmannite (Mn3O4) in the presence of the trihydroxamate siderophore desferrioxamine B', *Geochimica et Cosmochimica Acta*, 71: 5661-71.

Rai, V., N. Fisher, O. W. Duckworth, and O. Baars. 2020. 'Extraction and Detection of Structurally Diverse Siderophores in Soil', *Front Microbiol*, 11: 581508.

Rehr, John J., Joshua J. Kas, Fernando D. Vila, Micah P. Prange, and Kevin Jorissen. 2010. 'Parameter-free calculations of X-ray spectra with FEFF9', *Physical Chemistry Chemical Physics*, 12: 5503-13.

Reichard, Petra Ulrike. 2005. 'Effects of microbial plant siderophore ligands on the dissolution of iron oxides', ETH Zürich.

Reichman, S. M., and D. R. Parker. 2005. 'Chapter 4 - Metal complexation by phytosiderophores in the rhizosphere.' in P. M. Huang and G. R. Gobran (eds.), *Biogeochemistry of Trace Elements in the Rhizosphere* (Elsevier: Amsterdam).

Remucal, Christina K., and Matthew Ginder-Vogel. 2014. 'A critical review of the reactivity of manganese oxides with organic contaminants', *Environmental Science: Processes & Impacts*, 16: 1247-66.

Renshaw, Joanna C., Geoff D. Robson, Anthony P. J. Trinci, Marilyn G. Wiebe, Francis R. Livens, David Collison, and Robin J. Taylor. 2002. 'Fungal siderophores: structures, functions and applications', *Mycological Research*, 106: 1123-42.

Robin, A., G. Vansuyt, P. Hinsinger, J. M. Meyer, J. F. Briat, and P. Lemanceau. 2008. 'Chapter 4 Iron Dynamics in the Rhizosphere: Consequences for Plant Health and Nutrition.' in, *Advances in Agronomy* (Academic Press).

Römheld, V., and H. Marschner. 1986. 'Evidence for a specific uptake system for iron phytosiderophores in roots of grasses', *Plant Physiol*, 80: 175-80.

Sarier, Nihal, Emel Onder, and Sabri Ersoy. 2010. 'The modification of Na-montmorillonite by salts of fatty acids: An easy intercalation process', *Colloids and Surfaces A: Physicochemical and Engineering Aspects*, 371: 40-49.

Schwyn, B., and J. B. Neilands. 1987. 'Universal chemical assay for the detection and determination of siderophores', *Anal Biochem*, 160: 47-56.

Shenker, M., Y. Chen, and Y. Hadar. 1995. 'Rapid Method for Accurate Determination of Colorless Siderophores and Synthetic Chelates', *Soil Science Society of America Journal*, 59: 1612-18.

Simanova, Anna A., John S. Loring, and Per Persson. 2011. 'Formation of Ternary Metal-Oxalate Surface Complexes on α-FeOOH Particles', *The Journal of Physical Chemistry C*, 115: 21191-98.

Simanova, Anna A., Per Persson, and John S. Loring. 2010. 'Evidence for ligand hydrolysis and Fe(III) reduction in the dissolution of goethite by desferrioxamine-B', *Geochimica et Cosmochimica Acta*, 74: 6706-20.

Sparks, Donald L. 2003a. '2 - Inorganic Soil Components.' in Donald L. Sparks (ed.), *Environmental Soil Chemistry (Second Edition)* (Academic Press: Burlington).

———. 2003b. '5 - Sorption Phenomena on Soils.' in Donald L. Sparks (ed.), *Environmental Soil Chemistry (Second Edition)* (Academic Press: Burlington).

Strawn, Daniel G. 2021. 'Sorption Mechanisms of Chemicals in Soils', *Soil Systems*, 5: 13.

Suzuki, Motofumi, Atsumi Urabe, Sayaka Sasaki, Ryo Tsugawa, Satoshi Nishio, Haruka Mukaiyama, Yoshiko Murata, Hiroshi Masuda, May Sann Aung, Akane Mera, Masaki Takeuchi, Keijo Fukushima, Michika Kanaki, Kaori Kobayashi, Yuichi Chiba, Binod Babu Shrestha, Hiromi Nakanishi, Takehiro Watanabe, Atsushi Nakayama, Hiromichi Fujino, Takanori Kobayashi, Keiji Tanino, Naoko K. Nishizawa, and Kosuke Namba. 2021. 'Development of a mugineic acid family phytosiderophore analog as an iron fertilizer', *Nature Communications*, 12: 1558.

Tebo, Bradley M., John R. Bargar, Brian G. Clement, Gregory J. Dick, Karen J. Murray, Dorothy Parker, Rebecca Verity, and Samuel M. Webb. 2004. 'BIOGENIC MANGANESE OXIDES: Properties and Mechanisms of Formation', *Annual Review of Earth and Planetary Sciences*, 32: 287-328.

Villalobos, Mario, Brandy Toner, John Bargar, and Garrison Sposito. 2003. 'Characterization of the manganese oxide produced by Pseudomonas putida strain MnB1', *Geochimica et Cosmochimica Acta*, 67: 2649-62.

Wang, Yuheng, Sassi Benkaddour, Francesco Femi Marafatto, and Jasquelin Peña. 2018. 'Diffusion- and pH-Dependent Reactivity of Layer-Type MnO2: Reactions at Particle Edges versus Vacancy Sites', *Environmental Science & Technology*, 52: 3476-85.

Whitaker, Andrew H., and Owen W. Duckworth. 2018. 'Cu, Pb, and Zn Sorption to Biogenic Iron (Oxyhydr)Oxides Formed in Circumneutral Environments', *Soil Systems*, 2: 18.

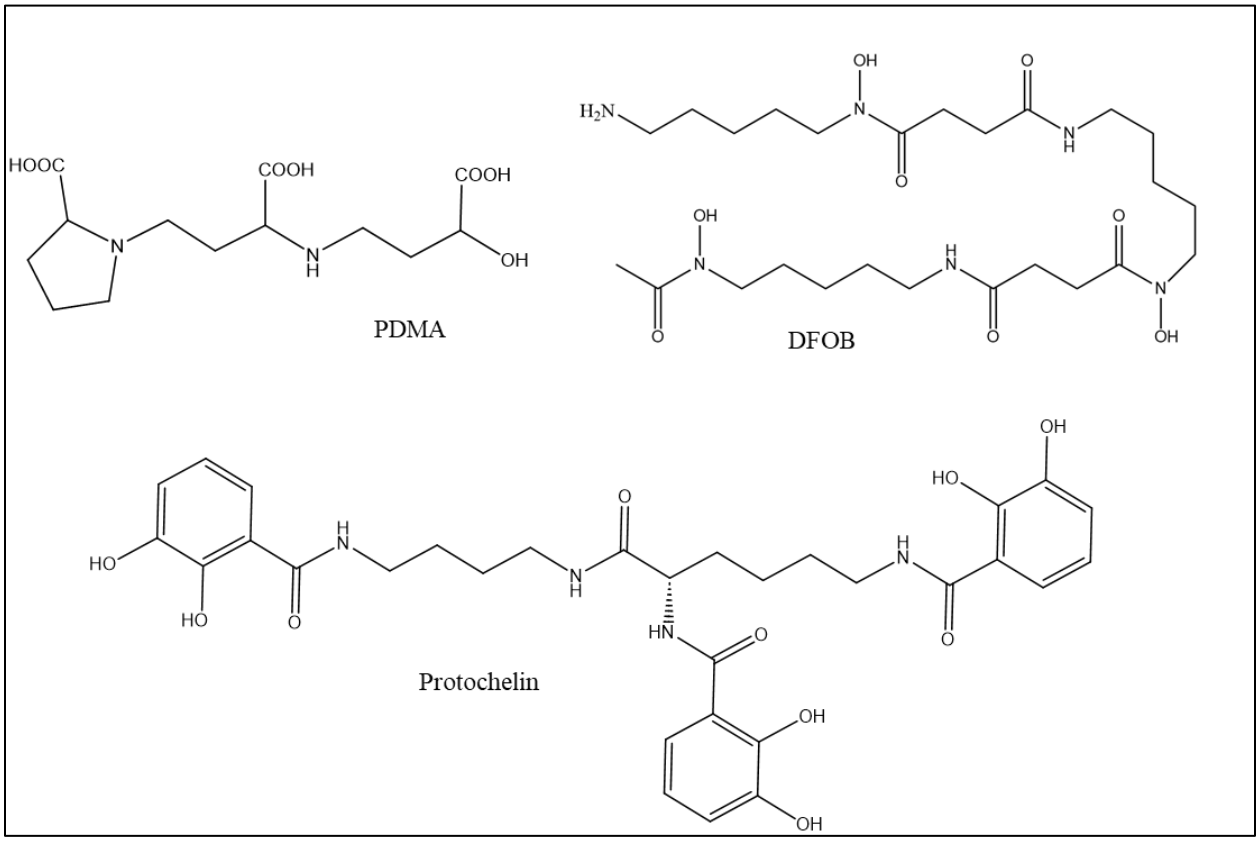

Figure 3.1. Structures of the siderophores proline-2᾽-deoxymugineic acid (PMDA), desferrioxamine-B (DFOB), and protochelin.

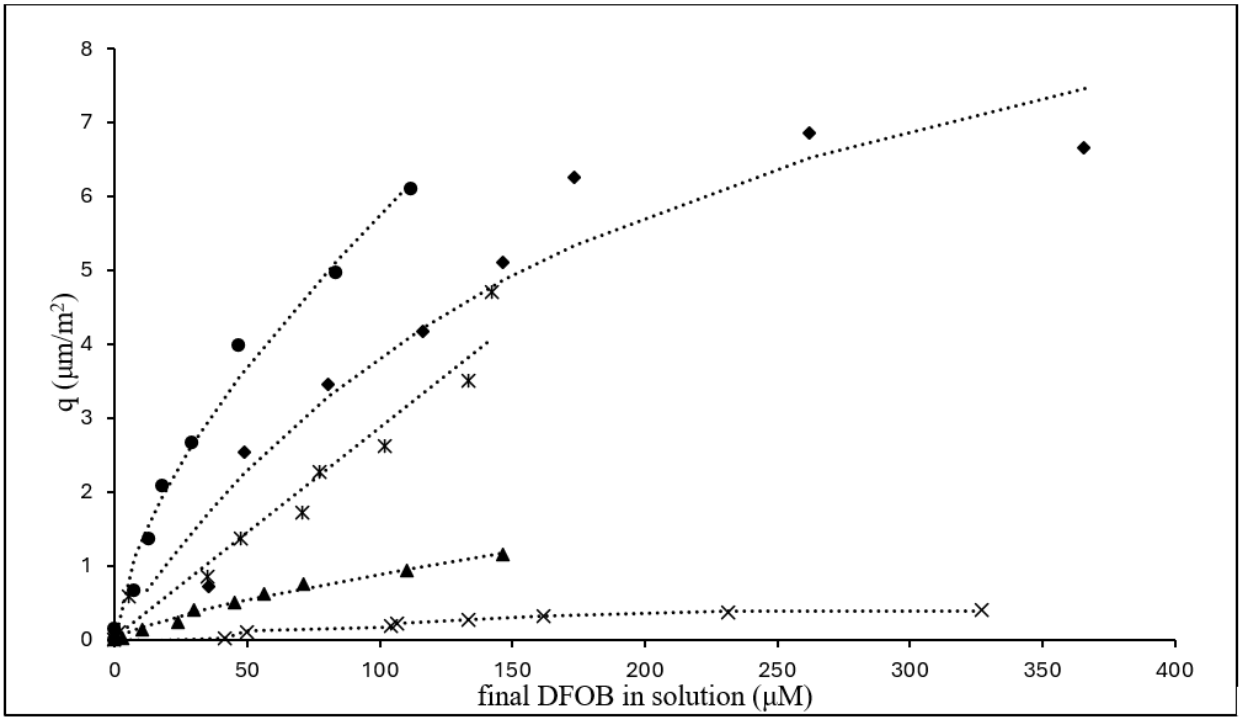

Figure 3.2. apo-DFOB isotherms (surface area normalized) onto δ-MnO_2 (triangles), goethite (asterisk), ferrihydrite (x's), montmorillonite (circles), and kaolinite (diamonds). Data sets were modeled with Freundlich sorption model (dashed line), with fit parameters shown in Table 1. Initial experimental conditions: 2 g L^{-1} sorbent, DFOB=0-500μM, pH=6.

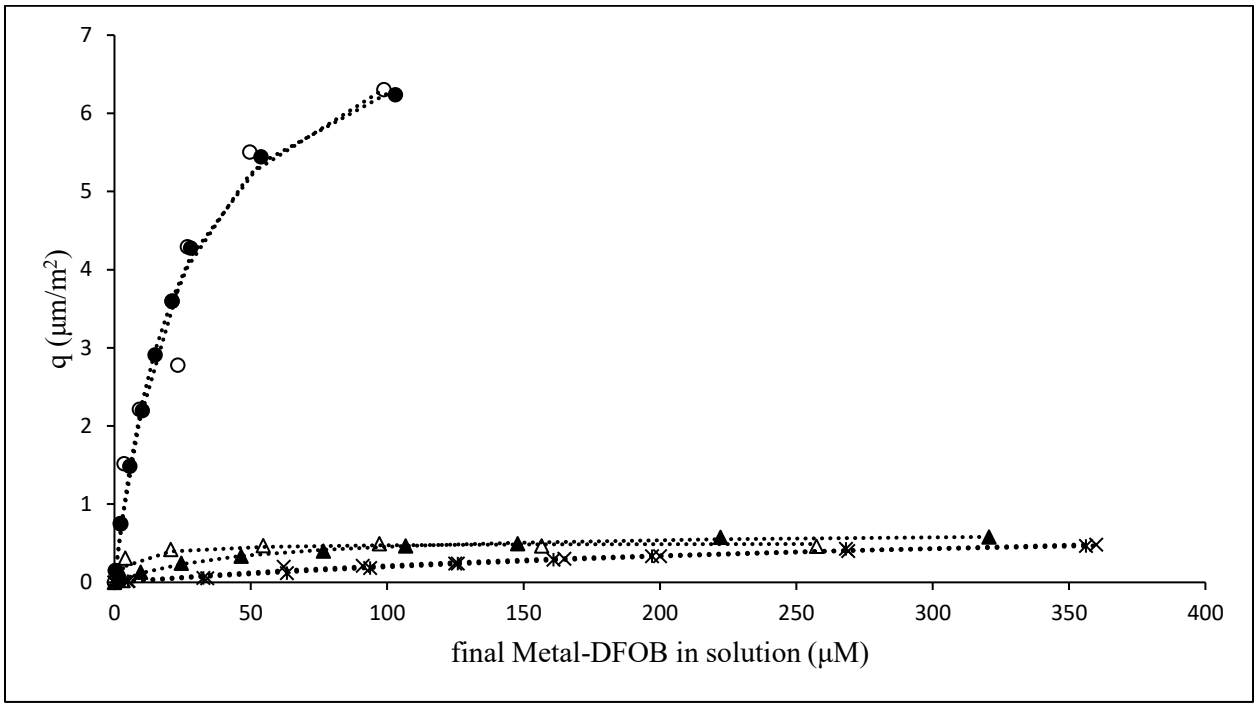

Figure 3.3. Fe(III)-DFOB (open and Ga(III)apo-DFOB isotherms (surface area normalized) onto δ-MnO_2 (triangles), ferrihydrite (x's), montmorillonite (circles). Data sets were modeled with Langmuir sorption model (dashed line), with fit parameters shown in Table 2. Initial experimental conditions: 2 g L^{-1} sorbent, DFOB=0-500μM, pH=6.

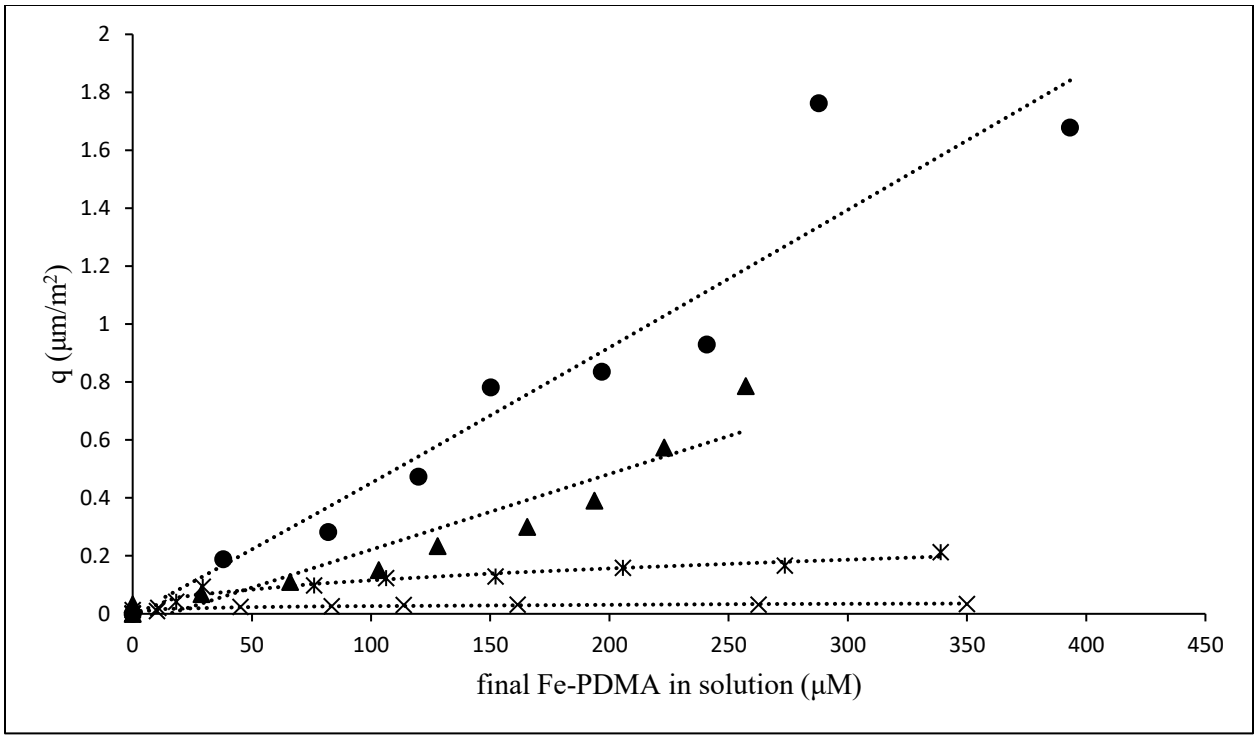

Figure 3.4. Fe(III)-PDMA isotherms (surface area normalized) onto δ-MnO_2 (triangles), goethite (asterisk), ferrihydrite (x's), and montmorillonite (circles). Data sets were modeled with Freundlich sorption model (dashed line), with fit parameters shown in Table 3. Initial experimental conditions: 2 g L^{-1} sorbent, Fe(III)-PDMA=0-500µM, pH=6.

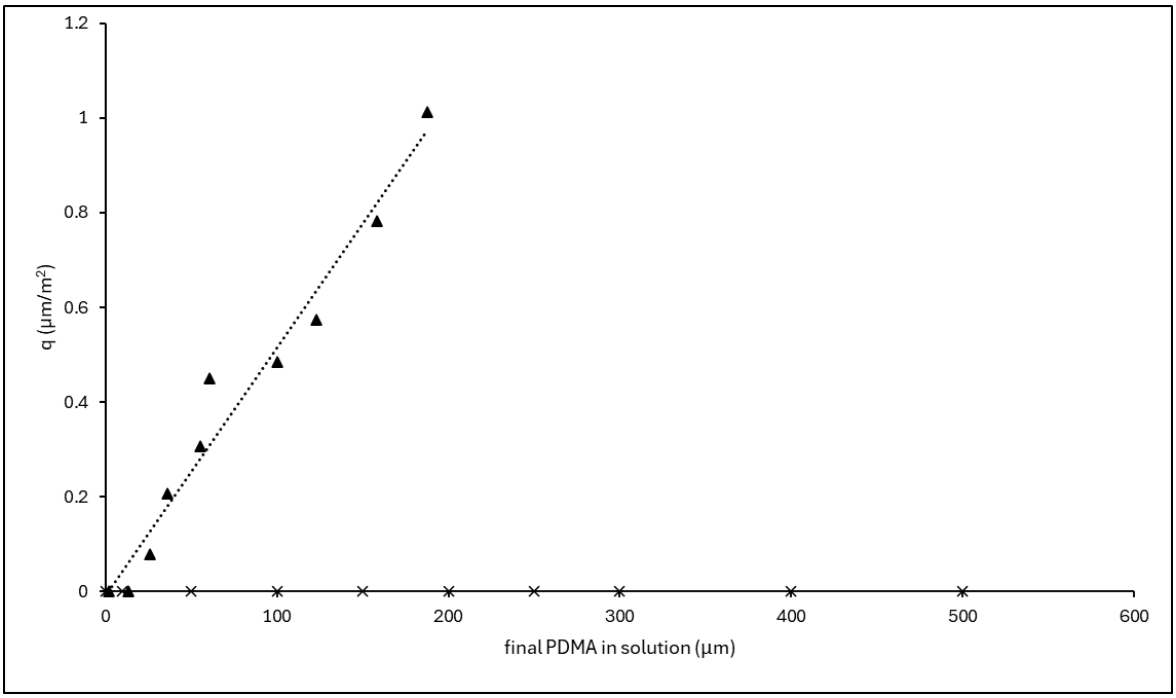

Figure 3.5. apo- PDMA isotherms (surface area normalized) onto δ-MnO_2 (triangles). Data sets were modeled with Freundlich sorption model (dashed line), with fit parameters shown in Table 4. Initial experimental conditions: 2 g L^{-1} sorbent, PDMA=0-500µM, pH=6.

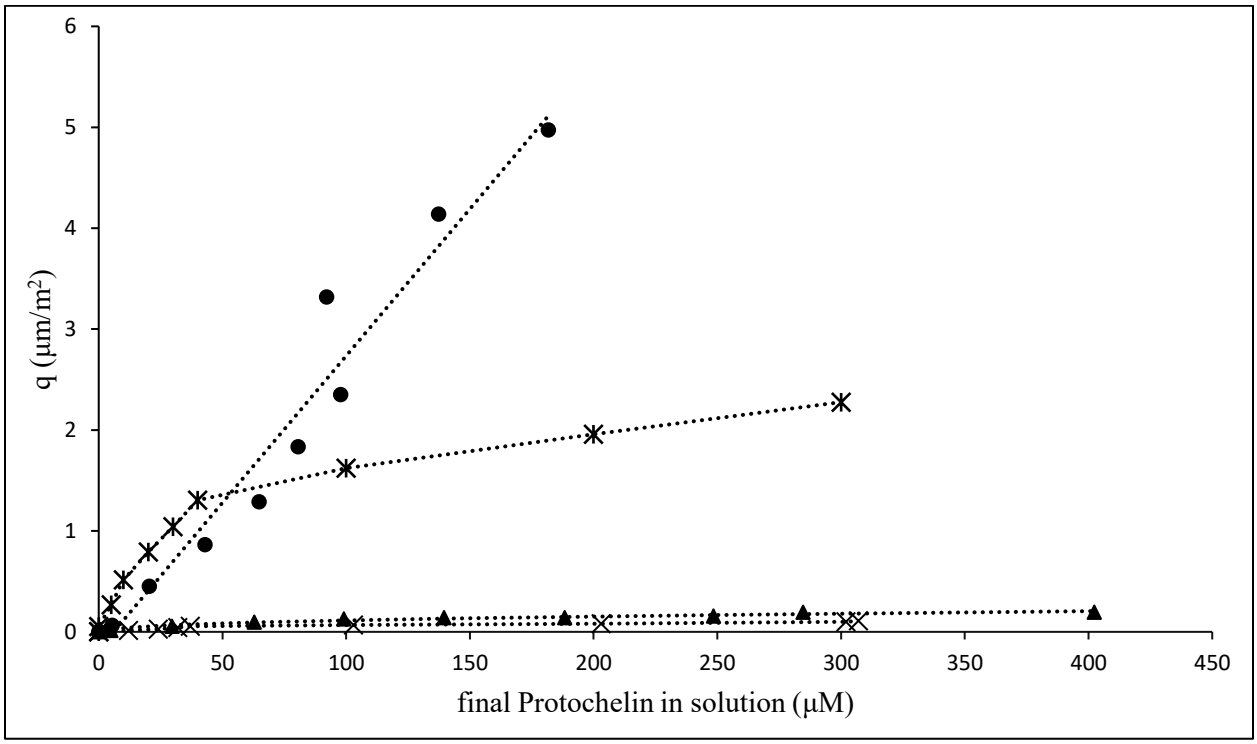

Figure 3.6. Protochelin isotherms (surface area normalized) onto δ-MnO_2 (triangles), goethite (asterisk), ferrihydrite (x's), and montmorillonite (circles). Data sets were modeled with Freundlich sorption model (dashed line), with fit parameters shown in Table 5. Initial experimental conditions: 2 g L^{-1} sorbent, Protochelin=0-500µM, pH=6.

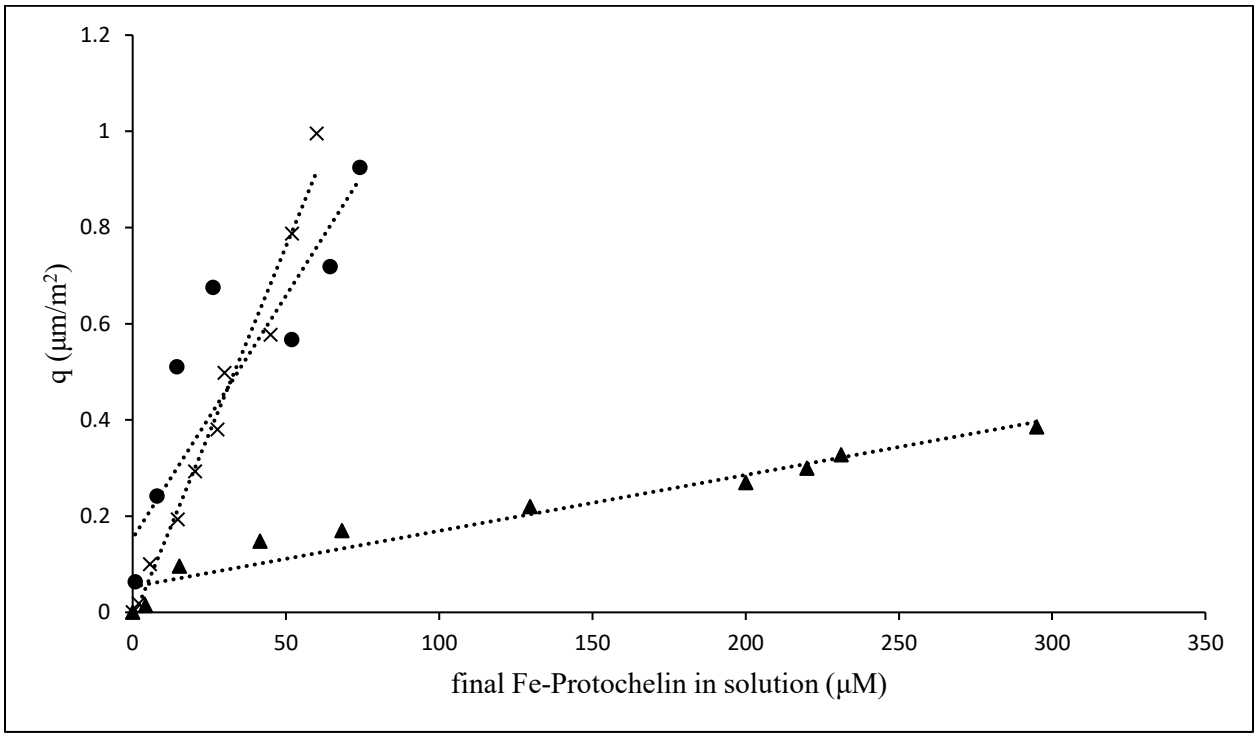

Figure 3.7. Fe(III)-protochelin isotherms (surface area normalized) onto δ-MnO_2 (triangles), goethite (asterisk), and montmorillonite (circles). Data sets were modeled with Freundlich sorption model (dashed line), with fit parameters shown in Table 6. Initial experimental conditions: 2 g L^{-1} sorbent, Fe(III)- protochelin=0-500µM, pH=6.

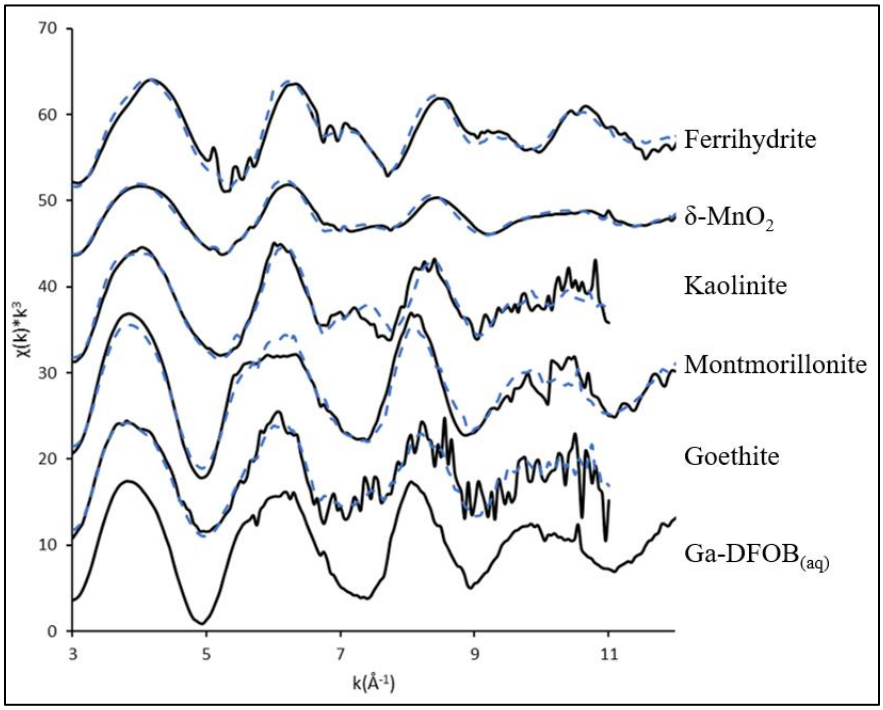

Figure 3.8. Chi EXAFS spectra for Ga(III)-DFOB onto ferrihydrite, MnO_2, kaolinite, goethite, montmorillonite, and aqueous Ga(III)-DFOB (1mm). Dashed lines represent fits.

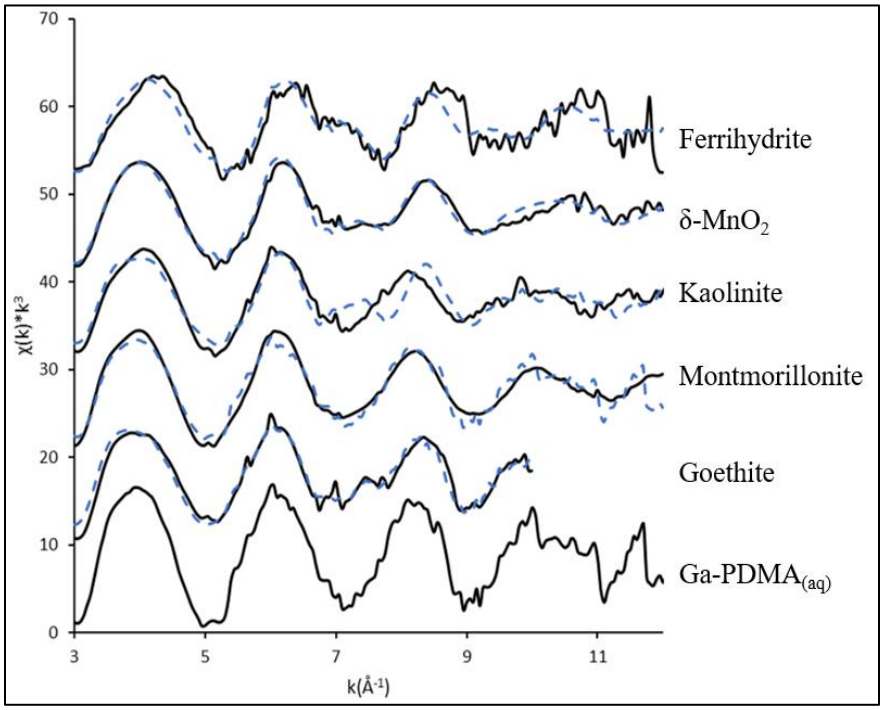

Figure 3.9. Chi EXAFS spectra for Ga(III)-PDMA onto ferrihydrite, MnO_2, kaolinite, goethite, montmorillonite, and aqueous Ga(III)-PDMA (1mm). Dashed lines represent fits.

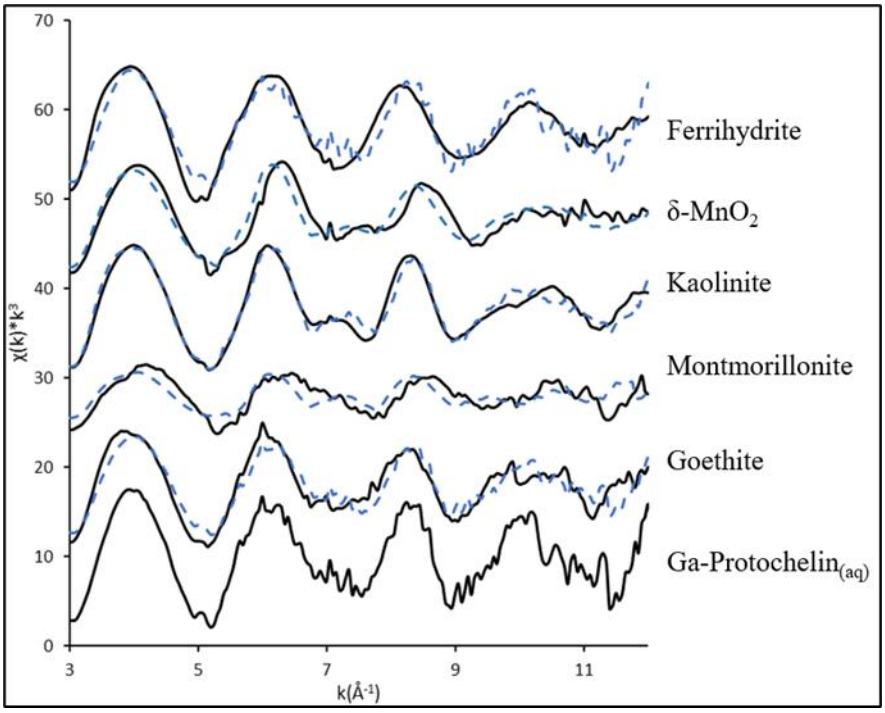

Figure 3.10. Chi EXAFS spectra for Ga(III)-protochelin onto ferrihydrite, MnO_2, kaolinite, goethite, montmorillonite, and aqueous Ga(III)-Protochelin (1mm). Dashed lines represent fits.

Table 3.1. Fitting parameters used to model DFOB sorption to montmorillonite, kaolinite, ferrihydrite, goethite, MnO_2. K_f = Freundlich sorption constant ($\mu mol/m^2$); n = exponential constant; E = model efficiency. Uncertainty is reported as standard error.

Apo-DFOB sorption to minerals (Freundlich Model)			
Adsorbent	**K_f ($\mu mol/m^2$)**	**n**	**E**
ferrihydrite	0.010 ± 0.004	0.75 ± 0.10	0.918
goethite	0.02 ± 0.03	1.0 ± 0.1	0.956
montmorillonite	0.311 ± 0.006	0.64 ± 0.05	0.984
kaolinite	0.16 ± 0.10	0.66 ± 0.01	0.848
δ-MnO_2	0.034 ± 0.005	0.74 ± 0.04	0.990

Table 3.2. Fitting parameters used to model Fe(III)-DFOB and Ga(III)-DFOB sorption to montmorillonite, goethite, and MnO_2. S_{max} = sorption maximum K = Langmuir binding coefficient; E = model efficiency. Uncertainty is reported as standard error.

Metal-DFOB sorption to minerals (Langmuir Model)				
Ion in complex	**Adsorbent**	**S_{max} (µmol/m^2)**	**K**	**E**
Fe(III)	montmorillonite	8.4 ± 1.0	0.031 ± 0.008	0.962
Ga(III)	montmorillonite	8.0 ± 0.8	0.038 ± 0.009	0.966
Fe(III)	δ-MnO_2	0.40 ± 0.05	0.23 ± 0.10	0.742
Ga(III)	δ-MnO_2	0.50 ± 0.02	0.022 ± 0.002	0.996
Fe(III)	goethite	0.80 ± 0.08	0.0020 ± 0.0003	0.995
Ga(III)	goethite	0.76 ± 0.09	0.003 ± 0.001	0.993

Table 3.3. Fitting parameters used to model Fe(III)-PDMA sorption to montmorillonite, ferrihydrite, goethite, δ-MnO_2. K_f = Freundlich sorption constant (μmol/m^2); n=exponential constant; E = model efficiency. Uncertainty is reported as standard error.

Fe(III)-PDMA sorption to minerals (Freundlich Model)			
Adsorbent	**K_f (μmol/m^2)**	**n**	**E**
goethite	0.020 ± 0.004	0.42 ± 0.05	0.964
montmorillonite	0.004 ± 0.003	1.0 ± 0.2	0.912
δ-MnO_2	0.0026 ± 0.0003	1.00 ± 0.04	0.901
ferrihydrite	0.010 ± 0.002	0.22 ± 0.04	0.936

Table 3.4. Freundlich parameters used to model PDMA sorption to MnO_2. K_f= Freundlich sorption constant (μmol/m^2); n = exponential constant; E = model efficiency. Uncertainty is reported as standard error.

Apo-PDMA sorption to minerals (Freundlich Model)			
Adsorbent	**K_f (μmol/m^2)**	**n**	**E**
δ-MnO_2	0.0052 ± 0.0003	0.001 ± 0.03	0.965

Table 3.5. Fitting parameters used to model protochelin sorption to montmorillonite, goethite, ferrihydrite, and δ-MnO_2. K_f = Freundlich sorption constant (μmol/m^2); n = exponential constant; E = model efficiency. Uncertainty is reported as standard error.

Apo-protochelin sorption to minerals (Freundlich Model)			
Adsorbent	**K_f(μmol/m^2)**	**n**	**E**
montmorillonite	0.02 ± 0.01	1.1 ± 0.1	0.955
δ-MnO_2	0.021 ± 0.003	0.43 ± 0.04	0.970
goethite	0.26 ± 0.04	0.38 ± 0.03	0.976
ferrihydrite	0.013 ± 0.002	0.43 ± 0.04	0.966
kaolinite	0.023 ± 0.004	0.46 ± 0.02	0.971

Table 3.6. Fitting parameters used to model Fe(III)-protochelin sorption to montmorillonite, goethite, and δ-MnO_2. K_f = Freundlich sorption constant (μmol/m^2); n = exponential constant; E= model efficiency. Uncertainty is reported as standard error.

Fe(III)-protochelin sorption to minerals (Freundlich Model)			
Adsorbent	**K_f (μmol/m^2)**	**n**	**E**
montmorillonite	0.10 ± 0.05	0.5 ± 0.1	0.862
δ-MnO_2	0.024 ± 0.005	0.52 ± 0.04	0.981
goethite	0.015 ± 0.003	1.11 ± 0.09	0.980

Table 3.7. EXAFS structure fitting results. Numbers represent the normalized best fit by the aqueous complex, with remainder of the fit from Ga(III)-mineral spectra. Fits were normalized to 100% but were 0.88 ± 0.11. Ferrihydrite, δ-MnO_2, kaolinite, and montmorillonite complexes were fit from k = 3–13 $Å^{-1}$, whereas goethite complexes were fit from k = 3–10 $Å^{-1}$.

Sorbent	Ga(III)-DFOB (%)	Ga(III)-PDMA (%)	Ga(III)-Protochelin(%)
ferrihydrite	0	0	100
δ-MnO_2	0	0	0
kaolinite	0	0	28
montmorillonite	100	70	33
goethite	36	35	38

Table 3.8. d(001) distances calculated from XRD for montmorillonite after sorption of siderophores, Ga(III)-siderophores, or Ga(III). $\Delta_{d(001)}$ refers to the change in basal spacing of the montmorillonite with adsorbed species compared to air dried montmorillonite. Positive $\Delta_{d(001)}$ represents an increase in basal spacing, and negative $\Delta_{d(001)}$ represents a decrease in basal spacing.

Adsorbate	***d*(001) (Å)**	***Δ*$_{d(001)}$ (Å)**
None	6.28	-
Ga(III)	5.22	-1.04
DFOB	6.78	0.52
PDMA	5.12	-1.14
Protochelin	5.66	-0.60
Ga(III)-DFOB	6.88	0.62
Ga(III)-PDMA	6.37	0.11
Ga(III)-protochelin	5.83	0.43

CHAPTER 4: Elucidating the Fate of Siderophores in Soil Systems through μ-XRF and μ-EXAFS

1. Introduction

Iron (Fe) is typically held in insoluble (oxyhydr)oxide mineral phases that are not readily available for biological uptake at circumneutral pH in soils. However, Fe is an essential element for all organisms that is widely used in electron transport and metabolic processes. In response to biological unavailability of Fe, microorganisms, fungi, and gramineous plants have evolved various strategies to promote its uptake from soil environments. One strategy involves the production of siderophores, low molecular weight compounds possessing high affinity and selectivity for Fe(III) (Schwyn and Neilands 1987). Siderophores are structurally diverse, with over 500 different structures containing combinations of chelating moieties including hydroxamate, carboxylate, α-hydroxycarboxylate and catecholate groups, each with unique chemical properties that behave differently in soil environments (Hider and Kong 2010).

For siderophore mediated uptake to occur, Fe must be solubilized from a bio-unavailable source and then a Fe-siderophore complex must travel back to the organism. Because of the complicated and dynamic nature of soil systems, a myriad of reactive agents, including mineral surfaces and organic matter, can disrupt this process. Currently, the complex roles siderophores play in the soil ecosystem, and the factors affecting their efficiency are not yet well understood. Abundant natural soil Fe convolutes efforts to study the fate of Fe-siderophore complexes in soil systems, leaving significant questions regarding where and when siderophore production becomes critical to organism nutrition, microbial competition, or soil biogeochemical processes unresolved.

Studies of siderophores in soils have traditionally relied on extraction followed by mass spectrometry or assay quantification (Rai et al. 2020; Powell et al. 1980). Ahmed and Holmström 2014 studied the distribution of hydroxamate siderophores in a podzol soil, as well as the

concentration of siderophores on buried polished mineral surfaces (Ahmed and Holmström 2014). The concentration of hydroxamates adsorbed to mineral surfaces was determined to be higher than that in the bulk soil. However, success with siderophore extraction has mostly been limited to hydroxamate type siderophores (Rai et al. 2020). Schenkeveld et. al. 2014 studied metal mobilization by phytosiderophores in individual soils experimentally and via multi surface models but did not consider complex adsorption in models (Schenkeveld et al. 2014). Recently, (*Evers in prep*) studied reactions between both apo siderophores and Fe(III)- siderophores complexes and antagonistic soil minerals. To study the fate of siderophore complexes, Ga(III), which is close to Fe(III) in size and electron configuration (Green and Welch 1989) and forms siderophore complexes with similar binding affinity and local structure (Evers et al. 1989; Nicolafrancesco et al. 2019; Duckworth, Bargar, and Sposito 2009), was used as a proxy for Fe in X-ray absorption spectroscopy (XAS) experiments. Results showed marked differences in the reactivity of siderophores with different structures with differing soils minerals, suggesting the possibly of applying analogous approaches in soil systems.

To better understand the fate of siderophore complexes in soils, micro-X-ray fluorescence (μ-XRF) mapping paired with micro-extended X-ray absorption fine structure (μ-EXAFS) spectroscopy was utilized to probe the fate of Ga(III) complexes with the trishydroxamate siderophore desferrioxamine B (DFOB), the triscatecholamide siderophore protochelin, and the carboxylate mugineic acid derivative phytosiderophore proline-2'-deoxymugeneic acid (PDMA) in soils with differing edaphic properties. Synchrotron-based μ-XRF allowed for in situ mapping and determination of chemical associations of elements in soils at the micron scale with high sensitivity (Majumdar et al. 2012). When paired with structural data from μ-EXAFS, the coordination environment of Ga(III) from siderophores and fate of Ga(III)-siderophore complexes

soil environments was observed. The results of this study provides unique insights into how structurally distinct siderophores behave in diverse soil environments, with the potential to guide future best management practices to develop sustainable methods of biofortifying our crops to combat nutrient deficiencies.

2. Methods

2.1. Materials. All **s**olutions were prepared using ASTM Type 1 (>18.2 MΩ·cm) deionized water (DI). Unless otherwise noted, all chemicals used were of reagent grade from Fisher Scientific (Hampton, NH) or Sigma-Aldrich (St. Louis, MO). The three siderophores examined in this study were chosen for their structural diversity. The mesylate salt of the trishydroxamate siderophore DFOB was purchased from Sigma Aldrich (>92.5%) and used without any further purification. Protochelin (a triscatecholamide siderophore) were synthesized by the Duke University Small Molecules Custom Synthesis Facility (Harrington et al. 2012). Proline-2′-deoxymugineic acid PDMA was provided as PDMA·2HCl by Aichi Steel Corporation (Japan) (Suzuki et al. 2021).

*2.3. Soils***.** Soils chosen for this study include a Cassville clay, Gruver series, and a Belhaven muck. All soils were air dried and passed through a 2 mm sieve. The Cassville series was sourced from Cassville County, NC and classified as a sandy clay loam (51.5% sand, 17.6% silt, 30.9% clay) with a pH of 6.5 ± 0.2. The Gruver series was sourced from Goodwell, Oklahoma, and is a no-till agricultural soil (irrigated corn into alfalfa) with a pH of 8.0 ± 0.4. The Belhaven series was sourced from a field in Plymouth, NC and is a poorly drained organic soil with a pH of 6.3 ± 0.3. Total Fe and Mn concentrations in the soils was determined via XRF (Niton 5XL+) in soils mode. The Cassville soil was selected as a high activity clay soil, the Belhaven muck as an organic soil, and the Gruver as an alkaline soil to cover a range of soil environments.

2.3. Ga(III)-siderophore complex reacted with soil. Aqueous Ga(III)-DFOB, Ga(III)-PDMA, and Ga(III)-protochelin complexes were adsorbed to the three soils previously mentioned. Aqueous (1mM, pH 6) solutions of Ga(III)-siderophore were reacted with the soil with a solid loading 2 g/L. Solutions were allowed to equilibrate for 24 h in the dark while mounted on a rotary wheel at 20 RPM. The supernatant was collected, passed through a 0.2 μm filter, and analyzed for aqueous Ga concentration via inductive coupled plasma-optical emission spectrometry (ICP-OES; Perkin Elmer Optima 800). Solids were collected, air dried, and stored in a freezer for analysis via bulk EXAFS as well as spatially resolved μ-XRF and μ-EXAFS.

2.4. Ga K-edge extended X-ray absorption fine structure spectroscopy. Bulk Ga K-edge XAS spectra were collected at the Stanford Synchrotron Radiation Lightsource (SSRL) under normal operating conditions on beamline 11−2 on samples consisting of Ga(III)-siderophore adsorbed to soils. Spectra were energy calibrated by adjusting the E_0 to an elemental Ga sample. Spectra were collected in fluorescence mode using a 100-element Ge detector or in transmission mode. The energy was selected by using a variable-exit Si(220) double-crystal monochromator and harmonics were rejected with a rhodium-coated mirror. Spectra were collected using Soller slits and a Zn X-ray filter improved the signal-to-noise ratio. Three spectra were collected for each sample, with no evidence of beam damage in successive scans, and averaged to improve the signal-to-noise ratio. For 2 samples, transmission data was used due to poor fluorescence data quality.

Ga K-edge spectra were energy calibrated, averaged, background-subtracted, splined, and linear combination fit (LCF) (Kelly, Hesterberg, and Ravel 2008) using the SIXPACK (Webb 2005) interface which makes use of the IFEFFIT code (Newville 2001). LCF analyses were conducted with previously published Ga(III)-siderophore mineral standards (Evers in prep) which are summarized in the SI. All spectral components used in fits were extensively characterized in Evers

et al. Because Ga(III)-DFOB and Ga(III)-PDMA were found to intercalate predominantly as intact complexes in montmorillonite, free Ga(III)-DFOB and Ga(III)-PDMA can be interpreted not mineral associated, outersphere complexes, or intercalated species. The presence of standards having Ga(III) sorbed to minerals in the absence siderophore in the fits of spectra from Ga(III)-siderophore complex sorption were interpreted as dissociation of the complex followed by sorption of Ga(III) to the surface, or as the formation of ternary surface complexes. Components found to make up less than 5% of the spectral reconstruction were removed, and fits were recalculated with the remaining standards.

To prepare mineral standards, Ga(III) (1mM) was exposed to mineral surfaces at pH 6 and a suspension loading of 2 g/L. After an equilibration period of either 24 hours or 2 hours (depending on mineral dissolution rates), the suspension was passed through 0.2 μm filter and the filtrate was analyzed for Ga concentration via inductive coupled plasma-optical emission spectrometry (ICP-OES; Perkin Elmer Optima 800). Solids were collected and air dried for XAS measurement, and Ga K-edge XAS spectra were collected at beamline 11-2 as described above.

2.5. μ-X-ray fluorescence spectroscopy. μ-XRF and μ-EXAFS spectroscopy were conducted at the Stanford Synchrotron Radiation Lightsource (SSRL) at Beamline 2-3. A thin layer of Ga(III)-siderophore soil was placed into a silicon mold, and a two-part epoxy resin (Epotek 301) was poured over the material and allowed to cure for 24 hours. Once dry, the epoxy block was glued to a quartz microscope slide (Chemglass) with the soil side down. These samples were thin-sectioned by grinding to ca. 200-300 nm in thickness (Buehler PetroThin). At beamline 2-3, incident beam energy was set to 11000 eV using a Si(111) monochromator and fluorescence data was collected for Ga using a CCD detector. Discrete areas were scanned in fluorescence mode using a vortex detector; scans were collected with a step size of 7 μm and a 15 ms dwell time. The

μ-XRF spatial maps were then used to identify points of high Ga concentration (hot spots) where μ-EXAFS spectra for Ga were collected using a Vortex silicon drift detector and a 5 μm beam size. μ-XRF maps were analyzed using SMAK (Webb 2011), and μ-EXAFS scans were analyzed in SIXPACK as described earlier. SMAK software was used to determine areas of high Ga concentration, as well as the spatial correlations between Ga and other elements. LCF fitting in SIXPACK was used to determine in what form the Ga was predominant in the hotspots.

3. Results

A summary of total Fe and Mn concentrations in the soils can be found in Supplementary Table 1. The Cassville clay soil contained the highest Fe content with 1,168.9 mmol Fe/kg. The Gruver contained the second highest Fe with 345.2 mmol/kg, and the Belhaven contained the lowest with 114.9 mmol Fe/kg. Altough the Belhaven soil contained the least total Fe, it had the greatest Fe dissolution (Table 1). The Cassville and Gruver had similair total Mn contents (8.1 and 7.8 mmol/kg, respectively), whereas the Belhaven contained low total Mn (0.38 mmol/kg).

Table 1 shows the amount of Ga sorbed (as determined by Ga lost from solution after experiments) onto each soil when Ga(III)-DFOB, Ga(III)-PDMA, and Ga(III)-protochelin complexes were allowed to react with Cassville clay, Belhaven muck, and Gruver soil. The greatest Ga(III) sorption to the Cassville clay occurred in Ga(III)-protochelin experiments, whereas Ga(III)-PDMA had the greatest sorption onto the Belhaven muck and Gruver soil. Ga(III)-Protochelin caused the most Fe and Mn dissolution from the Cassville, the Belhaven, and the Gruver soil.

Figure 1 shows Ga μ-XRF maps for Ga(III)-siderophore complexes adsorbed to Cassville clay soil (top row), Belhaven Muck (middle row) and Gruver soil (bottom row). Small areas on

the μ-XRF maps with the highest Ga signal were designated as Ga hotspots. For each Ga(III)-siderophore soil sample, μ-EXAFS spectra were collected from hotspots identified on μ-XRF maps using a 5 μm beam size. Bulk EXAFS data was also collected to give a broader understanding of the fate of Ga(III)-siderophore complexes in the whole sample. Spectra (*k*-space plots) and LCF fits and of both hotspot and bulk EXAFS can be found in Figure 2, 3, and 4, for the Cassville, Belhaven, and Gruver, respectively.

The top row of the figure shows interactions of siderophores with the Cassville soil. From the μ-XRF map (Figure 1), the Ga distribution for Ga(III)-DFOB adsorbing onto the Cassville clay was concentrated in three places, with one larger, irregularly shaped hotspot (200 μm), and two smaller hotspots (25 μm). The Ga(III)-PDMA distributed more evenly across the soil, with two small hotspots (20 and 30 μm). The Ga(III)-protochelin map shows Ga(III)associating with triangular soil particles evenly distributed across the map (300 μm). Sorption visually appeaers different across this soil for the three different siderophores, and this is reflected in the μ-EXAFS results (Table 2, 3, and 4), where fit components vary among the siderophores.

For the Belhaven muck (middle row), Ga(III)-DFOB, Ga(III)-PDMA, and Ga(III)-protochelin visually sorbed similarily, with Ga accumulating on a few small particles. Ga(III)-DFOB and Ga(III)-PDMA had small round hotspots (80 μm), with the Ga(III)-protochelin had a slightly larger elongated hotspot (120 μm). In contrast, for the Gruver series soils (bottom row) Ga(III)-DFOB sorbed more uniformly, with only one small round hotspot near the top of the map (30 μm). The Ga(III)-PDMA μ-XRF map shows Ga mostly accumulating on one specific elongated particle on the edge of the map (270 μm), with low Ga concentrations in the rest of the map. Ga(III)-protochelin also adsorbed onto elongated particles on the Gruver series (100 μm), with low concentrations in the rest of the sample. Additionally, the Gruver soil contained the

highest quantity and most concentrated areas of high Fe (20 μm) evenly distributed across the map (SI Figure 1).

Table 2 show the LCF fitting results for spectra of Ga(III)-DFOB, Ga(III)-PDMA, and Ga(III)-protochelin adsorbed to the Cassville clay soil. In the Ga(III)-DFOB sample, the spectra from the Ga hotspot in the map were best fit by 28% Ga(III)-DFOB complex, 40% Ga(III) sorbed to δ-MnO_2, and 25% Ga(III) sorbed to ferrihydrite. The R^2 value ($p<0.05$) of Ga correlated with Fe and Mn was 0.57 and 0.41, respectively over the entire map (SI table 2). When isolating the hotspot, significant ($p<0.05$) correlation coefficients of $R^2 = 0.63$ for Ga-Fe and $R^2 = 0.42$ for Ga-Mn were observed (SI Table 3). The bulk EXAFS spectra for Ga(III)-DFOB reacted with the Cassville soils were best fit by 11% Ga(III)-DFOB complex, 38% Ga(III) sorbed to ferrihydrite, 27% Ga(III) sorbed to Pahokee peat, and 23% Ga(III) sorbed to kaolinite. The hotspot contained a higher percentage of retained Ga(III)-DFOB than the bulk, whereas the bulk contained a higher percentage fit of Ga(III)-ferrihydrite.

Two sets of EXAFS hotspot data were collected for Ga(III)-PDMA adsorbed to the Cassville clay. The first hotspot spectrum was best fit with 49% Ga(III)-PDMA, 9.4% Ga(III) sorbed onto ferrihydrite, and 41.5% Ga(III) sorbed to montmorillonite. The second hotspot spectrum fit was composed of 67% Ga(III)-PDMA, 15.7% Ga(III) sorbed to ferrihydrite, and 15.7% Ga(III) sorbed to montmorillonite. The bulk EXAFS was composed of 5.7% Ga(III)-PDMA, 19.2% Ga(III) sorbed to ferrihydrite, 40.3% Ga(III) sorbed to montmorillonite, 24% Ga(III) sorbed to pahokee peat, and 10.6% Ga(III) sorbed to δ-MnO_2. Both hotspots consisted of the same components, while the bulk data contained additional organic and Mn components. Both Fe and Mn showed significant correlations ($p<0.05$) with Ga in the overall map (R^2 of 0.57 and 0.52, respectively) (SI table 2). In the first hotspot, an R^2 of 0.29 was observed for the Ga-Fe

correlation, and 0.18 for the second hotspot. The hotspots contained Ga-Mn R^2 of 0.41 and 0.006 respectively. In the hotspots in this sample, all correlations were either not significant ($p>0.05$) or had low Pearson coefficients (defined herein as $R^2 <0.5$).

Two sets of hotspot data were also collected for Ga(III)-protochelin adsorbed onto the Cassville clay. The first hotspot EXAFS spectrum LCF fit was composed of 25.9% Ga(III)-protochelin, 20.9% Ga(III) sorbed onto ferrihydrite, and 56.7% Ga(III) sorbed onto organic matter. The second hotspot spectrum was best fit with 11.5% Ga(III)-Protochelin complex, 62% Ga(III) sorbed to ferrihydrite, and 23% Ga(III) sorbed to montmorillonite. The bulk EXAFS spectrum fit was composed of 31.9% Ga(III)-protochelin complex, and 68% Ga(III) sorbed to ferrihydrite. The first hotspot fit contained a higher retained percentage than the second hotspot, however the most Ga(III)-protochelin complex was observed in the fit for the bulk sample. As with the other Cassville soil samples, the μ-XRF map showed high Ga-Fe and Ga-Mn correlations with an R^2 value of 0.60 and 0.62 ($p <0.05$) (SI table 2) for the overall map. The hotspot correlations were also statistically significant ($p <0.05$) for Fe and Mn (Ga-Fe R^2 of 0.81 and 0.69, and Ga-Mn R^2 of 0.85 and 0.76).

The correlations observed for Ga-Fe and Ga-Mn for all siderophores throughout the Cassville clay are further illustrated in the gradient plots shown in Supplementary Figure 2. These plots depict the spatial distribution of each element, with green hues indicating regions of elevated Ga concentration and red hues corresponding to areas enriched in Fe. Overlapping signals of these two elements produce orange hues, representing their co-localization. Consistent with the strong correlations, all siderophore Cassville plots display widespread orange coloration, indicating substantial spatial overlap between Ga and Fe.

Table 3 shows the LCF fitting results for spectra of Ga(III)-DFOB, Ga(III)-PDMA, and Ga(III)-protochelin adsorbed to the Belhaven muck. The Ga(III)-DFOB hotspot spectrum was best fit with 12.2% Ga(III)-DFOB and 88.0% Ga(III) sorbed to ferrihydrite. The bulk EXAFS spectrum was best fit with 27.5% Ga(III) sorbed to ferrihydrite, 37.6% Ga(III) sorbed to organic matter, and 31.8% Ga(III) sorbed to δ-MnO_2. The Belhaven muck is an organic soil, and correspondingly, the highest fit percentage in the bulk was Ga(III) associated with organic matter. In the Belhaven muck, Ga had low correlation coefficients R^2 of 0.23 and 0.10 with Fe and Mn, respectively, in the overall map (SI Table 2). However, R^2 correlations increased but remained low (to 0.35 and 0.44 for Fe and Mn, respectively) when focusing on hotspots (SI Table 3).

The spectrum of a Ga(III)-PDMA hotspot in the Belhaven Muck was best fit with 28.8% Ga(III) sorbed to kaolinite, 15.5% Ga(III) sorbed to ferrihydrite, 40% Ga(III) sorbed to montmorillonite, and 13.3% Ga(III) sorbed to organic matter. A spectrum from the second hotspot was best fit with 31% Ga(III) sorbed to ferrihydrite, and 69% Ga(III) sorbed to montmorillonite. The bulk EXAFS was best fit with 11% Ga(III) sorbed to kaolinite, 30% Ga(III) sorbed to ferrihydrite, 10% Ga(III) sorbed to montmorillonite, 38.5% Ga(III) sorbed to organic matter, and 8.2% Ga(III) sorbed to δ-MnO_2. The bulk EXAFS spectrum fit was the most components out of any spectra, and more varied than its accompanying hotspots, being comprised of every component. As with the Ga(III)-DFOB, the highest fit percentage was Ga(III) associated with organic matter. Fe and Mn correlations with Ga were low and not significant ($p>0.05$) in overall maps (R^2 of 0.07 and 0.02), and remained low when focusing on hotspot 1. The only significant correlation observed was an R^2 of 0.74 ($p<0.05$) for Ga-Fe in the second hotspot. (SI table 2 and 3).

The spectrum from hotspot for Ga(III)-protochelin adsorbed to the Belhaven muck was best fit with 65.6% Ga(III)-protochelin complex, and 33.3% Ga(III) sorbed to ferrihydrite. The bulk EXAFS spectra was best fit with 10% Ga(III)-protochelin complex, 18.8% Ga(III) sorbed to ferrihydrite, 45% Ga(III) sorbed to organic matter, and 18.8% Ga(III) sorbed to kaolinite. The hotspot contained a much higher percentage of whole complex than the bulk spectra. Although the bulk contained similar components as the hotspot, almost half the Ga(III) was found to be associated with organic matter. Ga was not found to correlate ($p>0.05$) with Fe or Mn in the overall map (SI table 2). However, Ga significantly correlated ($p <0.05$) with Fe (R^2 of 0.52) and Mn (R^2 of 0.51) in the hotspot.

The gradient plots presented in Supplementary Figure 2 support the low Pearson correlation coefficients observed in the Belhaven map. These plots reveal a clear spatial distinction between Ga and Fe, with only limited regions exhibiting co-localization of both elements. Overall, the distribution of Ga appears relatively uniform, whereas Fe is concentrated in discrete hotspots that lack corresponding Ga signals.

Table 4 shows the results of LCF fitting analysis for Ga(III)-DFOB, Ga(III)-PDMA, and Ga(III)-protochelin adsorbed to the Gruver soil. The spectrum of a hotspot for Ga(III)-DFOB was best fit with 100% Ga(III) sorbed to ferrihydrite. The bulk EXAFS spectrum was best fit with 13% Ga(III)-DFOB complex, and 86% Ga(III) sorbed to ferrihydrite. Ga showed low correlations or not significant ($p>0.05$) with Fe and Mn in the overall map (R^2 of 0.18 and 0.08, respectively) but was significantly correlated ($p<0.05$) in the hotspot (R^2 of 0.86 and 0.70, respectively).

The spectrum from hotspot for Ga(III)-PDMA adsorbed into the Gruver series soil was best fit with 44% Ga(III) sorbed to kaolinite, and 59% Ga(III) sorbed to ferrihydrite. The bulk EXAFS spectrum was best fit with 87% Ga(III) sorbed to ferrihydrite, and 12.9% Ga(III) sorbed

to organic matter. As with Ga(III)-DFOB, Ga had a low Pearson coefficient with Fe (R^2 of 0.21) and not was significantly ($p>0.05$) correlated with Mn in the overall map (R^2 of 0.06) (SI Table 2). The Ga-Fe correlation increased to $R^2 = 0.56$ in the hotspot but the Ga-Mn Pearson coefficient remained low ($R^2 = 0.26$)(SI Table 3).

For the bulk sample, the EXAFS spectra was best fit with 100% Ga(III) sorbed to ferrihydrite. However, Ga had a low Pearson coefficient with Fe in the overall map (R^2 of 0.14) (SI Table 3). We were unable to collect hotspot EXFAS spectra for this sample, most likely because of low Ga(III)-protochelin sorption onto the Gruver soil (Table 1),

The low Pearson correlation coefficients observed in the overall map for the Ga(III)-DFOB Gruver sample are further illustrated in Supplementary Figure 2. The map predominantly consists of regions containing either Ga or Fe individually, with only limited areas exhibiting orange hues, indicative of spatial co-localization of both elements. In comparison, the slightly higher Ga-Fe Pearson coefficient in the Ga(III)-PDMA Gruver sample is reflected in Supplementary Figure 2 by the increased presence of orange tones, though distinct regions of green and red remain apparent. Similarly, the Ga(III)-protochelin gradient map displays well-defined zones enriched in either Ga(III) or Fe(III), interspersed with localized orange regions corresponding to the co-occurrence of both metals.

4. Discussion

Bulk EXAFS spectra fit for all Ga(III)-siderophore complexes sorbed to soils, except that of Ga(III)-protochelin sorbed to Cassville clay, were best fit with a more components than hotspots were. The bulk EXAFS spectra may have received signal from a wide variety of sources, whereas the hotspots represent a smaller specific and presumably less chemically diverse area in the soil. However, if samples contain large quantities of similar hotspots with high amounts of Ga(III)

signal, these areas can dominate the bulk EXAFS spectra (e.g., the case with Ga(III)-protochelin Cassville clay (Figure 1)).

4.1 Cassville Clay

The Cassville clay is a high-activity clay soil, classified as a sandy clay loam containing 30.9% clay. This soil was selected to represent soils with high clay content, which are expected to strongly influence siderophore behavior due to their high sorptive capacity. Clays such as montmorillonite, which are common components of high-activity soils, are known to intercalate and adsorb a wide range of organic molecules, including siderophores, including DFOB and its Fe(III) complex (Haack, Johnston, and Maurice 2008). Studying siderophore interactions in this system allows assessment of whether high-activity clays act as strong sinks that limit siderophore mobility and bioavailability, thereby affecting Fe cycling and metal acquisition processes in natural environments.

4.1.1. Ga(III)-DFOB. Ga(III)-DFOB exhibited the lowest affinity for the Cassville clay soil, accompanied by minimal dissolution of both Fe and Mn. In the hotspot, the Ga(III)-DFOB complex constituted one third of the best-fit model, indicating its stability within the system. Previous work by Evers et al. demonstrated that Ga(III)-DFOB complexes remain intact upon intercalation into 2:1 clay minerals, suggesting the potential for similar intercalation processes within the Cassville soil, which contains high-activity clay phases. Spatial correlation analyses further revealed that Ga(III) was correlated with Fe and Mn in both whole-soil distributions and localized hotspots. These observations are consistent with hotspot fits indicating Ga(III) association with ferrihydrite and δ-MnO_2. Collectively, the significant Ga-Fe-Mn correlations, limited Fe and Mn release, and high complex retention suggest that Ga(III)-DFOB may be interacting into Fe- and Mn-oxide-coated clays domains within the Cassville soil. In the bulk fit,

intact complex reduced to 11%, and Ga(III) associated with ferrihydrite, kaolinite, and organic matter, indicating that the Ga(III)-DFOB complex is also interacting with other soil components.

4.1.2. Ga(III)-PDMA. Ga(III)-PDMA exhibited greater affinity for the Cassville clay soil than Ga(III)-DFOB, but less than Ga(III)-protochelin. This interaction was accompanied by slightly more dissolution of Fe and Mn compared to that induced by Ga(III)-DFOB. The Ga(III)-PDMA complex accounted for around 50% of the best-fit model in hotspots, indicating that the complex remained largely intact within the soil matrix. Consistent with previous observations that Ga(III)-PDMA complexes intercalate into 2:1 clays (Evers et al.), PDMA retention was particularly pronounced within localized hotspots, suggesting that these hotspots represent regions with high clay content. Both hotspots produced similar fit results and exhibited significant correlations between Ga(III), Fe, and Mn distributions. The strong elemental correlations, limited dissolution, and evidence of complex stability suggest that Ga(III)-PDMA is intercalating into clays coated with Fe and Mn oxides in the Cassville soil, similarly to the Ga(III)-DFOB complex. In the bulk fit, retained complex decreased to around 5%, and the remaining free Ga(III) associated with ferrihydrite, montmorillonite, organic matter, and δ-MnO_2. This wide variety of components suggests that although the PDMA does preferentially associate with the clay particles, since they are the hotspots, in the overall soil it distributes evenly, not exhibiting clear preferences for single components.

4.1.3. Ga(III)-protochelin. Ga(III)-protochelin exhibited the greatest sorption onto the Cassville soil and caused the most Fe and Mn dissolution. As with the other siderophore complexes, Ga(III)-protochelin remained intact in this soil, which is consistent with previous results showing 28% complex retention when Ga(III)-protochelin was adsorbed to montmorillonite clay (Evers et. al in prep). Ga(III)-protochelin has also been shown to dissolve Fe from montmorillonite (Evers et. al.),

which could contribute to the high Fe dissolution from this soil as it intercalates. Additionally, both hotspots and the bulk EXAFS in this soil contain Ga(III)-ferrihydrite as a fit, which is rationalized by high correlations between Ga and Fe in the hotspots as well as the bulk map. Ga(III)-protochelin has also been shown to remain intact upon sorption to ferrihydrite (Evers in prep), which could also contribute to portions of the percentage of whole siderophore complex in the fits, as well as Fe dissolution.

4.2. Belhaven Muck

The Belhaven muck is a poorly drained soil characterized by its dark color and high organic matter content. Humic substances within such soils are now understood as supramolecular associations in which numerous small, chemically diverse organic molecules cluster through hydrogen bonding and hydrophobic interactions (Piccolo 2001). This results in a micellar-like organization of organic matter, where hydrophilic exterior regions surround hydrophobic cores, shielding them from water molecules (Wandruszka, Engebreatson, and Yates 1999). Siderophores are expected to interact strongly with soil organic matter through a variety of mechanisms, including hydrogen bonding, complexation with metal-bridged organic matrices, and hydrophobic partitioning. For example, DFOB and its metal complexes have been shown to associate with organic matter via hydrophobic partitioning (M. Higashi, W-M. Fan, and N. Lane 1998). However, natural organic matter, particularly within soils, may also entrain particles that can interact with siderophore. Because of its high organic content and complex sorptive environment, the Belhaven muck was selected to represent organic-rich systems and to evaluate whether such soils act as strong sinks for siderophores, or a bioavailable source of Fe.

4.2.1. Ga(III)-DFOB. Ga(III)-DFOB exhibited a similar degree of sorption to the Belhaven muck as Ga(III)-protochelin but induced substantially lower Fe dissolution. The hotspot in this sample

consisted of 88% Ga(III) associated with ferrihydrite, along with 12% retained Ga(III)-DFOB complex. However, the Ga-Fe Pearson coefficient was low ($R^2 = 0.35$), suggesting that a portion of Ga(III) may have remained complexed and associated with particles low in Fe content. Bulk EXAFS fitting further indicated that Ga(III) was predominantly associated with organic matter (37.6%), consistent with expectations for a soil rich in humic substances. Fe in humic substances can be found as Fe(II) or Fe(III) bound to humic substances, or associated with humic substances in the form of Fe (hydr)oxide particles such as ferrihydrite (Allard et al. 2004). Fe bound within these organic associations has been shown to be readily mobilized by DFOB, raising the possibility of Ga(III)-Fe(III) exchange within the organic fraction (Kuhn et al. 2014). However, steric hinderances may limit DFOB's access to certain Fe microsites, resulting in partial complex retention. Together, these findings suggest that in the Belhaven muck, Ga(III)-DFOB predominantly interacts with organic matter and loosely with Fe-bearing humic components, with limited dissolution likely governed by the balance between complex stability and restricted site accessibility.

4.2.2.Ga(III)-PDMA. Ga(III)-PDMA showed the greatest sorption to the Belhaven muck out of the three siderophore complexes; however, this was accompanied by the least Fe and Mn dissolution. Although the Ga(III)-PDMA had a large affinity for the high organic soil, it did not have a particular affinity for certain minerals in the soil, and instead the Ga(III) associated with every component in the fit model. This overall distribution of Ga throughout the map can also be seen in Figure 1. The largest components of the fits were ferrihydrite and organic matter, perhaps suggesting a slight affinity for Fe bearing components. The overall Belhaven PDMA μ-XRF map had no correlation between Ga and Fe or Mn. The first hotspot also had no Ga-Fe correlation, and the fit was primarily composed of clays, and organic matter. The second hotspot did have a

significant Ga-Fe correlation, and the fit was composed of ferrihydrite and montmorillonite clay, verifying this correlation. None of the Ga in the hotspots was associated with Mn minerals, and the hotspots also showed no correlation between Ga and Mn, verifying this lack of association. The lack of Ga-Fe and Ga-Mn correlation in the maps is likely a result of the Ga(III)-PDMA complex having no strong affinities for specific soil minerals. Additionally, metal(III)-PDMA complexes have a net negative charge, and adsorption of negatively charged humic substances onto Fe(hydr)oxide phases in the soil will contribute to a lower affinity of metal(III)-PDMA complexes for Fe(hydr)oxide surfaces due to a decreased electrostatic attraction (Walter et al. 2016). This increase in repulsion between the PDMA complex and the Fe oxides may provide a possible explanation for the even distribution of the PDMA throughout the Belhaven soil.

4.2.3. Ga(III)-protochelin. Ga(III)-protochelin sorbed the least to the Belhaven muck and caused the most Fe and Mn dissolution from this soil. The Ga(III)-protochelin complex was also present in both the bulk and hotspot fits in greater proportion that the Ga(III)-PDMA and Ga(III)-DFOB complexes. Protochelin contains a highly hydrophobic backbone, which may promote intact complex interactions with domains within organic matter. The overall soil exhibited a weak correlation between Ga and Fe, and no correlation between Ga and Mn. For all Belhaven samples, low correlations with Mn are consistent with the inherently low Mn content in the muck.

Notably, the hotspot in this sample was composed of approximately one-third Ga(III) associated with ferrihydrite, as evidenced by a high Pearson correlation coefficient with Fe within the hotspot. Fe(III) has been shown to form complexes with oxygen-containing functional groups in organic matter, such as carboxylic and phenolic acids (Gustafsson et al. 2007). Hesterberg et al. (2012) reported that Fe in peat occurs either as mononuclear Fe-organic complexes or as a mixture of these complexes with polynuclear Fe species, the latter potentially comprising up to 20%

ferrihydrite-like phases (Morris and Hesterberg 2012). Given that siderophore-Fe stability constants exceed those of Fe-carboxylic acid complexes, Ga-Fe exchange may occur, resulting in Ga remaining associated with these ferrihydrite-like species. This, as well as the high Fe dissolution, indicates that protochelin may accumulate in Fe rich areas in the organic matter and facilitating Fe dissolution. The predominance of the Ga(III)-protochelin complex (65%) in the hotspot fit is consistent with previous work where Ga(III)-protochelin remained complexed when adsorbed to ferrihydrite while still facilitating Fe dissolution (Evers et.al). The high Fe dissolution may also indicate that the protochelin is able to access organic Fe; however, it can not be differentiated whether Fe associated with organic matter is an Fe source, or if all the Fe dissolution is a result of Fe (hydr)oxide particles within the organic matter. The Belhaven soil resulted in the highest amounts of Fe dissolution amongst all three Ga(III)-siderophore complexes while containing the lowest total Fe content, indicating that organic matter may be a viable Fe source for siderophores.

4.3. Gruver Soil.

The Gruver series soil is an alkaline (pH 8) no-till agricultural soil from an agricultural field rotating corn and alfalfa. Given this critical role of siderophores in facilitating Fe bioavailability in high-pH soils, the Gruver soil was selected as a representative system for investigating siderophore-driven Fe mobilization under agronomic conditions.

Supplementary Figure 1 reveals distinct Fe-rich regions distributed throughout the Gruver soil, yet Supplementary Figure 2 indicates that these Fe hotspots do not contain Ga. This lack of co-localization suggests that Ga is not preferentially associating with these specific Fe-rich mineral domains but is instead interacting with more diffusely distributed Fe phases across the sample. Additional mineralogical characterization, such as X-ray diffraction (XRD) or Fe XAS, is required

to determine the composition of these localized Fe accumulations. Despite this lack of association, Ga(III) sorbed to ferrihydrite was a predominant fit for all Ga(III)-siderophore complexes with the Gruver soil. This component presence is consistent with known trends that sorption of many metal cations to Fe-oxide surfaces increases with increasing pH (He et al. 2025), so the alkaline pH of the Gruver soil likely promotes strong Ga-ferrihydrite interactions. Across all Gruver maps, bulk Ga(III)-Fe correlations were low (SI Table 2). However, hotspot data available for Ga(III)-DFOB and Ga(III)-PDMA showed elevated Ga-Fe correlations within hotspots, supporting the interpretation that Ga interacts with ferrihydrite or other poorly crystalline Fe phases that are more diffusely distributed than the visually prominent Fe-rich regions.

4.3.1. Ga(III)-DFOB. The Ga(III)-DFOB had a low affinity for the Gruver soil and caused small amounts of Fe and Mn dissolution. The fit in the hotspot was solely composed of Ga(III) associated with ferrihydrite, which is accompanied by a high Ga-Fe correlation in this area (R^2 of 0.86). Ga(III)-DFOB was the only siderophore to remain complexed in the Gruver soil (around 13% in the bulk fit), which could be due to DFOB sorption to soil minerals being the most unaffected by changes in pH, or repulsion of positive Ga(III)-DFOB complexes with soil particles.

4.3.2. Ga(III)-PDMA. Ga(III)-PDMA had the highest affinity for this soil, which is consistent with trends seen in the other soils. Despite having the most sorption, it facilitated the least amount of Fe and Mn dissolution in this soil. As in the Belhaven and Cassville soils, the Ga(III)-PDMA EXAFS spectra were best fit with the highest variety of components compared to Ga(III)-DFOB and Ga(III)-protochelin. As in the other soils, the PDMA complex does not have as high of a preferential affinity for the Fe mineral as the other siderophore complexes. PDMA has previously been shown to exhibit either no or extremely low amounts of sorption to soil minerals such as clays and iron oxides (Hiradate and Inoue 1999; Reichard 2005), verifying the broader distribution of

PDMA throughout the soil. When in the soil system, the complex separates, and the resulting free metal associates with a variety of soil components.

4.3.3. Ga(III)-protochelin. The adsorption of Ga(III)-protochelin was very lowest out of the three complexes (0.004 mM). This limited sorption may be due to repulsive interactions between soil particles and the hydrophobic backbone of the protochelin, as well as potential steric hinderances arising from the larger complex size of the Ga(III)-protochelin complex compared with the Ga(III)-DFOB and Ga(III)-PDMA. Despite the limited sorption, the protochelin complex facilitated the highest amounts of Fe and Mn dissolution, similarly to the Cassville and Belhaven soils, indicating its capacity to solubilize metals from otherwise bio-unavailable pools. The bulk EXAFS was composed of Ga(III) associating solely with ferrihydrite, indicating that the protochelin complex reacts with Fe rich areas of the soil.

Sorption of the Ga(III)-protochelin complex resulted in substantially greater Mn dissolution from the Gruver soil than that observed for the Ga(III)-DFOB and Ga(III)-PDMA complexes (Table 1), consistent with previously observed trends. Notably, the Gruver soil was the only soil in which dissolved Mn concentrations exceeded those of dissolved Fe. This contrasts with the Cassville clay: although the Gruver and Cassville soils contain comparable total Mn, the Cassville soil released far less Mn relative to Fe. It is possible that the Gruver soil contains more active Mn minerals, while the Mn in the Cassville clay was associated with clay particles. XRD analysis is also necessary to confirm this.

4.4. Overall Reactions in the System

It is important to note that we are using Ga(III)-siderophore complexes to model the behavior of what would be Fe(III)-siderophore complexes in natural systems. When examining Ga(III)-siderophore complex behavior across individual mineral phases, Ga(III) was found to

serve as an effective proxy for interactions with clays and manganese oxides However, reactions with the Ga(III) may be occurring that would not typically occur in Fe systems. Notably, Ga(III) sorbed to ferrihydrite was identified as a contributing component in all EXAFS spectra, both within hotspot regions and in bulk samples, with an average fitted contribution of 41.2%. The slightly lower stability constant of the Fe(III)-siderophore complex relative to its Ga(III) counterpart (log K = 32.02 and 29.49, respectively) suggests the potential for metal exchange during sorption, wherein Ga(III) is retained on the ferrihydrite surface following displacement from the complex. On the other hand, ferrihydrite is an iron mineral with high surface area and reactivity, and it is possible that Fe(III)-siderophore complexes would also interact (perhaps cryptically) with the ferrihydrite surface, as cycling of Fe minerals has been shown to control key aspects of Fe biogeochemistry (Kappler and Bryce 2017).

Experiments with ferrihydrite demonstrated that the Ga(III)-DFOB and Ga(III)-PDMA complexes dissociated upon sorption, whereas Ga(III)-protochelin remained intact, likely adsorbing via an outer-sphere complexation mechanism. Given the abundance of reactive surface oxygens on ferrihydrite, ligand exchange involving Fe(III) cannot be ruled out for the DFOB and PDMA systems; however, it is equally plausible that similar behavior would occur for Fe(III)-DFOB and Fe(III)-PDMA complexes under comparable conditions. In contrast, sorption experiments with goethite indicated that Ga(III)-siderophore complexes formed ternary surface complexes. This observation is consistent with previous findings for Fe(III)-DFOB complexes (Simanova, Loring, and Persson 2011), suggesting that, for crystalline Fe(III) oxides such as goethite, Ga(III)-siderophore complexes effectively replicate the sorptive behavior of their Fe(III) analogs. Although methodological limitations are possible, it is noteworthy that previous studies have been unable to extract or detect protochelin in soils (Rai et al. 2020), due to its strong

adsorption to mineral surfaces. The approach developed here provides, at minimum, partial insight into its behavior in soil environments.

Across all soil systems examined, DFOB and PDMA promoted significantly less Fe dissolution than protochelin. This was also observed in adsorption isotherm experiments (Evers. et. al.), where PDMA promoted no dissolution from iron minerals. Although DFOB promoted some Fe release, the extent of dissolution remained markedly lower than that observed for protochelin. Protochelin is a reactive molecule, and previous studies have demonstrated that protochelin degrades slowly under low-pH conditions (Harrington et al. 2012) and upon interaction with montmorillonite clays or birnessite (Evers et al., in review; (Harrington et al. 2012). While the degradation mechanism associated with montmorillonite remains unresolved, protochelin oxidation during interaction with birnessite occurs via reductive dissolution, wherein catecholate moieties are oxidized to quinones. Given that the catecholate functional groups of protochelin are more redox-active than the hydroxamate and α-hydroxycarboxylate groups present in DFOB and PDMA, protochelin is inherently more susceptible to oxidative degradation. This reactivity contributes to higher levels of dissolved Fe observed in these systems.

Conclusions

Overall, this study demonstrates that siderophore-metal complex behavior in soils is strongly governed by the physicochemical characteristics of the soil matrix, including mineral composition, clay content, organic matter, and pH, and provides advances to the previous work of Evers et. al.. Although the fate of complexes on individual mineral surfaces provided necessary groundwork in order to track the Ga(III)-siderophore complexes in more complicated systems, they themselves did not provide insight into the competitive dynamics among minerals or indicate the ultimate distribution of the complexes within heterogeneous soil matrices. In this

study, it was found that in the Cassville clay, all siderophore interactions were dominated by intercalation and sorption processes within Fe- and Mn-oxide-coated clay domains, reflecting the high sorptive capacity of clay-rich systems, and their capacity to act as sinks for siderophores. In the organic-rich Belhaven muck, DFOB and protochelin siderophore complexes were partitioned as intact complexes with humic substances and associated Fe phases, while PDMA had low affinity for specific mineral phases and distributed evenly through the muck as a dissociated complex. All three siderophores associated with iron phases in the alkaline soil, emphasizing the critical role of siderophores in sustaining Fe cycling under such conditions. Protochelin induced the highest amount of Fe and Mn dissolution in all three soils, implying that protochelin undergoes degradation within the soil matrix, rendering it unable to re-bind Fe(III) after dissolution. Metal-PDMA complexes have the lowest stability constant with metals, which results in the release of the free metal into solution, where it is then available for plant uptake. This supports work from (Ueno et al. 2021), that metal-PDMA addition to soils could be useful as a plant fertilizer. Building on these findings, future work should focus on soil containing defined quantities of clays, organic matter, metal oxides, and sands, in order to access competition between soil components. Understanding how different siderophore structures behave in soils with varying edaphic properties represents an important step toward elucidating the mechanisms that control iron acquisition in plants and improving Fe bioavailability in agricultural systems.

References

Ahmed, Engy, and Sara J. M. Holmström. 2014. 'The effect of soil horizon and mineral type on the distribution of siderophores in soil', *Geochimica et Cosmochimica Acta*, 131: 184-95.

Akafia, Martin M., James M. Harrington, John R. Bargar, and Owen W. Duckworth. 2014. 'Metal oxyhydroxide dissolution as promoted by structurally diverse siderophores and oxalate', *Geochimica et Cosmochimica Acta*, 141: 258-69.

Allard, T., N. Menguy, J. Salomon, T. Calligaro, T. Weber, G. Calas, and M. F. Benedetti. 2004. 'Revealing forms of iron in river-borne material from major tropical rivers of the Amazon Basin (Brazil)1 1Associate editor: G. Sposito', *Geochimica et Cosmochimica Acta*, 68: 3079-94.

Duckworth, Owen W., John R. Bargar, and Garrison Sposito. 2009. 'Quantitative Structure−Activity Relationships for Aqueous Metal−Siderophore Complexes', *Environmental Science & Technology*, 43: 343-49.

Evers, Ann, Robert D. Hancock, Arthur E. Martell, and Ramunas J. Motekaitis. 1989. 'Metal ion recognition in ligands with negatively charged oxygen donor groups. Complexation of iron(III), gallium(III), indium(III), aluminum(III), and other highly charged metal ions', *Inorganic Chemistry*, 28: 2189-95.

Green, M. A., and M. J. Welch. 1989. 'Gallium radiopharmaceutical chemistry', *Int J Rad Appl Instrum B*, 16: 435-48.

Gustafsson, Jon Petter, Ingmar Persson, Dan Berggren Kleja, and Joris WJ Van Schaik. 2007. 'Binding of iron (III) to organic soils: EXAFS spectroscopy and chemical equilibrium modeling', *Environmental Science & Technology*, 41: 1232-37.

Haack, Elizabeth A., Cliff T. Johnston, and Patricia A. Maurice. 2008. 'Mechanisms of siderophore sorption to smectite and siderophore-enhanced release of structural Fe3+', *Geochimica et Cosmochimica Acta*, 72: 3381-97.

Harrington, James M., John R. Bargar, Andrzej A. Jarzecki, James G. Roberts, Leslie A. Sombers, and Owen W. Duckworth. 2012. 'Trace metal complexation by the triscatecholate siderophore protochelin: structure and stability', *BioMetals*, 25: 393-412.

Harrington, James M., Owen W. Duckworth, and Kurt Haselwandter. 2015. 'The fate of siderophores: antagonistic environmental interactions in exudate-mediated micronutrient uptake', *BioMetals*, 28: 461-72.

He, Bihong, Wentao Zhang, Yanan Diao, Shangchen Sun, Yonghe Zhang, Wenqing Zhao, Fei Wen, and Guangrui Yang. 2025. 'Mechanistic study of the adsorption capabilities of heavy metals on the surface of ferrihydrite: batch sorption, modeling, and density functional theory', *RSC Advances*, 15: 1072-80.

Hider, Robert C., and Xiaole Kong. 2010. 'Chemistry and biology of siderophores', *Natural Product Reports*, 27: 637-57.

Hiradate, S., and K. Inoue. 1999. 'Interactions of Mugineic Acid with Allophane, Imogolite, Montmorillonite and Gibbsite.' in J. Berthelin, P. M. Huang, J. M. Bollag and F. Andreux (eds.), *Effect of Mineral-Organic-Microorganism Interactions on Soil and Freshwater Environments* (Springer US: Boston, MA).

Kappler, Andreas, and Casey Bryce. 2017. 'Cryptic biogeochemical cycles: unravelling hidden redox reactions', *Environmental Microbiology*, 19: 842-46.

Kelly, S. D., D. Hesterberg, and B. Ravel. 2008. 'Analysis of Soils and Minerals Using X-ray Absorption Spectroscopy.' in, *Methods of Soil Analysis Part 5—Mineralogical Methods*.

Kuhn, Keshia M., Patricia A. Maurice, Elisabeth Neubauer, Thilo Hofmann, and Frank von der Kammer. 2014. 'Accessibility of Humic-Associated Fe to a Microbial Siderophore: Implications for Bioavailability', *Environmental Science & Technology*, 48: 1015-22.

M. Higashi, Richard, Teresa W-M. Fan, and Andrew N. Lane. 1998. 'Association of desferrioxamine with humic substances and their interaction with cadmium(II) as studied by pyrolysis–gas chromatography–mass spectrometry and nuclear magnetic resonance spectroscopy†', *Analyst*, 123: 911-18.

Majumdar, Sanghamitra, Jose R. Peralta-Videa, Hiram Castillo-Michel, Jie Hong, Cyren M. Rico, and Jorge L. Gardea-Torresdey. 2012. 'Applications of synchrotron μ-XRF to study the distribution of biologically important elements in different environmental matrices: A review', *Analytica Chimica Acta*, 755: 1-16.

Morris, Amanda J., and Dean L. Hesterberg. 2012. 'Iron(III) Coordination and Phosphate Sorption in Peat Reacted with Ferric or Ferrous Iron', *Soil Science Society of America Journal*, 76: 101-09.

Newville, Matthew. 2001. 'IFEFFIT: interactive XAFS analysis and FEFF fitting', *Journal of synchrotron radiation*, 8: 322-24.

Nicolafrancesco, Chiara, Francesco Porcaro, Igor Pis, Silvia Nappini, Laura Simonelli, Carlo Marini, Emanuela Frangipani, Daniela Visaggio, Paolo Visca, Settimio Mobilio, Carlo Meneghini, Ilaria Fratoddi, Giovanna Iucci, and Chiara Battocchio. 2019. 'Gallium- and Iron-Pyoverdine Coordination Compounds Investigated by X-ray Photoelectron Spectroscopy and X-ray Absorption Spectroscopy', *Inorganic Chemistry*, 58: 4935-44.

Piccolo, Alessandro. 2001. 'The supramolecular structure of humic substances', *Soil science*, 166: 810-32.

Powell, P. E., G. R. Cline, C. P. P. Reid, and P. J. Szaniszlo. 1980. 'Occurrence of hydroxamate siderophore iron chelators in soils', *Nature*, 287: 833-34.

Rai, V., N. Fisher, O. W. Duckworth, and O. Baars. 2020. 'Extraction and Detection of Structurally Diverse Siderophores in Soil', *Front Microbiol*, 11: 581508.

Reichard, Petra Ulrike. 2005. 'Effects of microbial plant siderophore ligands on the dissolution of iron oxides', ETH Zürich.

Schenkeveld, W. D. C., E. Oburger, B. Gruber, Y. Schindlegger, S. Hann, M. Puschenreiter, and S. M. Kraemer. 2014. 'Metal mobilization from soils by phytosiderophores – experiment and equilibrium modeling', *Plant and Soil*, 383: 59-71.

Schwyn, B., and J. B. Neilands. 1987. 'Universal chemical assay for the detection and determination of siderophores', *Anal Biochem*, 160: 47-56.

Simanova, Anna A., John S. Loring, and Per Persson. 2011. 'Formation of Ternary Metal-Oxalate Surface Complexes on α-FeOOH Particles', *The Journal of Physical Chemistry C*, 115: 21191-98.

Suzuki, Motofumi, Atsumi Urabe, Sayaka Sasaki, Ryo Tsugawa, Satoshi Nishio, Haruka Mukaiyama, Yoshiko Murata, Hiroshi Masuda, May Sann Aung, Akane Mera, Masaki Takeuchi, Keijo Fukushima, Michika Kanaki, Kaori Kobayashi, Yuichi Chiba, Binod Babu Shrestha, Hiromi Nakanishi, Takehiro Watanabe, Atsushi Nakayama, Hiromichi Fujino, Takanori Kobayashi, Keiji Tanino, Naoko K. Nishizawa, and Kosuke Namba. 2021. 'Development of a mugineic acid family phytosiderophore analog as an iron fertilizer', *Nature Communications*, 12: 1558.

Ueno, Daisei, Yuta Ito, Miho Ohnishi, Chikahiro Miyake, Takayuki Sohtome, and Motofumi Suzuki. 2021. 'A synthetic phytosiderophore analog, proline-2′-deoxymugineic acid, is efficiently utilized by dicots', *Plant and Soil*, 469: 123-34.

Walter, M., E. Oburger, Y. Schindlegger, S. Hann, M. Puschenreiter, S. M. Kraemer, and W. D. C. Schenkeveld. 2016. 'Retention of phytosiderophores by the soil solid phase – adsorption and desorption', *Plant and Soil*, 404: 85-97.

Wandruszka, R von, RR Engebreatson, and LM Yates, III. 1999. 'Humic acid pseudomicelles in dilute aqueous solution: fluorescence and surface tension measurements'.

Webb, S. M. 2005. 'SIXpack: a graphical user interface for XAS analysis using IFEFFIT', *Physica Scripta*, 2005: 1011.

———. 2011. 'The MicroAnalysis Toolkit: X-ray Fluorescence Image Processing Software', *AIP Conference Proceedings*, 1365: 196-99.

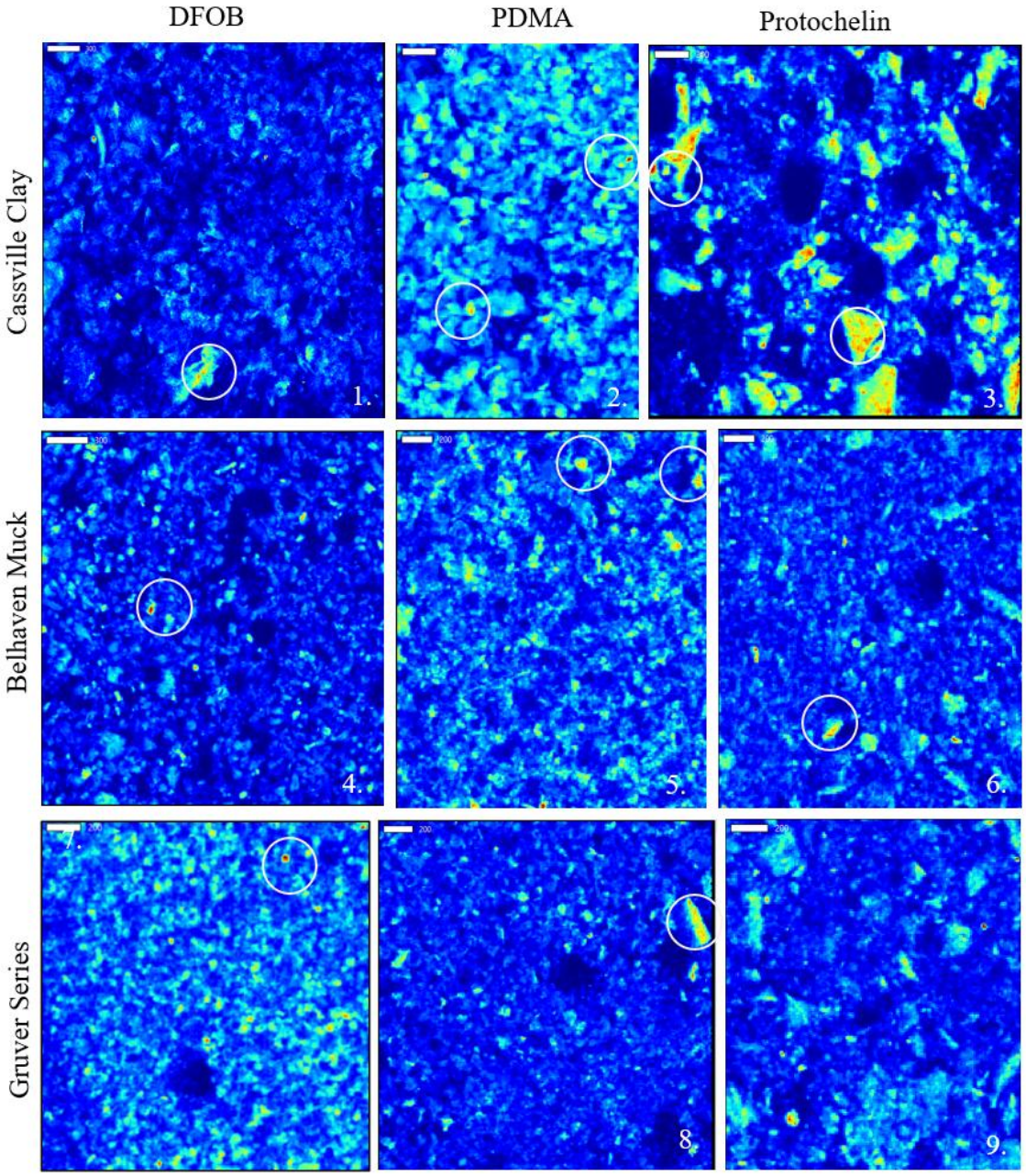

Figure 4.1. Ga μ-XRF maps for 1. Ga(III)-DFOB Cassville 2. Ga(III)-PDMA Cassville 3. Ga(III)-protochelin Cassville 4. Ga(III)-DFOB Belhaven 5. Ga(III)-PDMA Belhaven 6. Ga(III)-protochelin Belhaven 7. Ga(III)-DFOB Gruver 8. Ga(III)-PDMA Gruver and 9. Ga(III)-protochelin Gruver. White circles represent hotspots where μ-EXAFS measurements were taken.

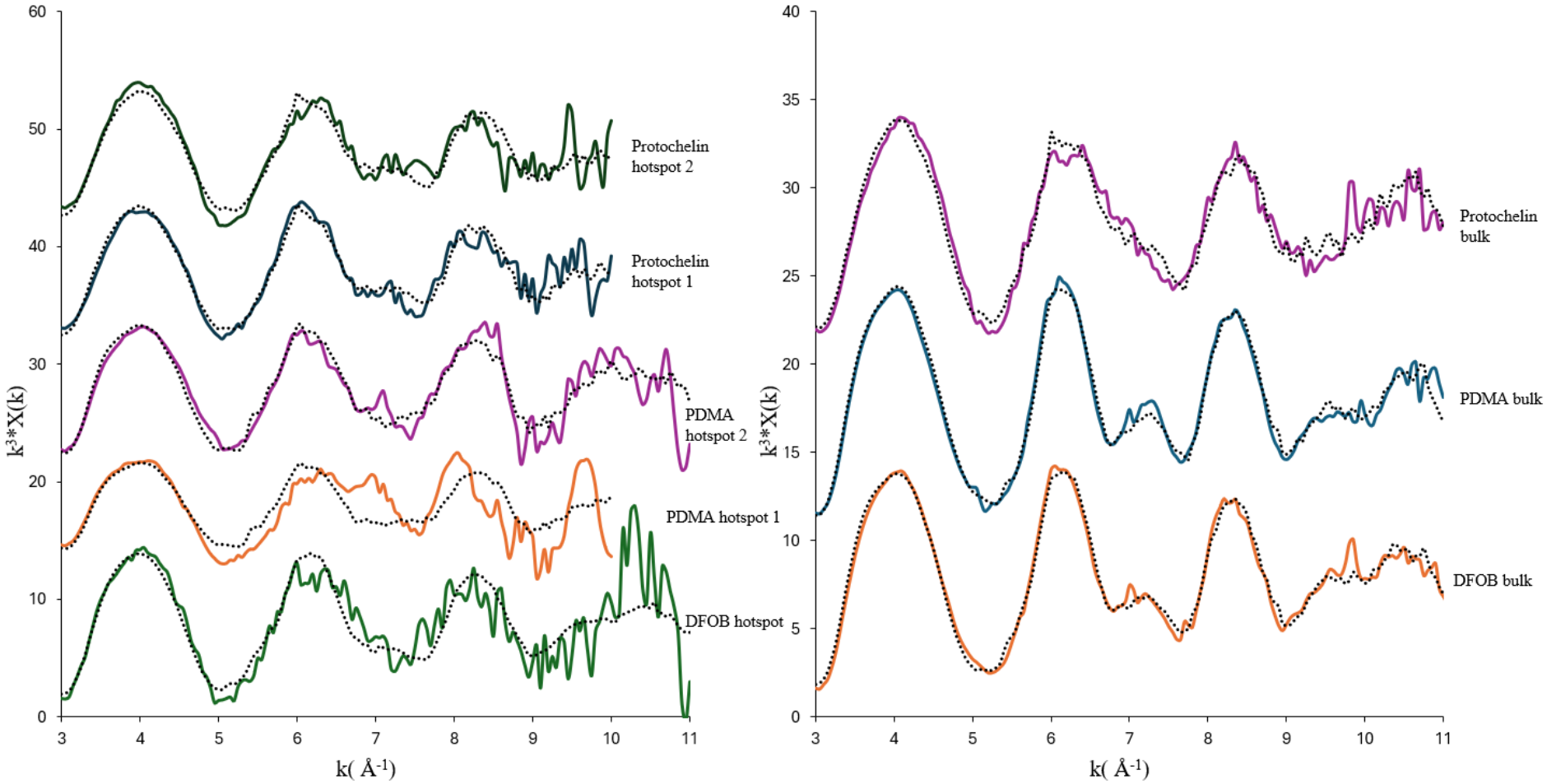

Figure 4.2. μ-EXAFS chi spectra and bulk EXAFS chi spectra for the Cassville clay soil. Dashed lined represent least square fits, with fit results shown in Table 2.

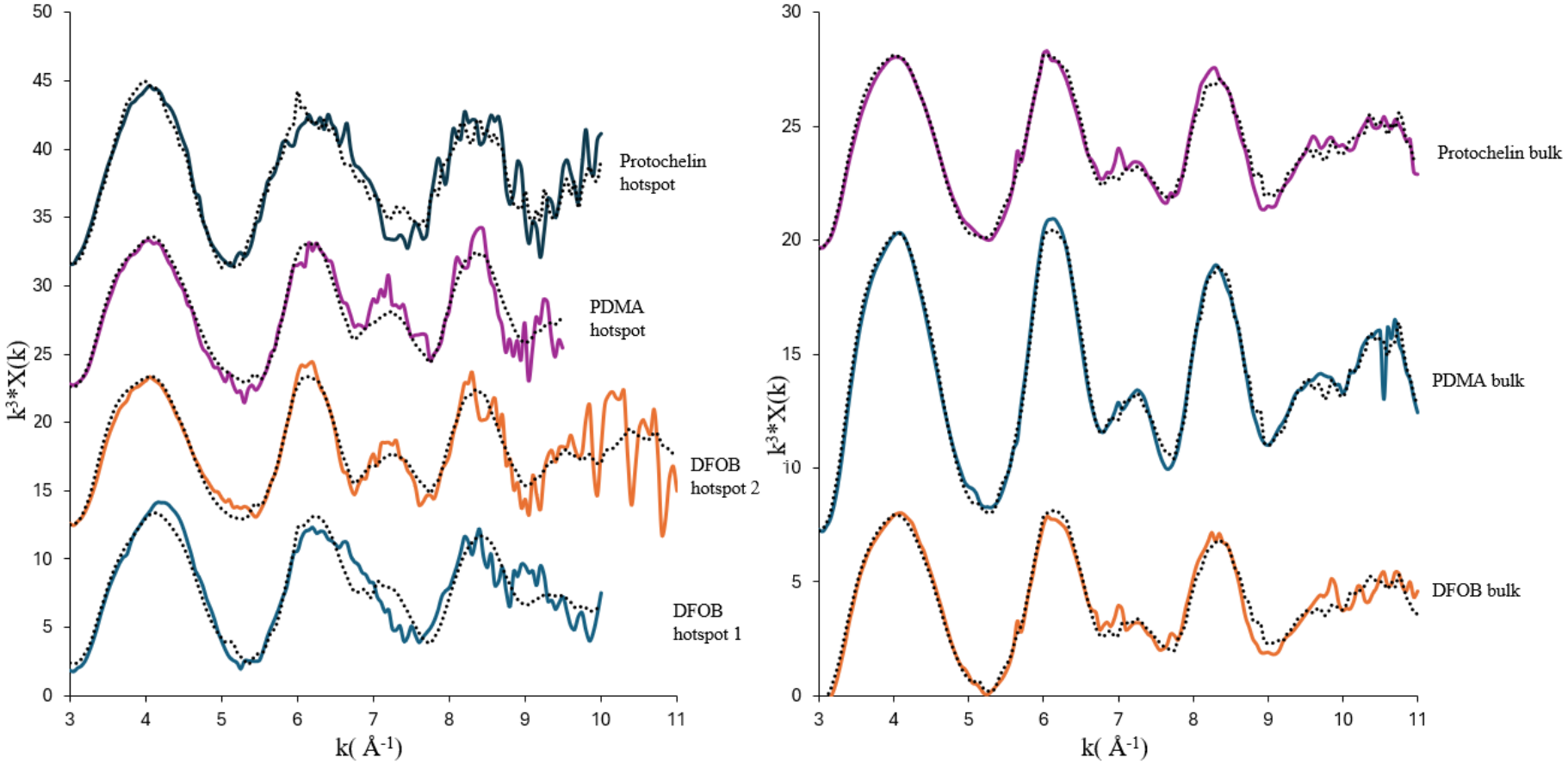

Figure 4.3. μ-EXAFS chi spectra and bulk EXAFS chi spectra for the Belhaven soil. Dashed lined represent least square fits, with fit results shown in Table 3.

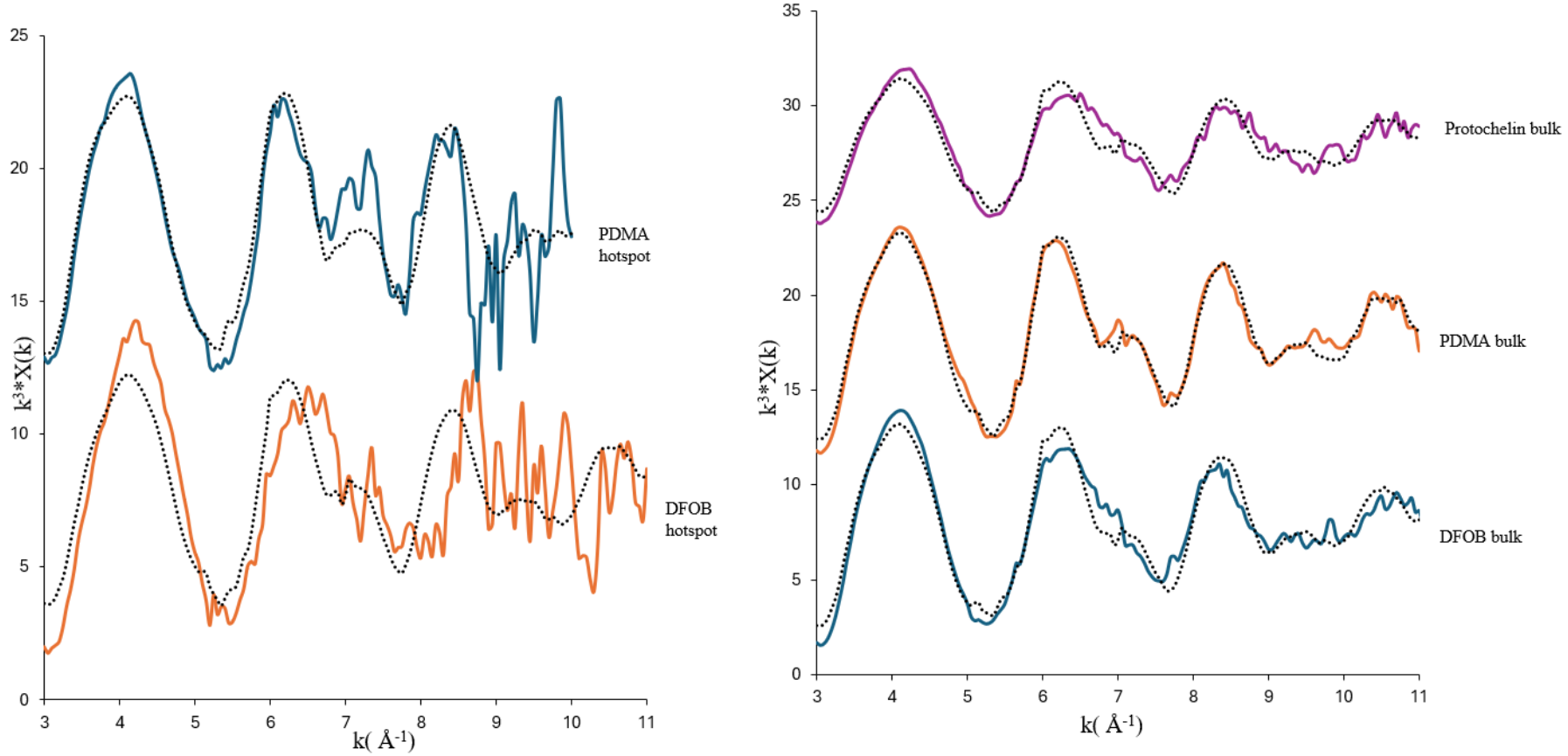

Figure 4.4. μ-EXAFS chi spectra and bulk EXAFS chi spectra for the Gruver soil. Dashed lined represent least square fits, with fit results shown in Table 3.

Cassville	**Ga loading (mmol Ga/g soil)**	**$Fe_{dissolved}$ (µM)**	**$Mn_{dissolved}$ (µM)**
Ga(III)-DFOB	0.0005	1.47	1.05
Ga(III)-PDMA	0.033	2.36	1.92
Ga(III)-Protochelin	0.075	6.19	2.66

Belhaven Muck	**Ga loading (mmol Ga/g soil)**	**$Fe_{dissolved}$ (µM)**	**$Mn_{dissolved}$ (µM)**
Ga(III)-DFOB	0.038	2.43	1.42
Ga(III)-PDMA	0.162	2.82	1.57
Ga(III)-Protochelin	0.03	11.69	2.12

Gruver	**Ga loading (mmol Ga/g soil)**	**$Fe_{dissolved}$ (µM)**	**$Mn_{dissolved}$ (µM)**
Ga(III)-DFOB	0.010	1.15	2.69
Ga(III)-PDMA	0.043	0.65	2.06
Ga(III)-Protochelin	0.001	1.51	10.05

Table 4.1. Gallium sorbed onto each bulk soil sample, and µm of iron and manganese dissolved from the soils. 1 mM initial concentration of Ga(III)-DFOB, Ga(III)-PDMA, Ga(III)-protochelin.

Cassville Clay	**DFOB**		**PDMA**			**Protochelin**		
Component	**hotspot**	**bulk**	**hotspot 1**	**hotspot 2**	**bulk**	**hotspot 1**	**hotspot 2**	**bulk**
Ga(III)-siderophore	28.0 ± 0.05	11.1 ± 0.02	49 ± 0.06	67 ± 0.03	5.7 ± 0.03	25.9 ± 0.05	11.5 ± 0.08	31.9 ± 0.03
Ga(III)-ferrihydrite	25.2 ± 0.11	38.2 ± 0.03	9.4 ± 0.17	15.7 ± 0.08	19.2 ± 0.05	20.9 ± 0.05	62 ± 0.19	68 ± 0.03
Ga(III)-montmorillonite	-	-	41.5 ± 0.18	15.7 ± 0.09	40.3 ± 0.05	-	23 ± 0.19	-
Ga(III)-kaolinite	-	23.5 ± 0.04	-	-	-	-	-	-
Ga(III)-organic	-	27.3 ± 0.04	-	-	24 ± 0.05	56.7 ± 0.06	-	-
Ga(III)- δ-MnO2	40.8 ± 0.15	-	-	-	10.6 ± 0.07	-	-	-

Table 4.2. LCF fitting results for Ga(III)-DFOB, PDMA, and Protochelin adsorbed onto Cassville clay. Results are normalized to 100%, but were 99 ± 1.4%, 77 ± 25% and 87 ± 6.5 respectively.

Belhaven Muck	**DFOB**		**PDMA**			**Protochelin**	
Component	**hotspot**	**bulk**	**hotspot 1**	**hotspot 2**	**bulk**	**hotspot 1**	**bulk**
Ga(III)-siderophore	12.2 ± 0.04	-	-	-	5.7 ± 0.03	65.6 ± 0.04	10 ± 0.02
Ga(III)-ferrihydrite	88.0 ± 0.03	27.5 ± 0.04	15.5 ± 0.08	31.4 ± 0.08	30.1 ± 0.04	33.3 ± 0.05	18.8 ± 0.03
Ga(III)-montmorillonite	-	-	40 ± 0.13	69.3 ± 0.07	10.2 ± 0.05	-	-
Ga(III)-kaolinite	-	-	28.8 ± 0.10	-	11.0 ± 0.06	-	18.8 ± 0.03
Ga(III)-organic	-	37.6 ± .03	13.3 ± 0.08	-	38.5 ± 0.4	-	45 ± 0.02
Ga(III)- δ-MnO2	-	31.8 ± .05	-	-	8.2 ± 0.07	-	-

Table 4.3**.** LCF fitting results for Ga(III)-DFOB, PDMA and protochelin adsorbed onto the Belhaven muck. Results are normalized to 100%, but were 82 ± 18%, 96 ± 11%, 82 ± 19% respectively.

Gruver	**DFOB**		**PDMA**		**Protochelin**
Component	**hotspot**	**bulk**	**hotspot 1**	**bulk**	**bulk**
Ga(III)-siderophore	-	13.7 ± 0.02	-	-	-
Ga(III)-ferrihydrite	100 ± 0.05	86 ± 0.02	59.2 ± 0.09	87.1 ± 0.02	100 ± 0.02
Ga(III)-montmorillonite	-	-	-	-	-
Ga(III)-kaolinite	-	-	44.8 ± 0.08	-	-
Ga(III)-organic	-	-	-	12.9 ± 0.02	-
Ga(III)- δ-MnO2	-	-	-	-	-

Table 4.4. LCF fitting results for Ga(III)-DFOB, PDMA and protochelin adsorbed to the Gruver series soil. Results are normalized to 100% but were 82 ± 12%, 88 ± 7% and 60% respectively.

CHAPTER 5: Summary and Conclusions

1. Summary of Major Findings

This dissertation broadly sought to elucidate the behavior of structurally distinct siderophores in soil environments, a topic that has remained challenging due to the overwhelming abundance and complexity of iron in soils. Three siderophores, including DFOB (hydroxamate), PDMA (α-hydroxycarboxylate), and protochelin (catecholate), were studied to represent major classes of siderophore ligands. The inclusion of PDMA and protochelin was notable, as measurable quantities of these compounds are rarely available and are accessible in only a limited number of laboratories.

Because PDMA is a synthetic analog of the natural phytosiderophore DMA, efforts were first directed toward improving the understanding of its binding behavior, particularly with respect to metals other than iron, as siderophores influence not only Fe acquisition but also the mobility and bioavailability of micronutrient trace metals. PDMA was found to form complexes with Cu(II), Ni(II), Co(II), and Zn(II), exhibiting stability constants comparable to those reported for DMA. This prompted the question of whether stability constants for phytosiderophores could be predicted in cases where direct measurement is constrained by limited compound availability. It was demonstrated that PDMA stability constants could be predicted from known stability constants of other phytosiderophores. Subsequently, predictive relationships were further expanded to phytosiderophore-metal pairs for which no experimental constants exist, using hydrolysis constants, ionic potential, and linear regressions based on DFOB-metal complexes. These findings provided insight into the potential utility of PDMA as a fertilizer component for metals beyond iron.

With a clearer understanding of PDMA's impact on trace metal biogeochemistry, we then evaluated how DFOB, PDMA, and protochelin interacted with mineral surfaces. Adsorption of apo-siderophores was compared to that of their Fe complexes. DFOB and its Fe complexes were found to exhibit similar degrees of sorption and generally sorbed more strongly than the other siderophores, likely due to the complex's overall positive charge. Apo-PDMA exhibited negligible affinity for mineral surfaces, although its Fe complex displayed measurable adsorption. Protochelin and its Fe complex both sorbed to most minerals examined, although protochelin frequently induced substantial mineral dissolution and underwent degradation, as indicated by repeated changes in solution color.

Because adsorption has the potential to disrupt the transport of siderophore-metal complexes to parent organisms, the mechanisms governing surface interactions were investigated. Traditional approaches have been limited by the inability to spectroscopically resolve Fe in siderophore complexes within Fe-rich matrices. This challenge was circumvented through the substitution of Ga(III) as a "pseudo-isotope," enabling analysis at the synchrotron. It was shown that all three siderophore complexes dissociated upon sorption to kaolinite and birnessite. All three intercalated into montmorillonite, although protochelin exhibited partial degradation and therefore did not fully intercalate. Ga-DFOB and Ga-PDMA dissociated upon sorption to ferrihydrite, whereas protochelin sorbed as an intact outer-sphere complex. On goethite surfaces, all siderophores formed type-A ternary complexes. These results demonstrated that Ga substitution is a viable strategy for tracing siderophore complexation processes in mineral systems that are otherwise analytically inaccessible.

Having established mineral level mechanisms, the fate of siderophore complexes in soils was then examined. A Cassville clay (high clay content), a Belhaven muck (high organic matter),

and a Gruver soil (alkaline) were selected to represent a variety of environmental conditions. Intercalation, and thus complex retention, of complexes was greatest in the Cassville soil. In the organic Belhaven soil, partial retention of all complexes occurred, likely driven by hydrophobic partitioning of intact species. In the alkaline Gruver soil, the complexes from all three siderophores dissociated, and free Ga(III) associated primarily with poorly crystalline iron phases. Consistent with mineral experiments, protochelin was the most susceptible to degradation and facilitated the highest levels of Fe dissolution.

Collectively, this work provided foundational thermodynamic and mechanistic insights needed to better understand PDMA reactivity in soils. The application of gallium as a spectroscopically traceable analog for iron introduced a novel methodological framework for tracking siderophores, and potentially other organic metal-binding ligands, through complex mineral and soil environments. Overall, the behavior of structurally distinct siderophores and their metal complexes in both mineral and soil matrices was elucidated, filling critical gaps in the understanding of their environmental fate.

2. Future Work

2.1. Improvement of present work

This dissertation advances our understanding of the fate of siderophores in soil environments; however, several opportunities for refinement became apparent in retrospect. The isotherm experiments, in particular, could have been expanded to yield a more comprehensive dataset. Incorporating more rigorous dissolution measurements across all minerals would have provided deeper insight into how ligand functional group identity affects nutrient release and availability. The inclusion of desorption experiments following initial adsorption would have further clarified siderophore cycling and potential re-mobilization. Conducting experiments across

a wider range of environmentally relevant pH values would also have strengthened interpretations of pH-dependent sorption behavior. Finally, the addition of adsorption isotherms with organic matter would have strengthened the interpretation of siderophore interactions in more complex environmental matrices.

2.2. Suggestions for future work

Several avenues for future research emerge from this work. Competition experiments, conducted both in simplified mineral systems and in more complex soil environments, would provide valuable insight into how siderophores interact when multiple surfaces are present simultaneously. For example, in the fourth chapter, the addition of a soil containing all major reactive components (clays, organic matter, metal oxides, and sands) would have provided valuable insight into competition among these phases and clarified the ultimate partitioning of siderophores within soil environments. Additional investigation into the degradation products formed during siderophore-mineral and siderophore-soil interactions would also be beneficial, however characterizing degradation in soils may be challenging, particularly for protochelin, which exhibits strong retention. However, such analyses are likely feasible in controlled mineral systems via LC-ICP-MS analysis of the supernatant. Finally, integrating a biotic component into soil experiments could offer a more realistic representation of siderophore cycling in natural environments, although this approach would require careful consideration of extraction challenges and analytical constraints.

3. Broader Impacts and Final Thoughts

This dissertation provides a better understanding of siderophore function, possibly including which structures retain metals, and can be uptake by strategy II plants, and which structures release metals, and can be utilized by strategy I plants. PDMA, in particular, has recently

been identified as a promising zinc fertilizer, capable of alleviating deficiencies in alkaline and flooded soils (Rocco et al. 2025). Additionally, PDMA has been shown to be accessible to dicot species (Ueno et al. 2021), as its complexes are more readily reduced, releasing iron in a form that can be taken up by Strategy I plants. This highlights the potential for leveraging specific siderophores to enhance micronutrient availability across a broad range of plant types and soil conditions.

At its core, this work aims to advance our understanding of how this remarkably diverse class of iron acquisition molecules behaves in soil environments, with the broader goal of informing strategies to mitigate iron deficiency in plants and, ultimately, in people — a pressing issue given that nearly two billion individuals worldwide experience anemia. Research in this area has historically focused on DFOB, and very little work has examined the behavior of siderophores in real soils. However, in understanding how different siderophores, such as PDMA and protochelin react in soils, we can potentially engineer plants to exude more efficient structures of siderophores or use them in fertilizer applications if cost effective pathways can be found. The findings presented here contribute an essential step toward the eventual use of siderophores in agricultural applications by demonstrating how different siderophores function across distinct environmental conditions. The potential applications of this research to nutrient management strategies underscores the importance of interdisciplinary collaboration. A mechanistic understanding of siderophore behavior is only valuable if it is translated to those capable of implementing changes in plant systems. While this dissertation provides foundational insights rather than direct solutions, such groundwork is necessary before meaningful advances can be made. As my advisor recently noted, the path from “study siderophores” to “solve

anemia" is not linear; several critical steps lie in between, and progress depends on building connections across disciplines to move the science forward

References

Rocco, Claudia, Motofumi Suzuki, Ramon Vilar, Enrique Garcia-España, Salvador Blasco, Gerald Larrouy-Maumus, Colin Turnbull, Matthias Wissuwa, Xuan Cao, and Dominik Weiss. 2025. 'Enhancing Zinc Bioavailability in Rice Using the Novel Synthetic Siderophore Ligand Proline-2′-Deoxymugineic Acid (PDMA): Critical Insights from Metal Binding Studies and Geochemical Speciation Modeling', *Journal of Agricultural and Food Chemistry*, 73: 8243-53.

Ueno, Daisei, Yuta Ito, Miho Ohnishi, Chikahiro Miyake, Takayuki Sohtome, and Motofumi Suzuki. 2021. 'A synthetic phytosiderophore analog, proline-2′-deoxymugineic acid, is efficiently utilized by dicots', *Plant and Soil*, 469: 123-34.

APPENDICES

Appendix A(Supplemental Information for Chapter 2)

Table S1. Log of stability constants for metal-siderophore complexes. DMA (Murakami et al. 1989), MA (Murakami et al. 1989); epi-HMA(Murakami et al. 1989); and DFOB (Duckworth and Sposito 2005; Evers et al. 1989; Hernlem, Vane, and Sayles 1996).

	MA	DMA	Epi-HMA	DFOB
Mn(II)	8.30	8.29	8.03	7.68
Ni(II)	14.92	14.78	14.38	11.78
Cu(II)	18.10	18.7	17.92	14.42
Zn(II)	12.69	12.84	12.43	10.43
Fe(III)	32.49	31.35	34.35	31.92

Table S2. Stability constants for metal-PDMA complexes estimated by regression with metal cation hydrolysis constant and DFOB complex stability constant. Stability constants are from: $\log\beta_{OH}$ (Baes and Mesmer 1976) and $\text{Log}\beta_{HDFOB}$ (Hernlem, Vane, and Sayles 1996; Duckworth and Sposito 2005; Evers et al. 1989; Kim, Duckworth, and Strathmann 2009).

ion	$\log K_{DFOB}$	$\log K_{OH}$	$\log KPDMA_{DFOB}$	$\log KPDMA_{KOH}$
Al(III)	25.5	-5.00	29.9± 5.9	27.0 ± 2.8
Ca(II)	3.5	-12.70	4.1± 2.7	2.8 ± 1.3
Cd(II)	8.8	-10.10	10.3 ± 3.4	10.9 ± 1.8
Co(III)	37.4	-1.13	44.1 ± 7.6	39.2 ± 3.6
Fe(II)	11.1	-9.40	13.1 ± 3.8	13.2 ± 1.9
Ga(III)	29.5	-2.90	34.7 ± 6.5	33.6 ± 3.3
In(III)	21.9	-4.00	25.8 ± 5.4	30.2 ± 3.0
La(III)	12.2	-10.04	14.4 ± 4.0	11.2 ± 1.8
Mg(II)	5.2	-11.40	6.1± 2.9	6.9± 1.5
Mn(III)	29.9	-0.60	35.2 ± 6.5	40.9 ± 3.7
Pb(II)	10.9	-7.60	12.8 ± 3.8	18.8 ± 2.3
Sr(II)	3.1	-13.18	3.7± 2.6	1.3 ± 1.1

Appendix B (Supplemental Information for Chapter 3)

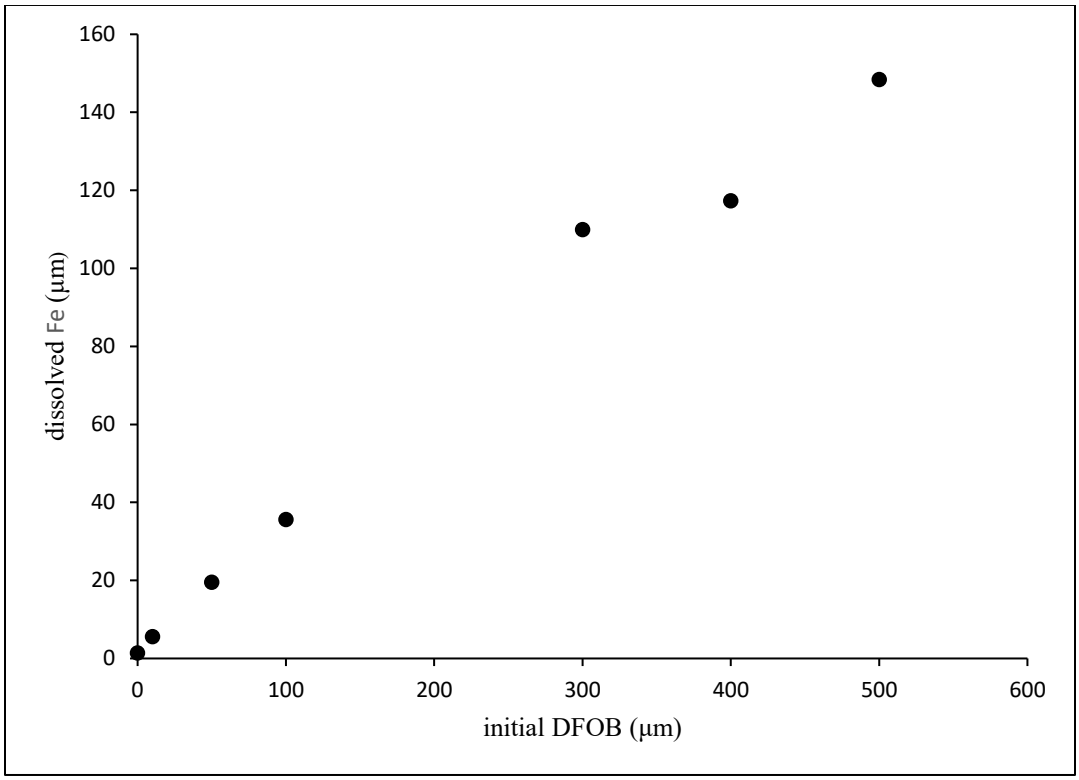

Figure S1. initial DFOB concentration (µm) vs dissolved Fe in solution (µm).

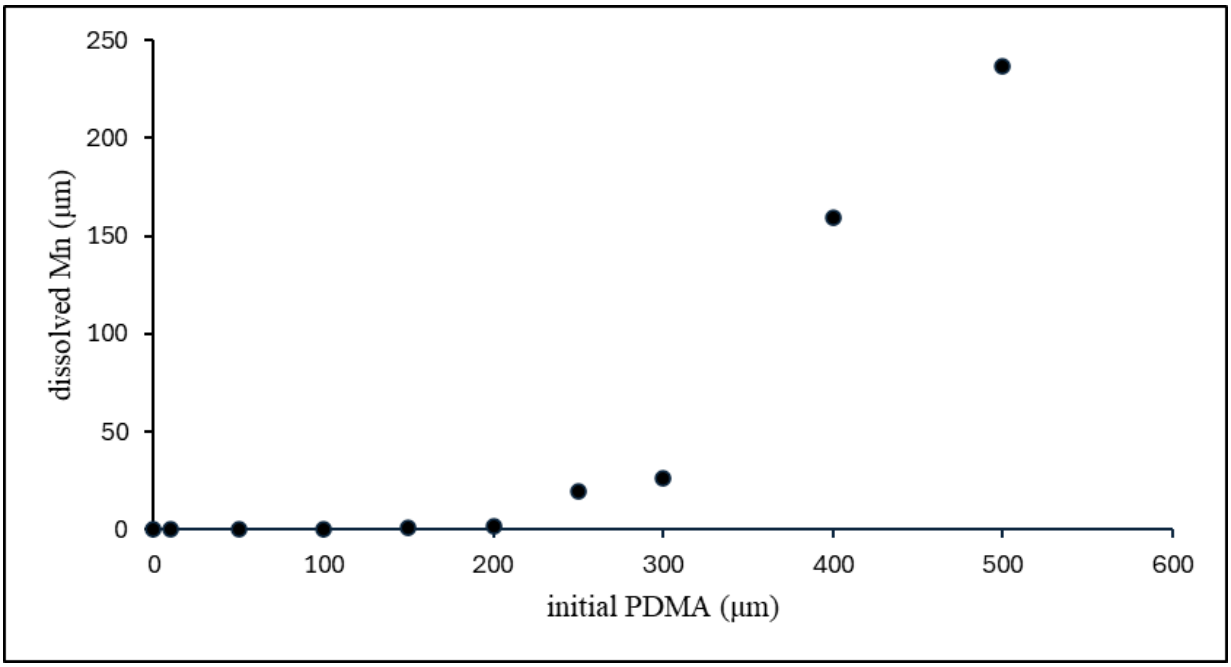

Figure S2. equilibrium PMDA concentration (µm) vs dissolved Mn in solution (ppm).

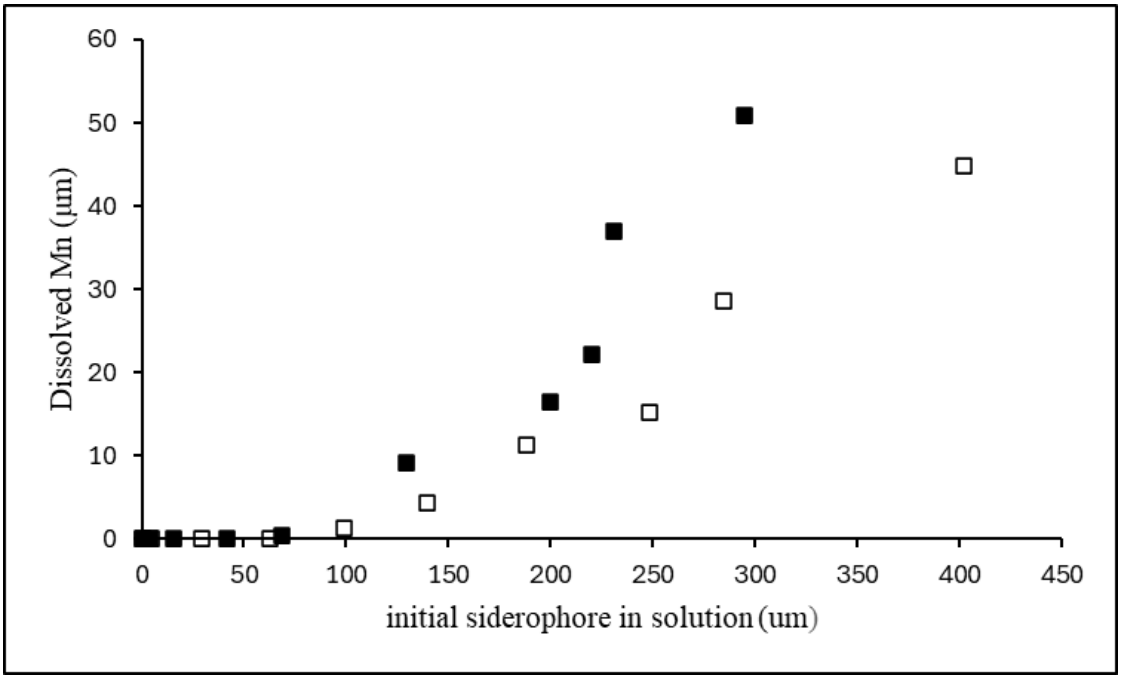

Figure S3. equilibrium protochelin (open square) and Fe-protochelin (dark square) concentration (µm) vs dissolved Mn in solution (ppm).

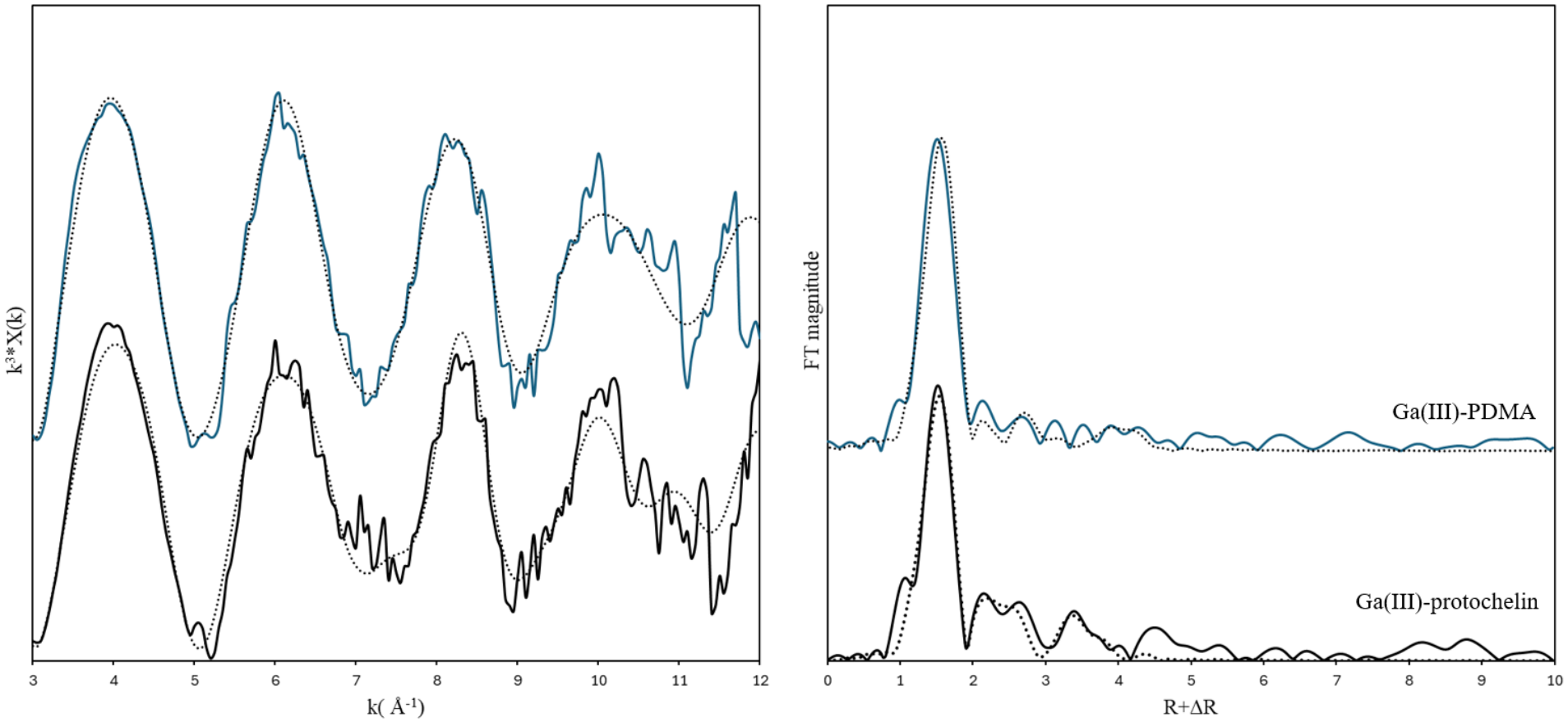

Figure S4. a) aqueous Ga(III)-PDMA and Ga(III)-protochelin EXAFS spectra and b) FT magnitude plots of Ga(III)-PDMA and Ga(III)-protochelin. Shell by shell (structural model) fits to the data are represented by dotted lines with fit parameters shown in SI table 1.

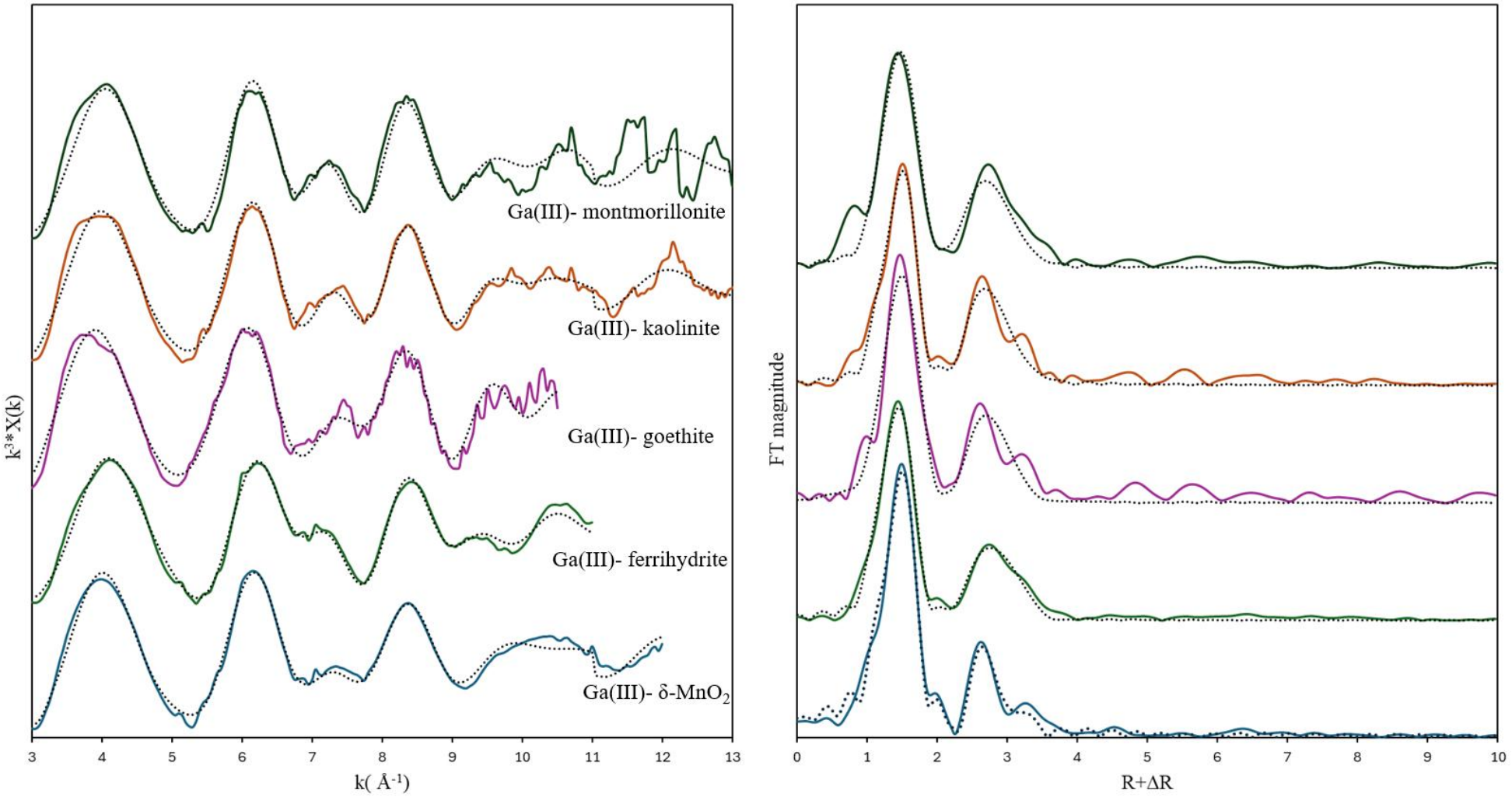

Figure S5. a) Ga(III)- mineral EXAFS spectra and b) FT magnitude plots of Ga(III)-mineral samples. Shell by shell (structural model) fits to the data are represented by dotted lines with fit parameters shown in SI table.

Table S1. Calculated and experimental (EXAFS) average, interatomic distances [Å], standard deviations (STDV: calc.) and Debye–Waller factors (DWF: expt.) for the first, second and third coordination shells.

	First Shell M-O				Second Shell M-C				Third Shell M-C			Carboxyl	
Ga(III) Species	**S_0^2**	**N_O**	**R_O (Å)**	**σ_O^2(Å^2)**	**$N_{C/N2}$**	**$R_{C/N2}$ (Å)**	**$\sigma_{C/N2}$ (Å^2)**	**multiple scattering**	**$N_{C/N3}$**	**$R_{C/N3}$**	**$\sigma_{C/N3}$ (Å^2)**	**R**	**σ (Å^2)**
Protochelin	1	5.78 (0.85)	1.963 (0.008)	0.006 (0.001)	6	2.72 (0.01)	0.0076 (0.002)	12	6	3.87 (0.02)	0.0027 (0.002)	x	x
PDMA	1	7.77 (0.83)	1.97 (0.01)	0.0066 (0.0001)	9	2.81 (0.11)	0.05 (0.02)	x	5	4.41 (0.12)	0.016 (0.018)	3.1 (0.03)	0.0037 (0.002)

	First Shell M-O				Second Shell M-C/N			Third Shell M-C/N		
Ga(III) Species	**S_0^2**	**N_O**	**R_O (Å)**	**σ_O^2(Å^2)**	**$N_{C/N2}$**	**$R_{C/N2}$ (Å)**	**$\sigma_{C/N2}$ (Å^2)**	**$N_{C/N3}$**	**$R_{C/N3}$**	**$\sigma_{C/N3}$ (Å^2)**
Goethite	1	8.23 (1.35)	1.98(0.01)	0.011 (0.001)	3.46 (0.85)	3.07 (0.02)	0.01	1.7 (1.05)	3.36 (0.04)	0.01
Ferrihydrite	1	6.77	1.91	0.011	1.98	3.05	0.01	1.55	3.46	0.01

	First Shell M-O				Second Shell M-C/N				Third Shell M-C/N		
Ga(III) Species	**S_0^2**	**N_O**	**R_O (Å)**	**σ_O^2(Å^2)**	**$N_{C/N2}$**	**$R_{C/N2}$ (Å)**	**$\sigma_{C/N2}$ (Å^2)**	**f_{DFS}**	**$N_{C/N3}$**	**$R_{C/N3}$**	**$\sigma_{C/N3}$ (Å^2)**
δ-MnO_2	1	7.47 (0.66)	1.95 (0.01)	0.011 (0.001)	2	3.03 (0.01)	0.0085 (0.001)	0.86 (.07)	6	3.50 (0.03)	0.0085

	First Shell M-O				Second Shell M-Al			Third Shell M-Ga		
Ga(III) Species	**S_0^2**	**N_O**	**R_O (Å)**	**σ_O^2(Å^2)**	**N_{al}**	**R_{Al} (Å)**	**$\sigma_{C/N2}$ (Å^2)**	**N_{Ga}**	**R_{Ga}**	**σ_{Ga} (Å^2)**
Kaolinite	1	7.44 (0.67)	1.95 (0.01)	0.011 (0.001)	0.91 (1.53)	3.68 (0.03)	0.0038 (0.012)	6.25 (2.50)	3.01 (0.010)	0.015 (0.004)
Montmorillonite	1	7.24 (0.85)	1.95 (0.01)	0.011(0.002)	1.97 (2.84)	3.74 (0.03)	0.008 (0.012)	5.85 (2.84)	3.03 (0.01)	0.014 (0.004)

Table S2. Dissolved Fe (μm) for Ga(III)-DFOB, Ga(III)-PDMA, and Ga(III)- Protochelin (1mM concentration) when reacted with ferrihydrite.

Species	**$Fe_{dissolved}$**
Ga-DFOB	20.3
Ga-PDMA	14.8
Ga-Protochelin	8.4

Appendix C (Supplemental Information for Chapter 4)

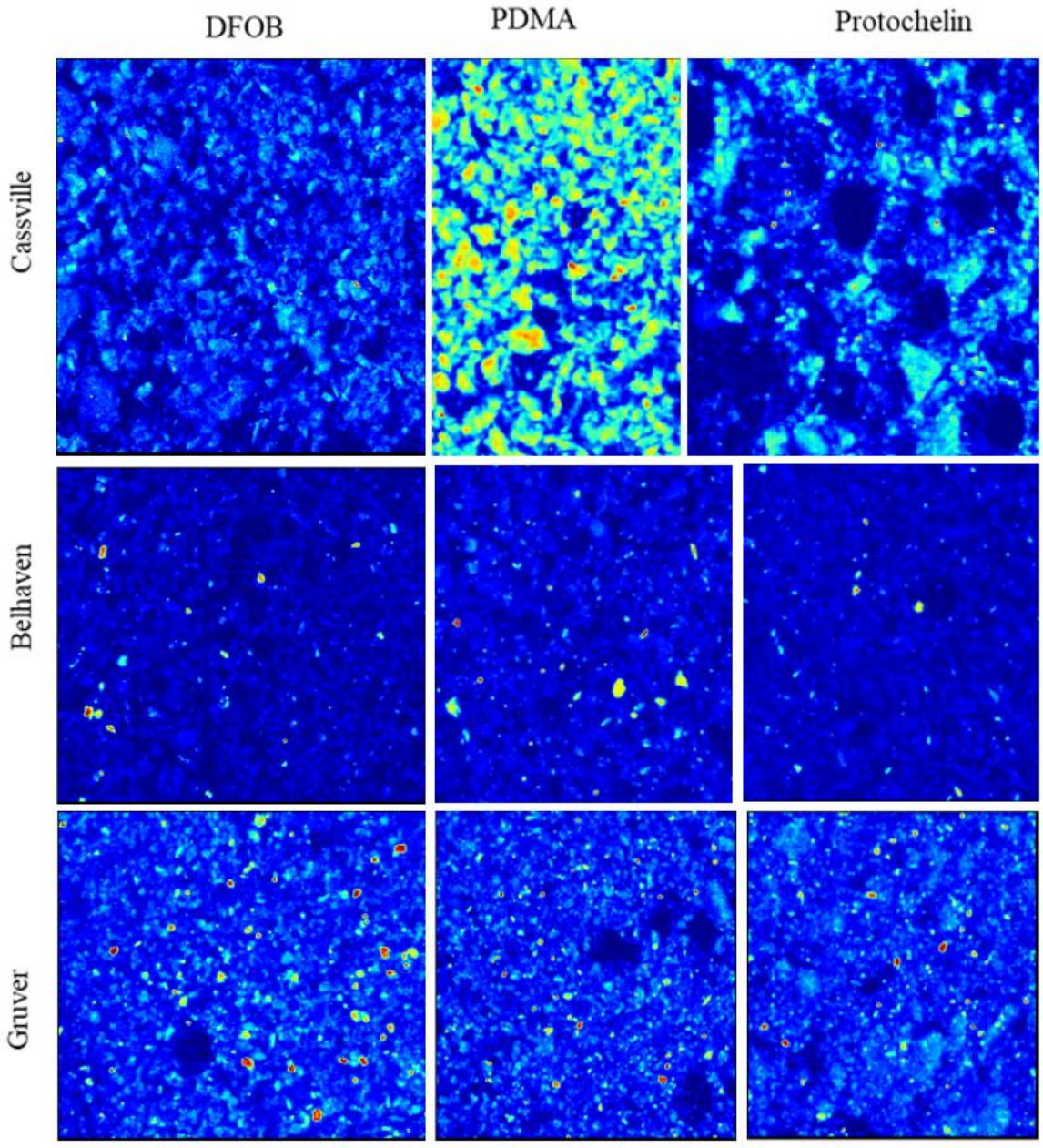

SI Figure 1. Fe μ-XRF maps. Red indicated areas of high concentration, and blue indicates areas of low concentration.

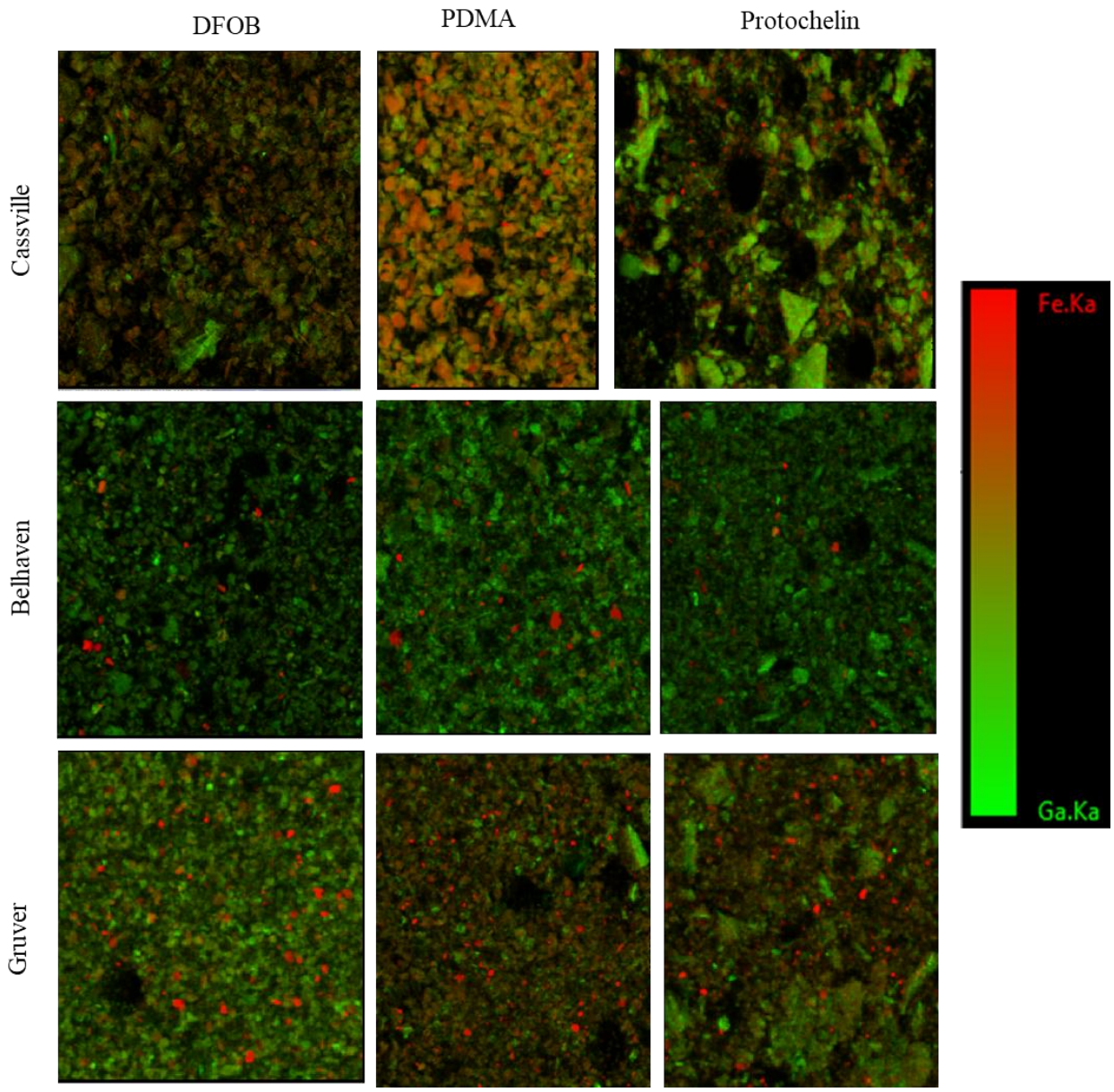

SI Figure 2. Ga(III)-Fe gradient maps.

SI Table 1. Total Fe and Mn concretions in the Cassville, Belhaven, and Gruver soils (mmol/kg).

Soils	Fe	Mn
Cassville Clay	1,168.9	8.1
Belhaven Muck	114.9	0.38
Gruver Soil	345.2	7.8

SI Table 2. R^2 values for Ga correlations with Fe and Mn in overall μ-XRF maps.

	Cassville		**Belhaven**		**Gruver**	
	Fe R^2	**Mn R^2**	**Fe R^2**	**Mn R^2**	**Fe R^2**	**Mn R^2**
Ga(III)-DFOB	0.57	0.41	0.23	0.10	0.18	0.08
Ga(III)-PDMA	0.57	0.52	0.07	0.02	0.21	0.06
Ga(III)-Protochelin	0.6	0.62	0.11	0.03	0.2	0.14

SI Table 3. R^2 values for Ga correlations with Fe and Mn in the hotspots for μ-XRF maps.

Fe R^2	**Cassville Fe R^2**		**Belhaven**		**Gruver**
	Hotspot 1	**Hotspot 2**	**Hotspot 1**	**Hotspot 2**	**Hotspot 1**
Ga(III)-DFOB	0.63	-	0.35	-	0.86
Ga(III)-PDMA	0.29	0.18	0.03	0.74	0.56
Ga(III)-Protochelin	0.81	0.69	0.52	-	-

Mn R^2	**Cassville**		**Belhaven**		**Gruver**
	Hotspot 1	**Hotspot 2**	**Hotspot 1**	**Hotspot 2**	**Hotspot 1**
Ga(III)-DFOB	0.42	-	0.44	-	0.70
Ga(III)-PDMA	0.41	0.006	0.04	0.02	0.26
Ga(III)-Protochelin	0.85	0.76	0.51	-	-

SI Table 4. EXAFS structure fitting results. Numbers represent the % best fit by the aqueous complex, with remainder of the fit from Ga(III)-mineral spectra. Fits were normalized to 100% but were 0.88 ± 0.11. Ferrihydrite, δ-MnO_2, kaolinite, and montmorillonite complexes were fit from k = 3-13 $Å^{-1}$, whereas goethite complexes were fit from k = 3-10 $Å^{-1}$.

Sorbent	**Ga(III)-DFOB (%)**	**Ga(III)-PDMA (%)**	**Ga(III)-Protochelin(%)**
ferrihydrite	0	0	100
δ-MnO_2	0	0	0
kaolinite	0	0	28
montmorillonite	100	70	33
goethite	36	35	38
Organic matter	55	80	0